



Calhoun: The NPS Institutional Archive
DSpace Repository

Theses and Dissertations

1. Thesis and Dissertation Collection, all items

2020-12

ROTATIONAL MOTION TRIBOELECTRIC NANOGENERATORS (TENG)

Capelle, June

Monterey, CA; Naval Postgraduate School

<http://hdl.handle.net/10945/66599>

This publication is a work of the U.S. Government as defined in Title 17, United States Code, Section 101. Copyright protection is not available for this work in the United States.

Downloaded from NPS Archive: Calhoun



Calhoun is the Naval Postgraduate School's public access digital repository for research materials and institutional publications created by the NPS community. Calhoun is named for Professor of Mathematics Guy K. Calhoun, NPS's first appointed -- and published -- scholarly author.

Dudley Knox Library / Naval Postgraduate School
411 Dyer Road / 1 University Circle
Monterey, California USA 93943

<http://www.nps.edu/library>



**NAVAL
POSTGRADUATE
SCHOOL**

MONTEREY, CALIFORNIA

THESIS

**ROTATIONAL MOTION TRIBOELECTRIC
NANOGENERATORS (TENG)**

by

June Capelle

December 2020

Thesis Advisor:
Second Reader:

Young W. Kwon
Jarema M. Didoszak

Approved for public release. Distribution is unlimited.

THIS PAGE INTENTIONALLY LEFT BLANK

REPORT DOCUMENTATION PAGE			<i>Form Approved OMB No. 0704-0188</i>	
Public reporting burden for this collection of information is estimated to average 1 hour per response, including the time for reviewing instruction, searching existing data sources, gathering and maintaining the data needed, and completing and reviewing the collection of information. Send comments regarding this burden estimate or any other aspect of this collection of information, including suggestions for reducing this burden, to Washington headquarters Services, Directorate for Information Operations and Reports, 1215 Jefferson Davis Highway, Suite 1204, Arlington, VA 22202-4302, and to the Office of Management and Budget, Paperwork Reduction Project (0704-0188) Washington, DC 20503.				
1. AGENCY USE ONLY (Leave blank)		2. REPORT DATE December 2020		3. REPORT TYPE AND DATES COVERED Master's thesis
4. TITLE AND SUBTITLE ROTATIONAL MOTION TRIBOELECTRIC NANOGENERATORS (TENG)			5. FUNDING NUMBERS	
6. AUTHOR(S) June Capelle				
7. PERFORMING ORGANIZATION NAME(S) AND ADDRESS(ES) Naval Postgraduate School Monterey, CA 93943-5000			8. PERFORMING ORGANIZATION REPORT NUMBER	
9. SPONSORING / MONITORING AGENCY NAME(S) AND ADDRESS(ES) N/A			10. SPONSORING / MONITORING AGENCY REPORT NUMBER	
11. SUPPLEMENTARY NOTES The views expressed in this thesis are those of the author and do not reflect the official policy or position of the Department of Defense or the U.S. Government.				
12a. DISTRIBUTION / AVAILABILITY STATEMENT Approved for public release. Distribution is unlimited.			12b. DISTRIBUTION CODE A	
13. ABSTRACT (maximum 200 words) The triboelectric nanogenerator (TENG) experiments conducted for this research are a continuation of previous research at the Naval Postgraduate School in Monterey, California. Teflon and copper were used as the primary materials to generate electricity through contact. Teflon tape, copper tape, and a variety of readily available materials were used to reduce the cost and increase the viability of mass production. The TENG consists of three parts: a flexible plastic in which the copper tape is applied, a PVC pipe in which the Teflon tape is applied, and a wooden shaft that supports and rotates the PVC pipe with the flexible plastic wrapped around the pipe. A DC motor is connected to the wooden shaft to generate rotational motion for the TENG, causing a potential change within the copper taping configuration. Five TENG models were analyzed for their capability to store and discharge electricity through capacitors and LEDs. The chosen model was also adapted to a stationary bicycle to demonstrate its capability to independently generate electricity.				
14. SUBJECT TERMS triboelectric nanogenerators, electronegativity, friction, energy storage			15. NUMBER OF PAGES 105	
			16. PRICE CODE	
17. SECURITY CLASSIFICATION OF REPORT Unclassified	18. SECURITY CLASSIFICATION OF THIS PAGE Unclassified	19. SECURITY CLASSIFICATION OF ABSTRACT Unclassified	20. LIMITATION OF ABSTRACT UU	

THIS PAGE INTENTIONALLY LEFT BLANK

Approved for public release. Distribution is unlimited.

ROTATIONAL MOTION TRIBOELECTRIC NANOGENERATORS (TENG)

June Capelle
Lieutenant, United States Navy
BS, Embry-Riddle Aeronautical University, 2008
BS, ECPI College of Technology, 2012

Submitted in partial fulfillment of the
requirements for the degree of

MASTER OF SCIENCE IN MECHANICAL ENGINEERING

from the

**NAVAL POSTGRADUATE SCHOOL
December 2020**

Approved by: Young W. Kwon
Advisor

Jarema M. Didoszak
Second Reader

Garth V. Hobson
Chair, Department of Mechanical and Aerospace Engineering

THIS PAGE INTENTIONALLY LEFT BLANK

ABSTRACT

The triboelectric nanogenerator (TENG) experiments conducted for this research are a continuation of previous research at the Naval Postgraduate School in Monterey, California. Teflon and copper were used as the primary materials to generate electricity through contact. Teflon tape, copper tape, and a variety of readily available materials were used to reduce the cost and increase the viability of mass production. The TENG consists of three parts: a flexible plastic in which the copper tape is applied, a PVC pipe in which the Teflon tape is applied, and a wooden shaft that supports and rotates the PVC pipe with the flexible plastic wrapped around the pipe. A DC motor is connected to the wooden shaft to generate rotational motion for the TENG, causing a potential change within the copper taping configuration. Five TENG models were analyzed for their capability to store and discharge electricity through capacitors and LEDs. The chosen model was also adapted to a stationary bicycle to demonstrate its capability to independently generate electricity.

THIS PAGE INTENTIONALLY LEFT BLANK

TABLE OF CONTENTS

I.	INTRODUCTION	1
A.	MOTIVATION	1
B.	LITERATURE REVIEW	2
1.	Principle Modes of TENG	4
2.	TENG Applications.....	7
3.	Design Challenges	9
II.	DESIGN DRAFTS.....	11
A.	PREVIOUS NPS TENG ROTATIONAL DESIGN	11
B.	DEVELOPMENT	12
C.	MATERIALS	13
D.	MODEL DESIGN AND CONSTRUCTION.....	14
E.	DESIGN MODELS.....	18
III.	EXPERIMENTATION PROCESS	25
A.	EXPERIMENTAL EQUIPMENT	25
B.	EXPERIMENTAL PROCEDURES	25
1.	Initial Voltage and Frequency Data Collection.....	26
2.	Electricity Storage and Display Procedures.....	27
3.	Series/Parallel Testing Procedures.....	28
IV.	RESULTS AND DISCUSSION.....	33
A.	INDIVIDUAL TENG MODEL VOLTAGE TESTING.....	33
1.	Initial Voltage Data.....	33
2.	Performance Comparison	38
B.	OPTIMUM PERFORMANCE ANALYSIS.....	39
1.	Performance with Capacitor.....	41
2.	Performance with LEDs.....	42
C.	SERIES/PARALLEL TESTING RESULTS	46
1.	Experimental Results for Model 3.....	46
2.	Experimental Results for Model 1A and 1B in Parallel/ Series	47
D.	SUMMARY OF ANALYSIS RESULTS	49
E.	DISCUSSION	53

V.	CONCLUSIONS AND FUTURE WORK	61
A.	CONCLUSIONS	61
B.	RECOMMENDATIONS.....	63
C.	FUTURE RESEARCH.....	64
APPENDIX	65
A.	MODEL 1A DATA	65
B.	MODEL 1B DATA	68
C.	MODEL 2A DATA	71
D.	MODEL 2B DATA	73
E.	MODEL 3 DATA	75
F.	MODEL 1A AND 1B SERIES/PARALLEL TEST DATA	77
G.	CAPACITOR STORAGE DATA	79
	LIST OF REFERENCES.....	81
	INITIAL DISTRIBUTION LIST	83

LIST OF FIGURES

Figure 1.	Triboelectric materials according to their Triboelectric polarities. Source: [4].....	3
Figure 2.	Four fundamental modes of TENG. Source: [3].....	4
Figure 3.	Vertical Contact-Separation Mode. Source: [3].....	5
Figure 4.	Linear Sliding Mode. Source: [3].	5
Figure 5.	Single Electrode Mode. Source: [3].....	6
Figure 6.	Freestanding Triboelectric-Layer Mode. Source: [3].	7
Figure 7.	Micro-scale TENG applications. Source: [3].....	8
Figure 8.	NPS TENG Rotational Model (Internal View). Source: [6].....	11
Figure 9.	NPS TENG Rotational Model (External View). Source: [6].....	12
Figure 10.	Dayton PMDC Motor with Controller (Model: 2Z846)	15
Figure 11.	Mounting Hub and Flexible Coupling	15
Figure 12.	PVC Pipe with Teflon Tape Outboard and Hardwood Shaft Inboard	16
Figure 13.	(From left to right) Copper Outboard and Copper Inboard	17
Figure 14.	TENG Model (1.27cm Copper Taping).....	17
Figure 15.	Spacing Example of Model 1A Copper and Teflon.....	19
Figure 16.	(Internal) Model 1A (left) and Model 1B (right)	20
Figure 17.	(External) Model 1A (left) and Model 1B (right).....	20
Figure 18.	Model 2A (Internal)	21
Figure 19.	Model 2B (Internal)	22
Figure 20.	Model 2B (External)	22
Figure 21.	Model 3 (Internal)	23
Figure 22.	Model 3 (External).....	23

Figure 23.	Motor Connected to TENG Model with Mounting Hub and Flexible Coupling.....	26
Figure 24.	Left TENG Initial Data Collection	29
Figure 25.	Right TENG Initial Data Collection	29
Figure 26.	Model 3 Series Connection.....	30
Figure 27.	Model 3 Parallel Connection	30
Figure 28.	Models 1A and 1B Series Connection	31
Figure 29.	Models 1A and 1B Parallel Connection.....	31
Figure 30.	TENG Model 1A Voltage Data	34
Figure 31.	TENG Model 1B Voltage Data.....	35
Figure 32.	TENG Model 2A Voltage Data	36
Figure 33.	TENG Model 2B Voltage Data.....	37
Figure 34.	Effective Voltage (V_{rms}) Comparison between Models	38
Figure 35.	Frequency Comparison between Models.....	38
Figure 36.	Oscilloscope Resistance = 10 M Ω	39
Figure 37.	Validation of Cable Resistance.....	40
Figure 38.	Configuration with Capacitor for electricity storage	41
Figure 39.	Voltage and Time to charge a 10 μ F Capacitor using TENG Model 1B.....	42
Figure 40.	Nine LEDs at 24 Volts from TENG	43
Figure 41.	30 LEDs at 90 Volts from TENG	44
Figure 42.	120 LEDs	45
Figure 43.	TENG Model 3 Voltage Data	47
Figure 44.	Series/Parallel Test (Model 1A and 1B).....	48
Figure 45.	Current without Transformer (left); Current with Transformer (right)	49

Figure 46.	Model 1A and 1B at 60 RPM Shaft Speed	50
Figure 47.	Model 2A and 2B at 60 RPM Shaft Speed	50
Figure 48.	Voltage and Current for Model 1B at 50 RPM.....	51
Figure 49.	Voltage and Current for Model 1B at 100 RPM.....	51
Figure 50.	Series/Parallel Data for Model 3.....	52
Figure 51.	Series/Parallel Data for Model 1A and 1B	53
Figure 52.	Gap in Surface Contact.....	54
Figure 53.	Stationary Bike with Mounted Gears and Chain	56
Figure 54.	Stationary Bike with TENG.....	57
Figure 55.	TENG Voltage Data at 20 RPM (Bike Speed)	58
Figure 56.	120 LEDs connected to TENG with Stationary Bike	58
Figure 57.	120 LEDs when Stationary Bike is operating at 20 RPM (left) or greater (right)	59
Figure 58.	Model 1A Shaft Speed at 60 RPM.....	65
Figure 59.	Model 1A Shaft Speed at 90 RPM.....	65
Figure 60.	Model 1A Shaft Speed at 120 RPM.....	66
Figure 61.	Model 1A Shaft Speed at 150 RPM.....	66
Figure 62.	Model 1A Shaft Speed at 180 RPM.....	66
Figure 63.	Model 1A Shaft Speed at 210 RPM.....	67
Figure 64.	Model 1A Shaft Speed at 240 RPM.....	67
Figure 65.	Model 1A Shaft Speed at 270 RPM.....	67
Figure 66.	Model 1A Shaft Speed at 300 RPM.....	68
Figure 67.	Model 1A Shaft Speed at 397 RPM.....	68
Figure 68.	Model 1B Shaft Speed at 60 RPM.....	68
Figure 69.	Model 1B Shaft Speed at 90 RPM.....	69

Figure 70.	Model 1B Shaft Speed at 120 RPM.....	69
Figure 71.	Model 1B Shaft Speed at 150 RPM.....	69
Figure 72.	Model 1B Shaft Speed at 180 RPM.....	70
Figure 73.	Model 1B Shaft Speed at 210 RPM.....	70
Figure 74.	Model 1B Shaft Speed at 240 RPM.....	70
Figure 75.	Model 1B Shaft Speed at 270 RPM.....	71
Figure 76.	Model 1B Shaft Speed at 300 RPM.....	71
Figure 77.	Model 1B Shaft Speed at 398 RPM.....	71
Figure 78.	Model 2A Shaft Speed at 60 RPM.....	72
Figure 79.	Model 2A Shaft Speed at 90 RPM.....	72
Figure 80.	Model 2A Shaft Speed at 120 RPM.....	72
Figure 81.	Model 2A Shaft Speed at 150 RPM.....	73
Figure 82.	Model 2A Shaft Speed at 180 RPM.....	73
Figure 83.	Model 2B Shaft Speed at 60 RPM.....	73
Figure 84.	Model 2B Shaft Speed at 90 RPM.....	74
Figure 85.	Model 2B Shaft Speed at 120 RPM.....	74
Figure 86.	Model 2B Shaft Speed at 150 RPM.....	74
Figure 87.	Model 2B Shaft Speed at 180 RPM.....	75
Figure 88.	Left Side of Model 3 at 90 RPM.....	75
Figure 89.	Right Side of Model 3 at 90 RPM	75
Figure 90.	Model 3 Right and Left sides in Series at 90 RPM.....	76
Figure 91.	Model 3 Right and Left sides in Parallel at 90 RPM	76
Figure 92.	Model 1A prep for Series/Parallel Test	77
Figure 93.	Model 1B prep for Series/Parallel Test.....	77
Figure 94.	Model 1A and 1B in Series at 90 RPM.....	78

Figure 95.	Model 1A and 1B in Parallel at 90 RPM	78
Figure 96.	Model 1B Charging 10 μ F Capacitor at 50 RPM	79
Figure 97.	Model 1B Charging 10 μ F Capacitor at 75 RPM	79
Figure 98.	Model 1B Charging 10 μ F Capacitor at 100 RPM	80
Figure 99.	Model 1B Charging 10 μ F Capacitor at 125 RPM	80

THIS PAGE INTENTIONALLY LEFT BLANK

LIST OF TABLES

Table 1.	List of Required Materials	13
Table 2.	Model Dimensions	18
Table 3.	List of Required Equipment.....	25
Table 4.	Model 1A Voltage Data	33
Table 5.	Model 1B Voltage Data	35
Table 6.	Model 2A Voltage Data	36
Table 7.	Model 2B Voltage Data	37
Table 8.	Complete Charging of 10 μ F Capacitor.....	42
Table 9.	LEDs Used in 1st Display Test.....	43
Table 10.	Model 3 Voltage Data.....	46
Table 11.	Series/Parallel Test (Model 1A and 1B).....	47

THIS PAGE INTENTIONALLY LEFT BLANK

LIST OF ACRONYMS AND ABBREVIATIONS

AC	alternating current
DC	direct current
EMG	electromagnetic generator
FO-TEEM	floating oscillator-embedded triboelectric-electromagnetic
LED	light emitting diode
MIN	minimum
MAX	maximum
NPS	Naval Postgraduate School
PENG	piezoelectric nanogenerator
PLA	polylactic acid
PTFE	polytetrafluorethylene
PVC	polyvinyl chloride
RMS	root mean square
RPM	rotations per minute
TENG	triboelectric nanogenerator
VAC	Voltage Alternating Current

THIS PAGE INTENTIONALLY LEFT BLANK

ACKNOWLEDGMENTS

Foremost, I would like to thank my family, most specifically my wife, Louisa, and two kids, Adassah and K-Vaun, for their unwavering support throughout my Navy career in addition to my time here at Naval Postgraduate School. In addition, I want to give my special thanks to Professor Young Kwon and Professor Jarema Didoszak for their mentorship, guidance, and support throughout my research and experiments. The majority of this research was successful due to the exceptional guidance received from Professor Young Kwon and Professor Jarema Didoszak. I also want to give my special thanks to Dr. Seol Myeonglok from NASA Ames for helping me get over some of the greater hurdles encountered during my research. Also, I would like to thank Lieutenant Katherine Mann and Lieutenant Joseph Kessopha for their research and help in leading me to my interest in developing these triboelectric nanogenerator models.

From the Engineering Department staff, I would like to thank Warren Rogers, Daniel Sakoda, and Joseph Klamo. From NPS Public Works, I would like to thank Roy Carius and William Lee. Their unselfish support also played a significant role in my pursuit to complete my research.

THIS PAGE INTENTIONALLY LEFT BLANK

I. INTRODUCTION

A. MOTIVATION

We live in an age where technology is no longer a luxury but a necessity. With the high demands for modern technology, the requirement for electricity has exponentially increased, with no limit in sight. Fossil fuels (coal, gas, and oil) continue to be the primary source of energy being supplied to the world. And although the use of fossil fuels is reliable, cheap, and well-established, the by-products of such energy sources have deeply affected our environment, especially through global warming. Additionally, the increase in the world's population will eventually lead to a point where the supply of fossil fuels will not be able to meet the demand.

To avoid a potential energy crisis in the near future and combat global warming, stakeholders have been seeking to improve renewable energy methods, with intentions to overtake the roles of fossil fuels. Renewable energy has now overtaken nuclear power, which makes up of 4.3% of the world's total energy consumption [1]. Renewable energy sources include sunlight, wind, waves, tides, rain, rivers, and practically anything that can generate heat and/or motion. The primary problem with all renewable energy methods is that the source is inconsistent and harvesting methods are still inefficient compared to fossil fuels. Although improvements have been made to the renewable energy methods, we should not limit ourselves to these current methods if we expect to exceed the capabilities of fossil fuels. Other methods should also be considered to ensure all possibilities are not overlooked.

This research considers methods of generating energy by means of motion. For example, wind flowing through wind turbines and rivers flowing through dams are both renewable energy methods that can only be constructed in areas with reasonable wind and rivers. That is because air and water motion are the sole factors used to generate electricity. And although they can be reliable, this limits the locations where these methods can be utilized. And what happens if there is no wind? Or the rivers dry up? The keyword in this example is "motion." Without motion, there is no energy generation.

Both energy methods require motion to generate electricity. So, what if we had a renewable energy method that could harvest energy from any type of motion?

One possible solution is triboelectric nanogenerators (TENGs). A TENG generates an electrical output “based on contact electrification between two materials and charge transfer between the electrodes due to electrostatic induction” [2]. This research focuses on constructing a device capable of extracting the mechanical energy generated from rotational motion and discovering how to use such motion to generate electrical energy.

B. LITERATURE REVIEW

Triboelectricity is generated when a material gains electric charge through contact with a different material. “A chemical bond is formed between some parts of the two surfaces, called adhesion, and charges move from one material to the other to equalize their electrochemical potential” [3]. In your everyday life, many call this type of electric charge static electricity. When you rub your shoes against carpets, balloons against hairs, or even silk sheets against plastic, you will eventually generate enough charge to shock you -widely known as static electric shock. This is conceptually true since static electricity is the imbalance of electric charges within a material; however, to complete the analogy, triboelectricity is the process in which the imbalance of electric charges is actually being harvested rather than discharged naturally. Overall, an effective TENG would require the use of two different materials where one of the materials has a greater tendency to lose electrons while the other material has a greater tendency to gain electrons. In addition, there has to be a certain relative motion between the two materials to ensure electric charges are generated.

Over the last decade, research teams from the United States, South Korea, and China have been conducting experiments on various TENG models to accommodate a range of applications. Currently, the primary market aimed for TENG technology is for personal electronic devices and sensors. Most of these designs are for smaller applications and low-power devices; however, it is a mission for this research to expand the horizon of this technology with the possibility to meet higher demands.

Current research on TENG aim towards optimizing the type of materials being used, the size of the models being constructed, and the configuration of material contact. In terms of materials being used, Figure 1 shows a list of possible combinations that could be used for a TENG model.



Triboelectric Polarity	
 POSITIVE	Silicone elastomer with silica filler
	Borosilicate Glass
	Aniline – formol resin
	Polyformaldehyde 1.3-1.4
	Polymethylmethacrylate
	Ethycellulose
	Polyamide 11
	Polyamide 6-6
	Rock Salt
	Melamine formol
	Wool, knitted
	Silk, woven
	Poly-ethylene glycol succinate
	Cellulose - Cellulose acetate
	Polyethylene glycol adipate
	Cotton, woven
	Polyurethane elastomer
	Styrene – acrylonitrile copolymer
	Styrene – butadiene copolymer
	Steel (Neutral)
 NEGATIVE	Wood
	Hard Rubber
	Acetate, Rayon
	Polyvinil alcohol
	Polyester (Dacron)
	Polyisobutylene
	Polyurethane flexible sponge
	Polyethylene glycol terephthalate
	Polyvinyl butyral
	Formo-phenelique
	Epoxide resin
	Natural Rubber
	Polystyrene
	Polyethylene
	Polypropylene
	Polyimide (Kapton)
	Polyethylene terephthalate
	Polyvinyl Chloride (PVC)
	Polytrifluorochloroethylene – Silicon
	Polytetrafluoroethylene (Teflon) – Flourinated PEI

Figure 1. Triboelectric materials according to their Triboelectric polarities. Source: [4].

From the list in Figure 1, it should be noted that choosing the most positive and negative materials is not practical. For instance, the chemical reaction between two materials have to be considered to ensure that the generated byproducts are not hazardous to the environment -which could result in this technology being denied as a renewable energy source. Another consideration is the conductivity of the material that will be carrying the charge. For instance, aluminum may have a better tendency to lose electrons

than copper; however, copper is more conductive than aluminum. Overall, many factors must be considered when constructing a TENG for application. For the purpose of this research, we will concentrate on practical materials that are readily available with assurance of the possibility of mass production at an affordable global rate.

1. Principle Modes of TENG

For a material to generate an electric charge after contact with a different material, the concept can be easy to grasp since all that is needed is contact. In any dimension, contact horizontally or vertically has the probability to generate electricity depending on the materials being used. But for simplification, the understanding of this technology is better explained starting with the four principle modes for a TENG, which are vertical contact-separation, linear sliding, single electrode, and freestanding triboelectric layer mode (see Figure 2) [3].

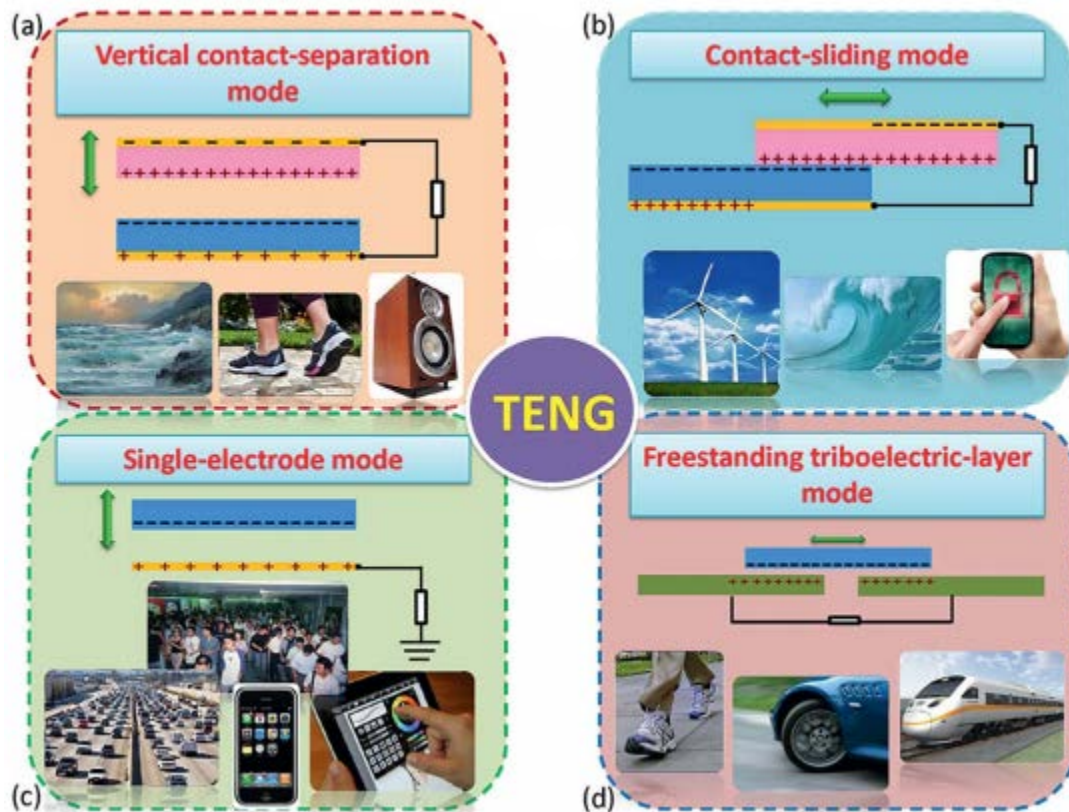


Figure 2. Four fundamental modes of TENG. Source: [3].

a. Vertical Contact Separation

The vertical contact separation mode is the simplest of the four modes. For this mode, two dissimilar dielectric films are oriented with their main surface areas facing each other and two electrodes attached to the outer surface area of both films. The two electrodes are wired together to allow for flow of electrons as shown in Figure 3.

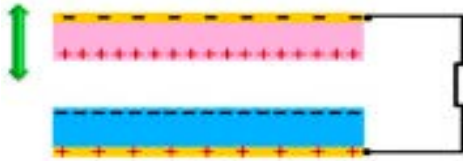


Figure 3. Vertical Contact-Separation Mode. Source: [3].

When the dielectric films make vertical contact, an opposite charge is generated on the surfaces of the films. When the surfaces are separated, electricity is generated due to a voltage drop from when electrons flow through the connected electrodes on the outer surface of the films with an attempt to neutralize the charged surfaces.

b. Linear Sliding

Linear sliding mode has the same components required for vertical contact separation mode. The difference is that linear sliding mode requires sliding contact between the two dielectrics to generate a charge on the two surfaces (see Figure 4).

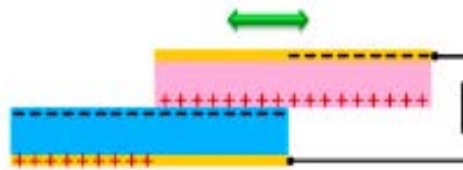


Figure 4. Linear Sliding Mode. Source: [3].

The amount of charge generated depends on the amount of surface in contact during the sliding motion. This induces a lateral polarization in the sliding direction

resulting in transferring electrons to the top and bottom electrodes, which balances the area created by triboelectric charges [5].

c. Single-Electrode

Single-electrode mode has a dielectric and a “single electrode” confined within a system as shown in Figure 5.

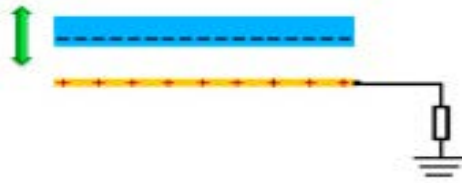


Figure 5. Single Electrode Mode. Source: [3].

The reasoning behind this type of mode is to allow the dielectric the freedom of movement with no connections to the load. Therefore, an electric charge is generated whenever the dielectric contacts the electrode. The electrode is grounded allowing current to flow towards the grounding. And in order to harvest the electricity generated by this mode, a load is placed before the grounding causing a voltage drop across the load. Motion above the electrode will transfer electrons between the bottom electrode and ground, therefore allowing a potential change [5].

d. Freestanding Triboelectric Layer

The freestanding triboelectric-layer mode is similar to the single electrode mode except for the fact that, instead of grounding a single electrode, two electrodes are connected to transfer electrons between them in an attempt to balance a potential distribution as the dielectric slides in contact over both electrodes [3]. The configuration of the freestanding triboelectric-layer mode is as shown in Figure 6.

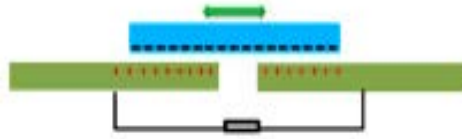


Figure 6. Freestanding Triboelectric-Layer Mode. Source: [3].

When the dielectric is on top of only one of the electrodes, a charge is generated and will tend to send the electrons to the other electrode in order to neutralize the materials in contact. And as the dielectric passes over both electrodes, the electric charges generated on both electrodes will depend on their surface area contacts with the dielectric. Therefore, current flow will generally be coming from the electrode with most surface area contact with the dielectric; however, as the surface area contact increases between the dielectric and the second electrode, there will still be current flow between the electrodes but now the current will change its directions. This mode is ideal in generating a potential with alternating current.

2. TENG Applications

Based on the four modes discussed in the previous section, TENG technology shows great potential in generating electricity for a range of applications. It has the substantial advantage of being a Blue Energy source; and with the proper design, TENG can be fabricated into a cheap, lightweight, durable, efficient, and safe source of electricity. To research further into TENG, one must consider the applications for TENG at a micro-scale and then the possible integrations that may be necessary to introduce TENG for macro-scale power sources.

a. *Micro-scale Power Source*

TENG has only been truly studied and considered as an alternate power source within the last decade. For us to understand its potential, we have to first consider its application in small electronics. At a micro-scale, TENG have a good fit in providing electricity for small sensors and LEDs usually found in doorbells, garage doors,

cellphones, toys, buoys, weather monitors, and many more. Innovation has revealed great use for TENG at a micro-scale, as shown in Figure 7.

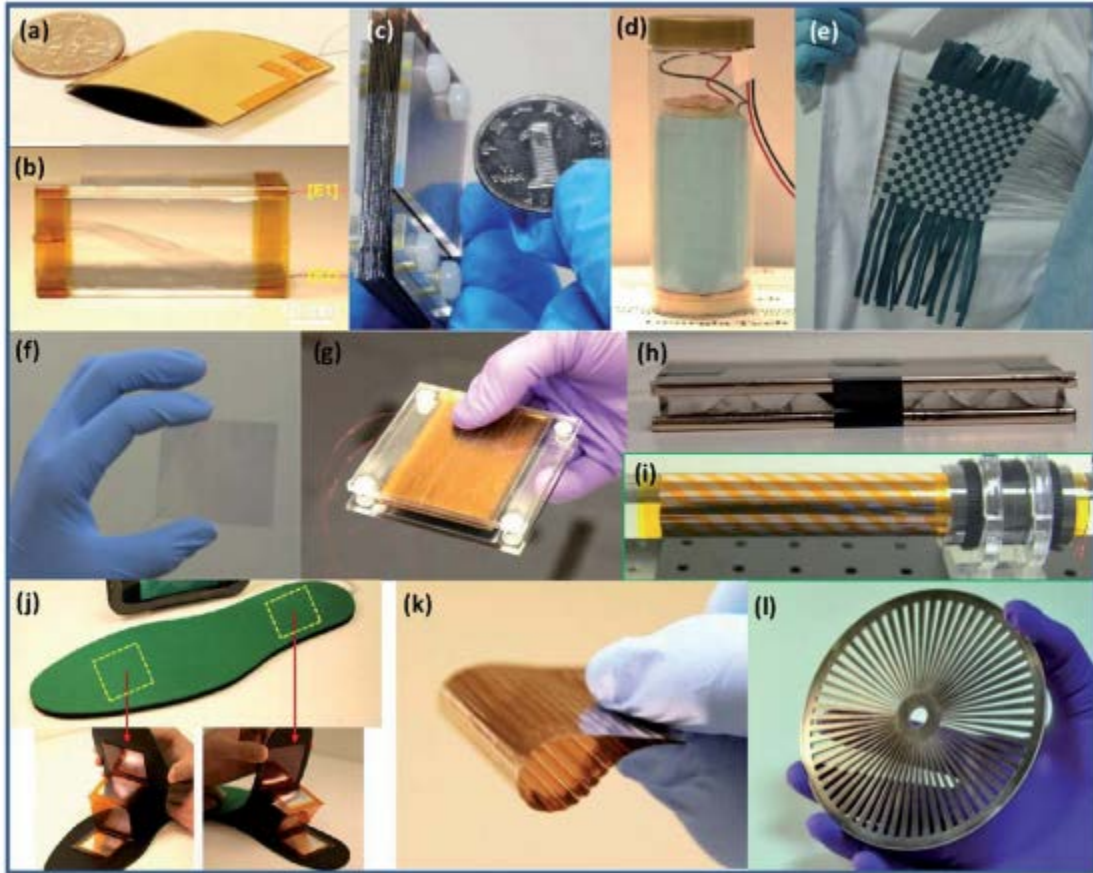


Figure 7. Micro-scale TENG applications. Source: [3].

The figure above shows “some triboelectric nanogenerators fabricated for harvesting: (a) finger tapping energy; (b) air-flow/wind energy; (c) relative in-plane sliding energy; (d) enclosed cage for harvesting oscillating/disturbing energy in water or mechanical vibration; (e) fabric for harvesting body motion energy; (f) transparent TENG for harvesting energy in touchpad; (g) foot/hand pressing energy; (h) water impact energy; (i) cylindrical rotation energy; (j) shoe insole for walking energy; (k) flexible grating structure for harvesting sliding energy; and (l) disc shape rotation energy” [3].

Due to the size of these TENGs, these electricity generators are highly durable and can easily be incorporated into our everyday lives. However, the size will certainly limit the amount of energy produced and the efficiency will highly depend on the precision of the design. The dimensional layout of the materials being used will have the greatest effect on the efficiency of a micro-scale TENG; but other considerations would be the production, maintenance, and life cycle of the device. Overall, current research has shown high power output from micro-scale TENGs that are feasible to power small electronics. This sets the foundation for us to start considering the use of TENG at a macro-scale.

b. Macro-scale Power Source

When using TENG to generate electricity at a larger scale, we are not necessarily talking about a change in design of the micro-scale TENGs mentioned earlier. However, the greatest difference would be that these TENGs will be using naturally high-potential energy generators such as oceans, rivers, and winds. In this case, multiple TENGs could be interconnected to generate high power. In addition, having a larger motion generator allows room to increase the size of the TENG being used. This is an advantage in the point that larger parts would be easier to produce and replace compared to micro-parts. The potential of macro-scale TENGs would increase from small electronics to possibly harvesting enough energy for household appliances.

3. Design Challenges

For this research, a TENG will be designed capable of harvesting energy via self-generation, wind, and/or water motion. With such a design, the first challenge would be its adaptability. A multipurpose mechanism would need to be implemented to ensure the TENG is capable of interchanging between different energy sources. But for the sake of discussion, we will concentrate on designing the actual TENG first. Depending on the environmental setting, wind or water motion may not always be available; therefore, the majority of discussions on the design will be under the impression that the TENG is being powered by self-generation. Nonetheless, the input source of the TENG will have

an “open” design to allow possibility of alterations to accommodate for change in energy input source ensuring its adaptability.

Another challenge will be stability. The consistency of the data accumulated may vary even if the same test was conducted twice; therefore, multiple data sets will need to be collected to verify the performance and stability of the design.

And finally, the last challenge will be the efficiency of the model. The efficiency will highly depend on the precision of the construction. Since almost all the materials that will be used for the design will be readily available, efficiency may prove to be a challenge depending on the quality of the materials being used.

There will be more challenges encountered as this research progresses, but the TENG being built will first have to produce positive results prior to concentration on its adaptability, stability, efficiency, and other challenges to follow.

II. DESIGN DRAFTS

A. PREVIOUS NPS TENG ROTATIONAL DESIGN

A previous NPS rotational model had the primary mediums for the electrode and the dielectric constructed using Polylactic Acid (PLA) via 3D printing [6]. The Teflon and copper taping were implemented as shown in Figure 8 and Figure 9.

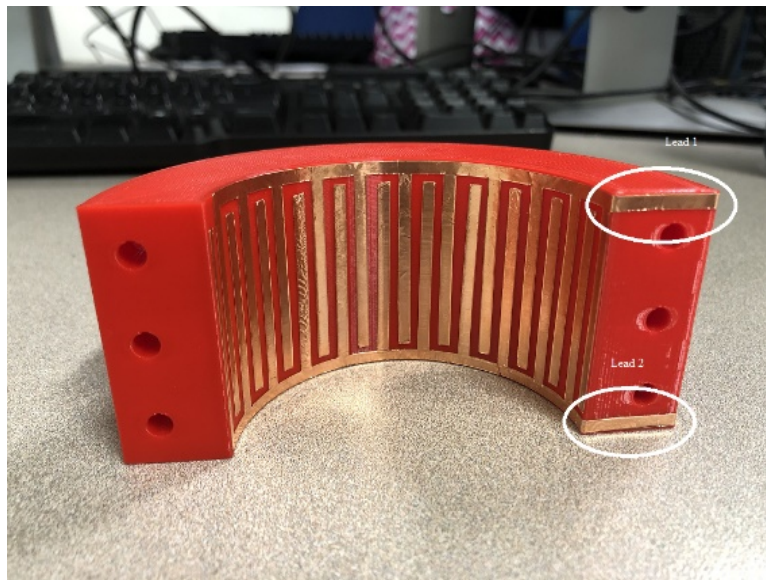


Figure 8. NPS TENG Rotational Model (Internal View). Source: [6].



Figure 9. NPS TENG Rotational Model (External View). Source: [6].

The inboard cylinder which had the Teflon taping was rotated using a DC motor. And as the inboard cylinder was being rotated, electron charges were harvested from the copper taping by wiring via connection leads to a load.

B. DEVELOPMENT

Previous TENG designs at the Naval Postgraduate School (NPS) in Monterey, California, were based off the freestanding triboelectric-layer mode. The initial designs were made to harvest energy through linear motion and a later design was made to harvest energy through rotational motion [6], [7], [8]. The previous designs also relied on 2D and 3D printing to generate most of the materials that were being used. And although both designs proved the feasibility of the TENG concept, further research is encouraged to increase the amount of energy generated to a reasonable value acceptable for application.

Since rotational motion has continuity, the design for this research will emulate the previous NPS rotational design. However, instead of using 2D and 3D printed material, most of the materials will be purchased based on its availability and fabricated without the use of printed material.

Overall, a DC motor will be used to test the TENG models. After testing, the TENG will be connected to a stationary bicycle via chain and gears to demonstrate self-generation of electricity.

C. MATERIALS

The primary materials used for this design are listed in Table 1. The attaching hardware (tape, nuts, bolts, clamps, safety wire, glue, etc.) are not mentioned in the list since these materials may vary based on personal preference. However, attaching hardware will be mentioned in the next section as the construction of the TENG is explained.

Table 1. List of Required Materials

Material	Notes
Copper Foil Tape	Electrode
Polyethylene Plastic	Electrode Mounting Surface
Polytetrafluoroethylene (Teflon) Tape	Dielectric
PVC Pipe	Dielectric Mounting Surface
Cylindrical Hardwood	Shafting
18 Gauge Wiring	TENG connection to a load
Rectifier	Convert AC to DC
Transformers	Increase current
Various LEDs	Load
Various Capacitors	Load

D. MODEL DESIGN AND CONSTRUCTION

The dielectric and electrodes used in this TENG design will be the same as the previous NPS rotational design. Copper foil tape will be the electrode medium and Teflon tape will be the dielectric medium. The copper tape was mounted on a very thin Polyethylene Plastic and the Teflon tape was mounted on a PVC pipe. A cylindrical hardwood was then be inserted inside the PVC pipe and secured to serve as the shaft attachment between the TENG and the energy source. Additionally, 18 Gauge wires were used to connect the copper tape from the TENG to a circuit load.

Since freestanding triboelectric-layer mode generates an alternating voltage/current, a rectifier was used to ensure that the output from the TENG has single polarity prior to handling the load(s). The LEDs were used to display that there is electricity generated from the design; and the capacitors were used to show that charges generated during rotational motion can be stored. And finally, a transformer was added to evaluate the change in current and how that may affect lighting from LEDs and/or storage from the capacitors.

The idea behind this design in its simplest form is as follows:

1. The energy source moves the Teflon.
2. The Teflon agitates the copper.
3. Charge build up in the copper is harvested using a capacitor or displayed using LEDs.

The energy source (either from wind, waves, self-generation, etc.) will translate rotational motion through the shaft which will in turn rotate the PVC pipe since it is secured to the shaft. For data collection purposes, an electric DC motor was used to rotate the shaft as shown in Figure 10:



Figure 10. Dayton PMDC Motor with Controller (Model: 2Z846)

A piece of hardwood is secured unto a mounting hub using 1.27cm ($\frac{1}{2}$ ") set screws. The mounting hub is then secured unto the motor shaft with a slot key. A 3.81cm ($1\frac{1}{2}$ ") flexible coupling is also placed at the end of the hardwood to make it easier to swap out multiple TENG models during testing (see Figure 11).



Figure 11. Mounting Hub and Flexible Coupling

The PVC pipe has Teflon taped on its external surface area and parallel to the rotational axis. And a hardwood shaft is secured inside the PVC pipe for attachment to the energy source as shown in Figure 12.

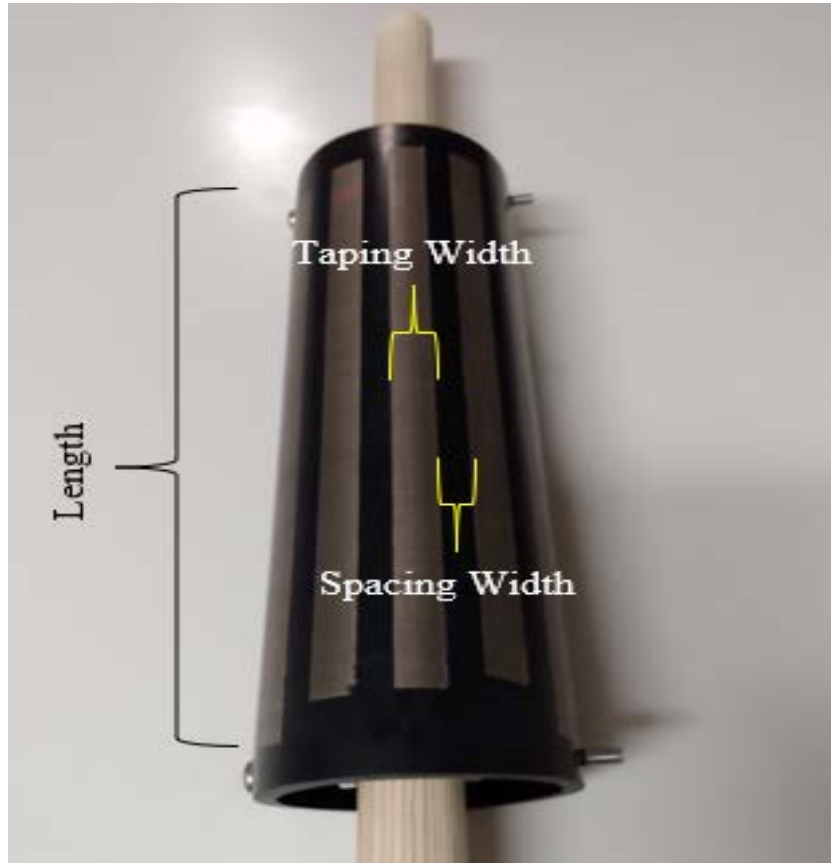


Figure 12. PVC Pipe with Teflon Tape Outboard and Hardwood Shaft Inboard

The outer diameter of the PVC pipe is 8.89cm (3.5”) and the diameter of the hardwood is 5.08cm (2”). The model lengths that were tested for this research is 15.24cm (6”) and 25.4cm (10”). In terms of securing the shaft to the PVC pipe, holes were drilled through the hardwood and the edges of the pipe with 0.635cm (1/4”) nuts and bolts being used to keep the shaft in the center of the pipe.

The copper taping was wrapped around a flexible polyethylene plastic as shown in Figure 13.

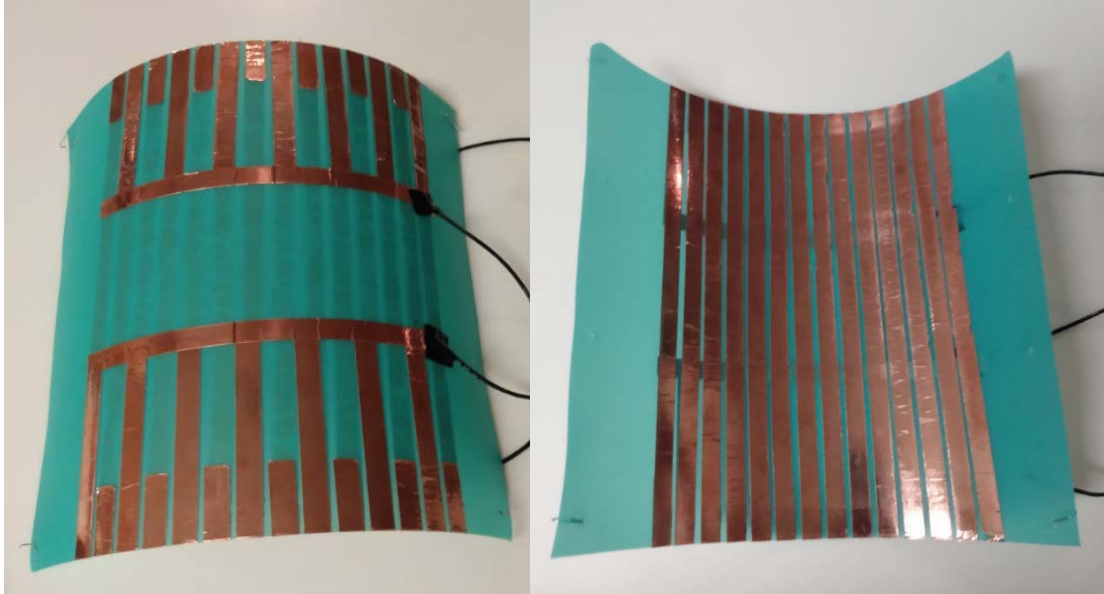


Figure 13. (From left to right) Copper Outboard and Copper Inboard

On the outboard surface of the plastic, wires were secured using electric tape to the copper leads. The copper leads are the taping that connects every other strip of copper taping together. And finally, the copper is overlaid onto the Teflon using clamps as shown in Figure 14.



Figure 14. TENG Model (1.27cm Copper Taping)

Figure 14 shows a template of the TENG model. Since the plastic sheet medium for the copper is 0.056cm (0.022”) thick, a hair dryer was used to help form the shape of the plastic to fit easily over the PVC pipe. The configuration of the copper and the Teflon orientation were set up to mirror the freestanding triboelectric-layer mode. Therefore, rotational motion will allow the Teflon to pass over two separate sets of copper taping causing the flow of charges. The charge flow within the two sets of copper taping were connected to a rectifier using 18-gauge wires which was later passed on to a load.

E. DESIGN MODELS

The models that were tested are shown in Table 2.

Table 2. Model Dimensions

Model	Copper Width (cm)	Copper Spacing (cm)	Teflon Width (cm)	Teflon Spacing (cm)	Length (cm)
1A	1.27	0.127	1.27	1.52	15.24
1B	0.635	0.0635	0.635	0.76	15.24
2A	1.27	0.127	1.27	1.524	25.40
2B	0.635	0.0635	0.635	0.76	25.40
3	0.635	0.0635	0.635	0.76	12.7

The width of the copper and Teflon were chosen based on available manufactured designs. The copper spacing and Teflon spacing were determined to ensure full overlap between the Teflon and either one set of copper taping (odd numbers) or the other set of copper taping (even numbers) as shown in Figure 15.

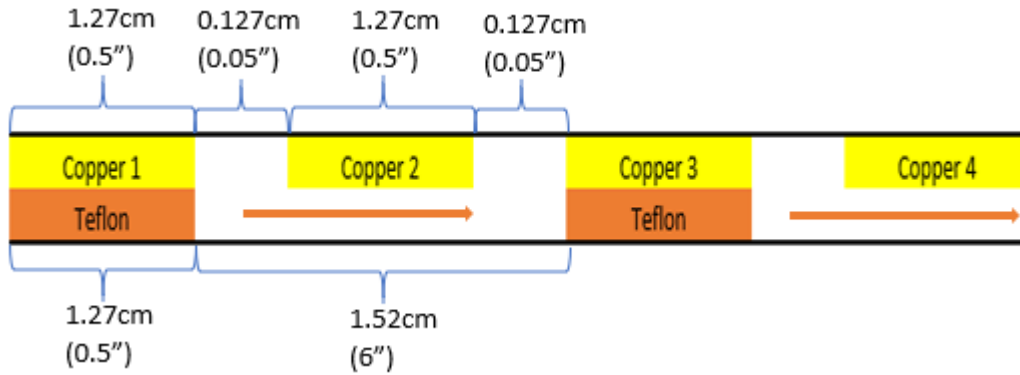


Figure 15. Spacing Example of Model 1A Copper and Teflon

To clarify, Model 1A had 1.27cm (0.5”) copper taping laid out at 0.127cm (0.05”) apart. Therefore, since the Teflon had to completely overlap either the even or odd number of copper linings, the spacing for the Teflon taping had to be 1.52cm (0.6”) as shown in Figure 15. All other models were spaced accordingly to ensure complete overlap depending on the width and spacing of the copper tape being used.

The first four models were tested to analyze how the change in length and width of the copper and Teflon taping effects its performance. The last model (Model 3) was used to analyze the effects of parallel or series connection between two models with the same dimensions. And Models 1A and 1B were also used to analyze the effects of parallel or series connections between two different models.

Models 1A and 1B are both 15.24cm (6”) in length but have different widths, as shown in Figure 16 and Figure 17.

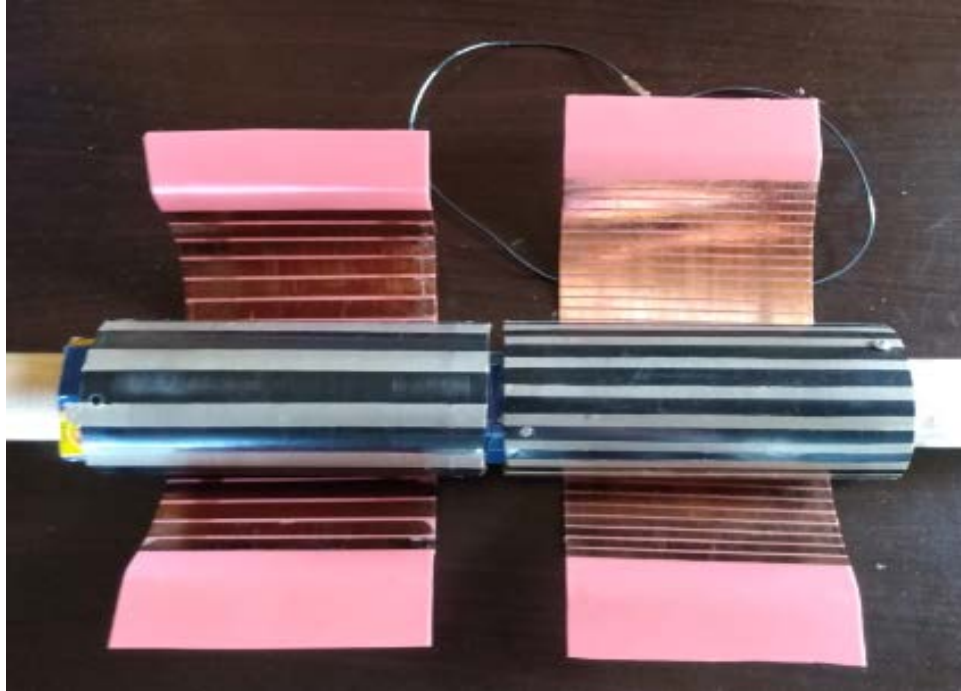


Figure 16. (Internal) Model 1A (left) and Model 1B (right)

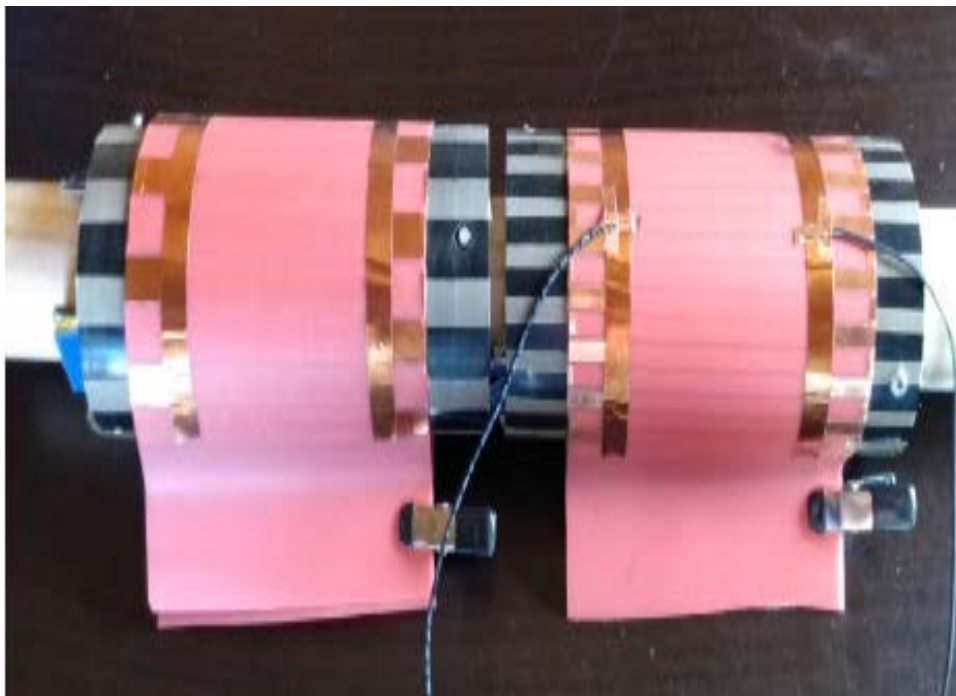


Figure 17. (External) Model 1A (left) and Model 1B (right)

An external view of Model 2A was previously shown in Figure 14. An internal view of Models 2A is shown in Figure 18.

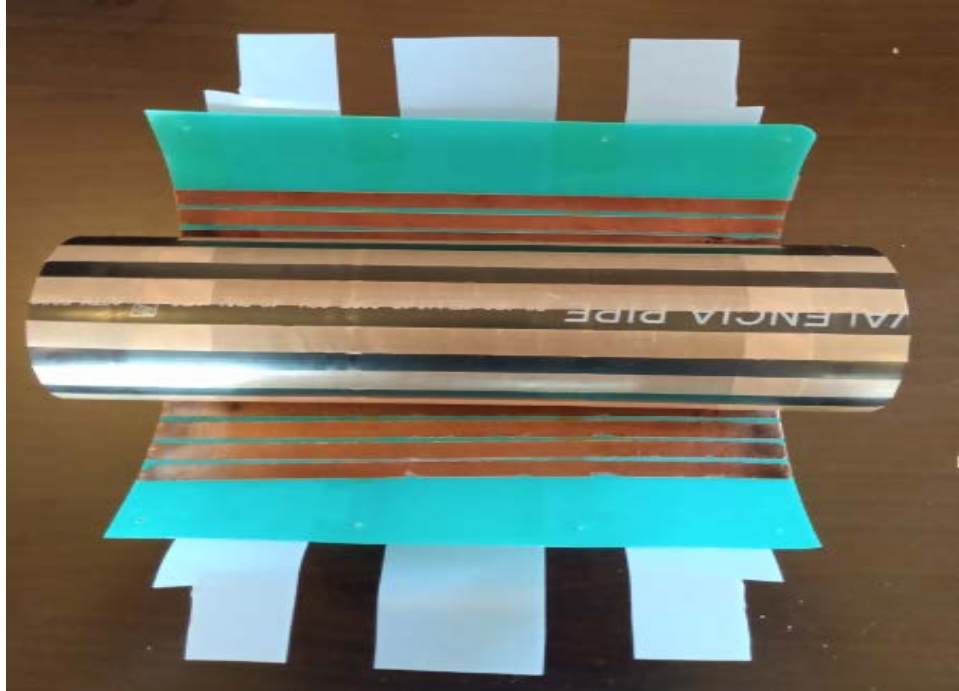


Figure 18. Model 2A (Internal)

Model 2B is similar in length as Model 2A, but with 0.635cm taping of copper and Teflon as shown in Figure 19 and Figure 20.



Figure 19. Model 2B (Internal)

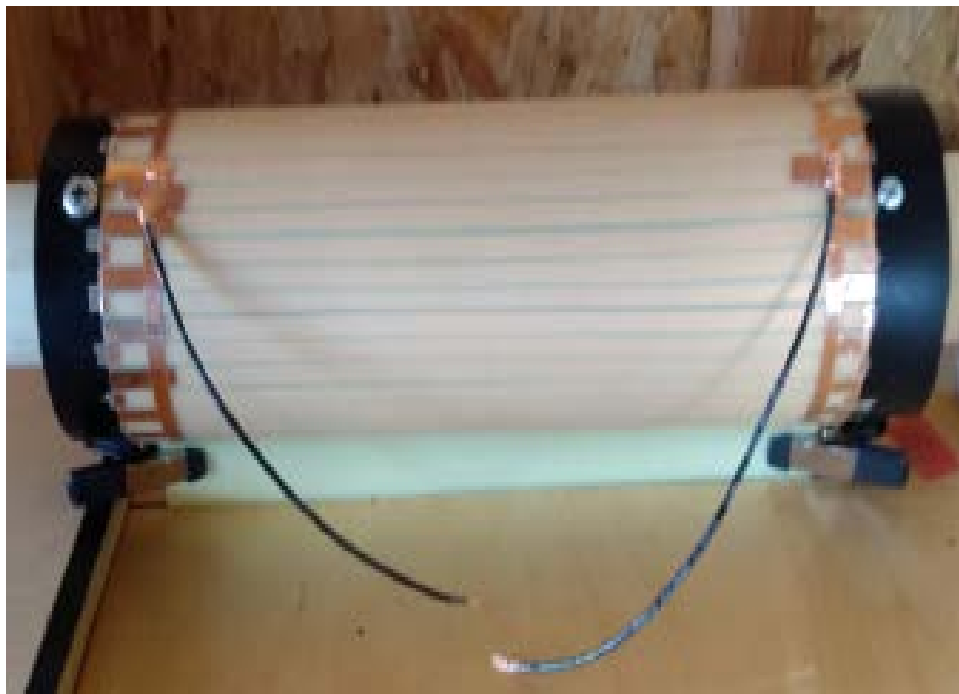


Figure 20. Model 2B (External)

Model 3 is as shown in Figure 21 and Figure 22.

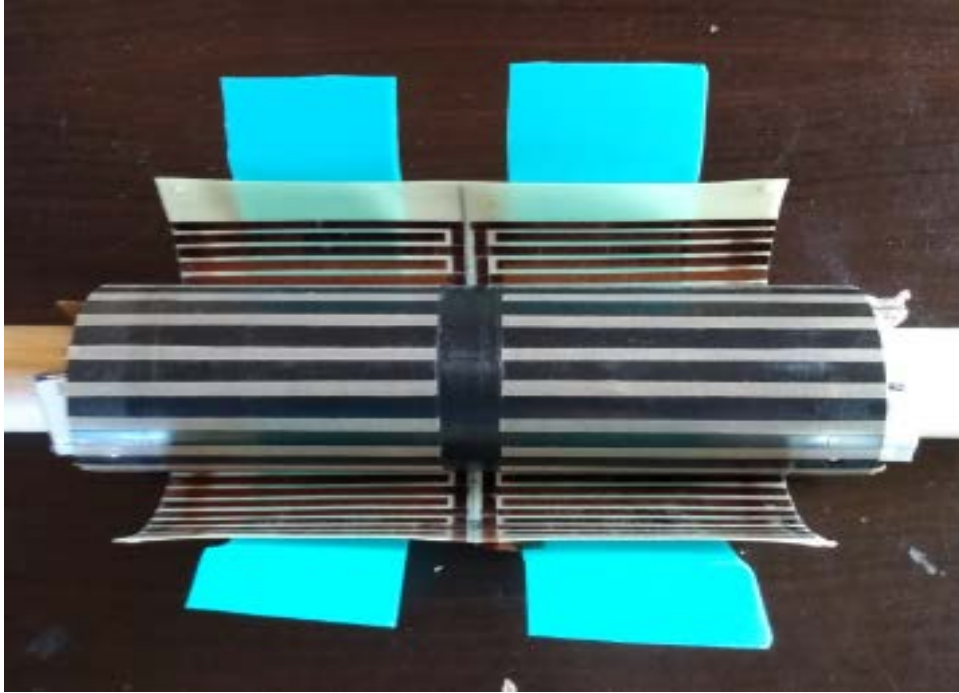


Figure 21. Model 3 (Internal)



Figure 22. Model 3 (External)

THIS PAGE INTENTIONALLY LEFT BLANK

III. EXPERIMENTATION PROCESS

A. EXPERIMENTAL EQUIPMENT

The primary data extracted from this experiment includes voltage, current, frequency, and shaft rotational speed. The equipment(s) used to collect the data are as listed in Table 3.

Table 3. List of Required Equipment

Equipment	Notes
Tachometer	Gain Express (Model #: DT-2236C)
Oscilloscope	Keysight (Model #: DSO1052B)
Ammeter	Keithley (Model #: 6514)
Voltmeter	Commercial Electronics (Model #: 8301S)

The tachometer ensures proper shaft speed is recorded for every test set. The oscilloscope was used to measure the voltage and frequency generated from the TENG. The Keithley ammeter measured the current flow through a load when the TENG is in operation. And the voltmeter was the mobile unit used to validate continuity within the circuit while a test is being conducted.

B. EXPERIMENTAL PROCEDURES

The data collected from this experiment were used to determine how much electricity can be generated based on configuration, size, and speed of the TENG. The first step in the experimental process was to validate that the constructed models can generate electricity. In order to do this, the shaft was connected to the DC motor using a flexible coupling as shown in Figure 23.

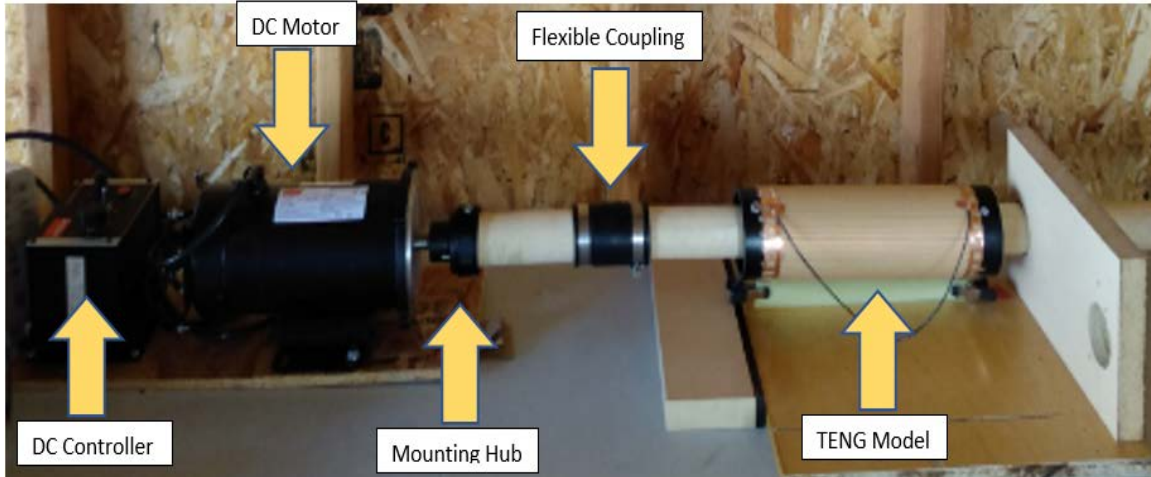


Figure 23. Motor Connected to TENG Model with Mounting Hub and Flexible Coupling

The end of the shaft was placed through a woodblock. The hole in the woodblock is drilled and sanded to allow the shaft to rotate freely when the motor is turned on. The tachometer was held against the shaft to monitor its rotational speed while the oscilloscope is connected to the wire leads to measure the initial voltages generated from the TENG.

1. Initial Voltage and Frequency Data Collection

Once the model shows a voltage reading validating electricity generation, voltage and frequency readings were taken from each model at different speeds. The steps to be taken are as follows:

1. Ensure wire leads from TENG are connected to oscilloscope.
2. Turn DC motor ON.
3. Using the tachometer, ensure the DC motor is rotating the shaft at 60 RPM.
4. Save the voltage and frequency readings on the oscilloscope.
5. Transfer oscilloscope data to a computer to be analyzed.

6. Adjust the DC controller to add 30 RPM to the current speed of DC motor.
7. Repeat steps 4), 5), and 6) until the oscilloscope reaches maximum voltage reading capability (in this case 400 Volts).
8. Turn DC motor OFF.

For this experiment, models 1A, 1B, 2A, and 2B were tested.

2. Electricity Storage and Display Procedures

Depending on the performance of the four models, the model with the best performance was proceeded for further analysis. In this case, capacitors and LEDs were loaded on the circuit to evaluate the performance of the chosen model. The steps for this experiment are as follows:

1. Turn DC motor ON.
2. Using the tachometer, ensure the DC motor is set to rotate the shaft at 50 RPM.
3. Turn DC motor OFF.
4. Safety Note: DO NOT make any connections while DC motor is ON. Live wires may result in electric shock, burns, and/or serious injuries.
5. Using a circuit board, connect wire leads from TENG to rectifier input.
6. Connect capacitor to rectifier output.
7. Connect oscilloscope in parallel with capacitor to take readings.
8. Turn DC motor ON (should already be set at 50 RPM at this point).
9. Use oscilloscope to measure the voltage accumulated by the capacitor.
10. Make note of the amount of time it took to fully charge the capacitor.
11. Save data on oscilloscope and transfer to computer to be analyzed.

12. Adjust the DC controller to add 25 RPM to the current speed of DC motor.
13. Repeat steps 8) – 11) until capacitor charging data is collected for when the model is operating at 50, 75, 100, and 125 RPM.

After collecting data showing the TENG's capability to store electricity, the next experiment was using LEDs to display the electricity generated directly from the TENG. The steps for this portion of the experiment are as follows:

1. Using a circuit board, connect wire leads from TENG to rectifier input.
2. Connect proper number of LEDs in series to rectifier output.
3. Set DC motor speed to 0 RPM.
4. Turn DC motor ON.
5. Adjust DC motor speed until LEDs start to light up.
6. Test multiple numbers of LEDs at different speeds.
7. Turn DC motor OFF.

3. Series/Parallel Testing Procedures

Two separate tests were conducted to show how multiple TENG models react to being connected in series or parallel with each other. First, Model 3 was tested simulating two models operating at the same phase. Then Model 1A and 1B were tested simulating two models operating at different phases.

The configurations for each test set are as shown in Figure 24–Figure 29.

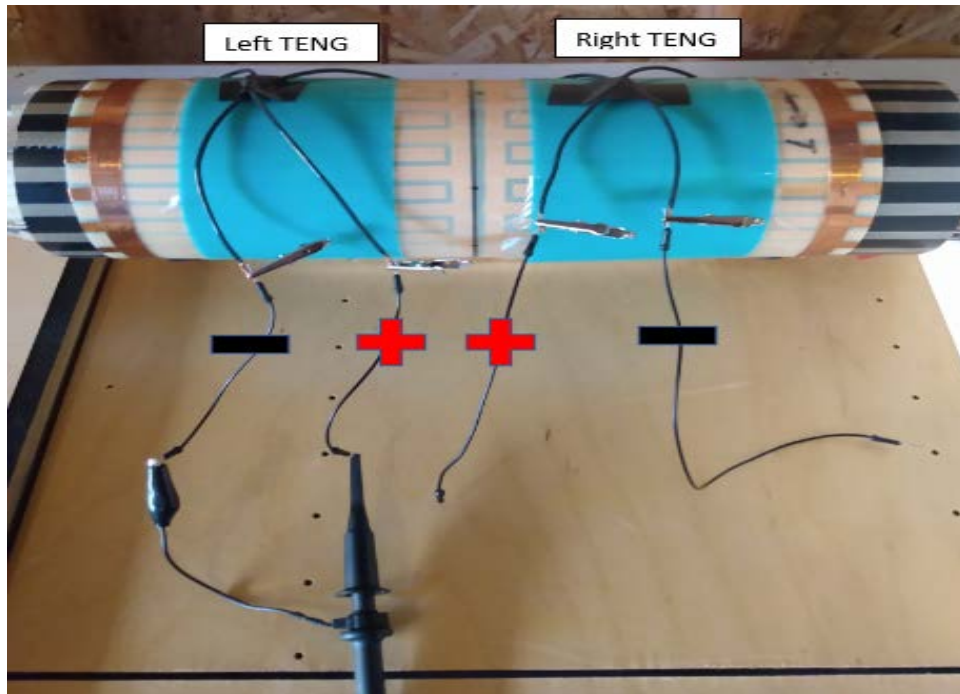


Figure 24. Left TENG Initial Data Collection

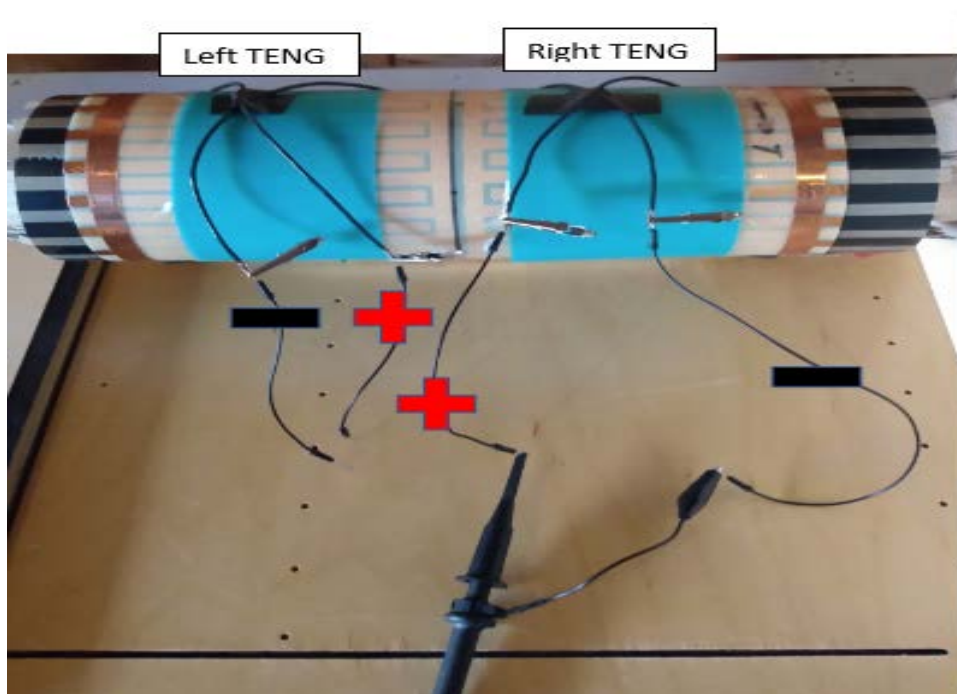


Figure 25. Right TENG Initial Data Collection

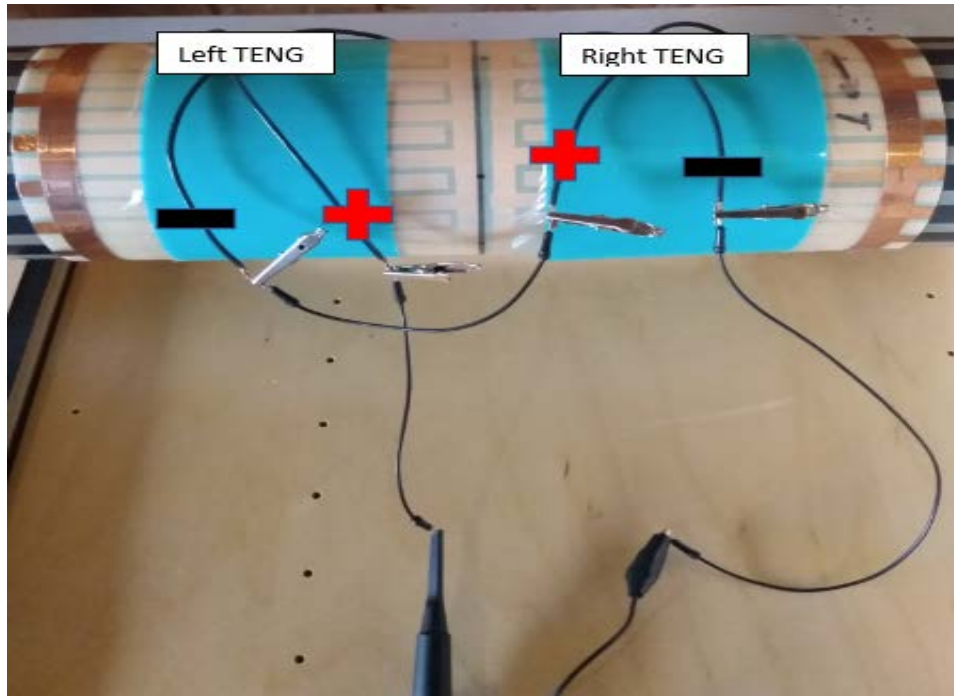


Figure 26. Model 3 Series Connection

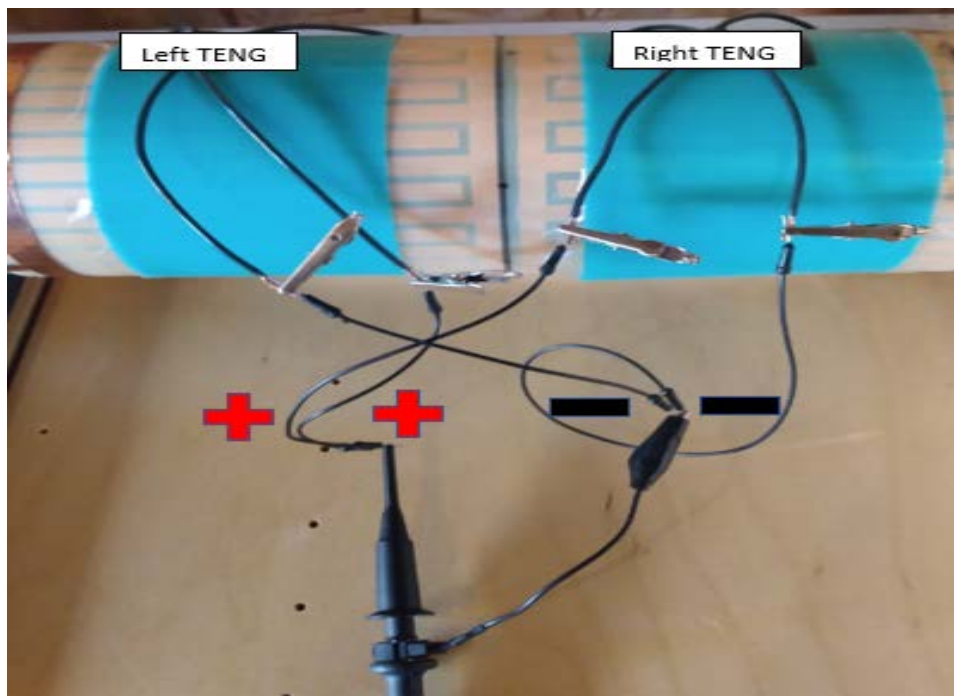


Figure 27. Model 3 Parallel Connection

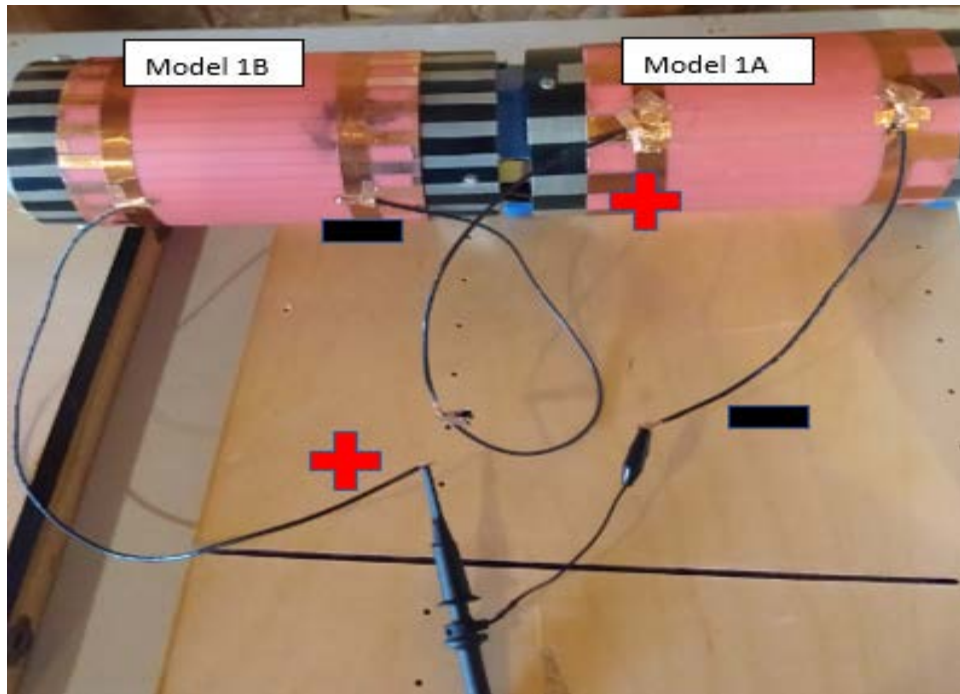


Figure 28. Models 1A and 1B Series Connection

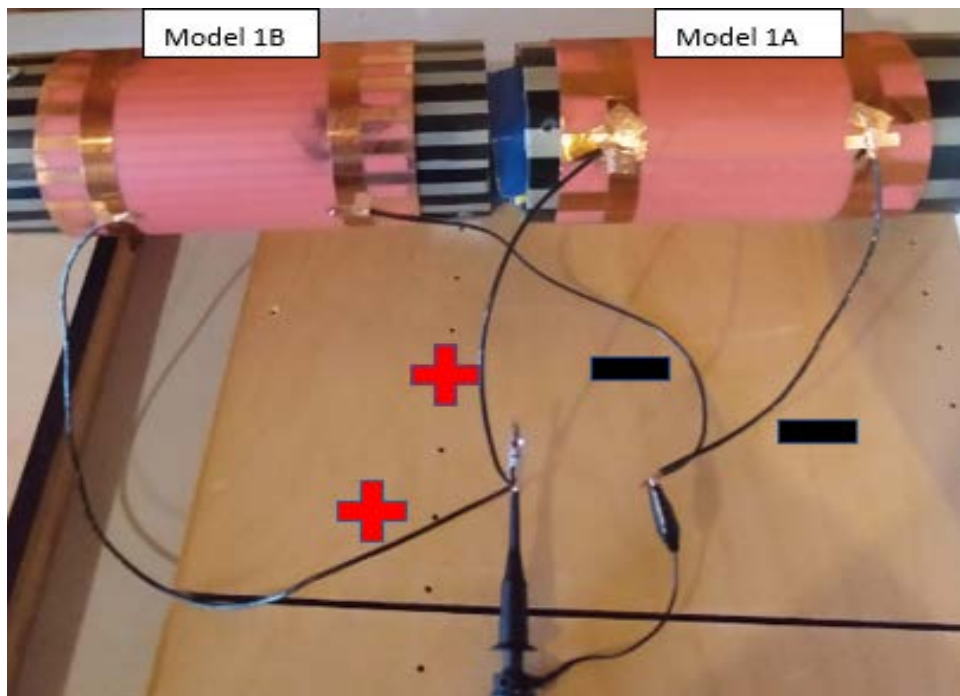


Figure 29. Models 1A and 1B Parallel Connection

THIS PAGE INTENTIONALLY LEFT BLANK

IV. RESULTS AND DISCUSSION

The first set of tests collected data on Models 1A and 1B. These models have the same length; but the copper and Teflon widths are different. Model 1A uses 1.27cm width copper and Teflon; and Model 1B uses 0.635cm width copper and Teflon. The objective of the first set of data was to determine the electricity generation capability of the TENG depending on the width of the materials being used.

Model 2A and 2B used the same 1.27cm and 0.635cm taping; however, now the length of the Model 2A and 2B is 25.4cm rather than 15.24cm. Data collection from these models were used to show how the change in length affects the electricity generation capabilities of the TENG.

Model 3 has the same width and spacing as Model 1B; however, this model is a special design constructed to analyze how a TENG would respond to either a series or parallel configuration.

A. INDIVIDUAL TENG MODEL VOLTAGE TESTING

1. Initial Voltage Data

The voltage data for Model 1A are tabulated in Table 4.

Table 4. Model 1A Voltage Data

RPM	Shaft Freq. (Hz)	Source Freq. (Hz)	Vmax (+)	Vmin (-)	Vrms
60.6	1.01	7	54	58	26.8
90.7	1.51	11.45	98	102	48
121	2.02	18.67	128	132	68.6
150.2	2.50	22.44	146	150	82.7
180.4	3.01	26.9	170	184	102
210.1	3.50	31.41	212	220	130
239.8	4.00	35.99	248	256	157
269.9	4.50	40.27	276	284	175
300.4	5.01	45.02	312	308	193
397	6.62	59.42	388	396	257

Note that the shaft frequency is a measurement of how fast the shaft is rotating and the source frequency is the actual frequency of the alternating voltage measured by the oscilloscope. The shaft frequency and source frequency are proportional to each other but serve as references for how fast the model is spinning (shaft frequency) and how fast the voltage is alternating (source frequency). The voltage for Model 1A is graphed against the shaft speed as shown in Figure 30.

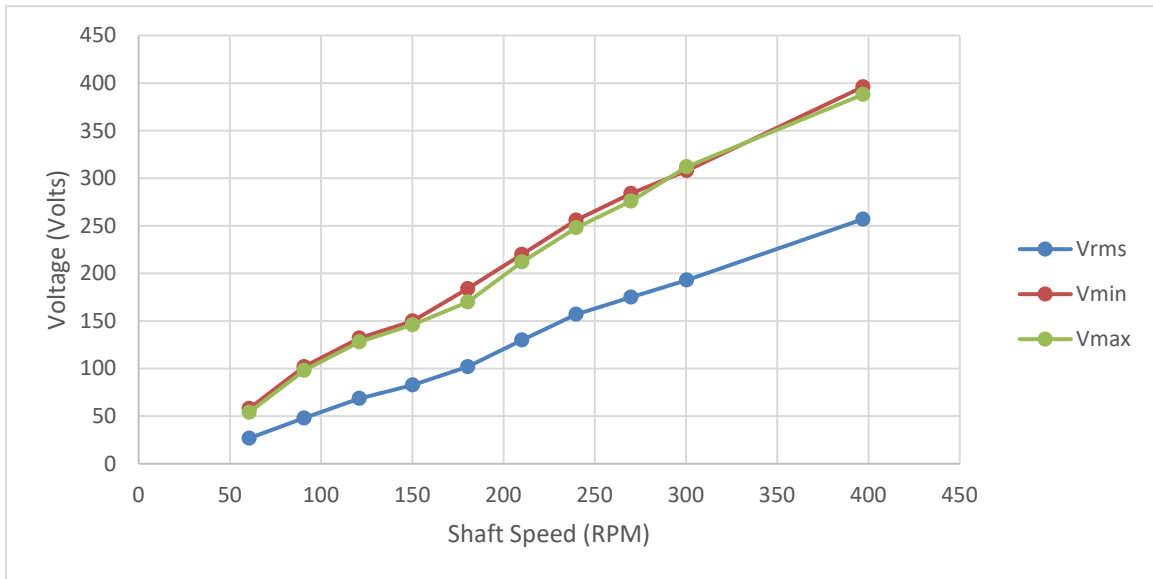


Figure 30. TENG Model 1A Voltage Data

The voltage data for Model 1B are tabulated in Table 5.

Table 5. Model 1B Voltage Data

RPM	Shaft Freq. (Hz)	Source Freq. (Hz)	Vmax (+)	Vmin (-)	Vrms
60.8	1.01	19.25	82	90	54.6
90	1.50	27.93	128	134	96.7
120.5	2.01	38.15	178	182	150
149.5	2.49	47.44	220	228	185
180.8	3.01	56.78	252	256	214
210.4	3.51	67.03	276	280	234
240.9	4.02	76.45	300	304	262
271.1	4.52	85.5	332	332	287
300.6	5.01	95.03	356	352	303
398	6.63	131.34	396	392	339

The voltage for Model 1B is graphed against the shaft speed as shown in Figure 31.

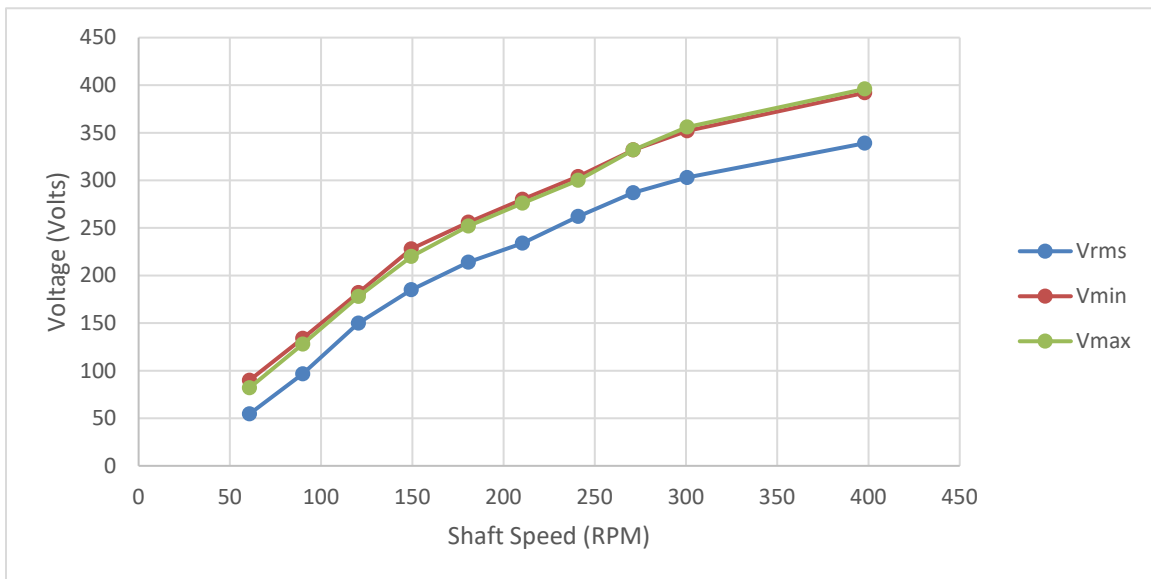


Figure 31. TENG Model 1B Voltage Data

The voltage data for Model 2A are tabulated in Table 6.

Table 6. Model 2A Voltage Data

RPM	Shaft Freq. (Hz)	Source Freq. (Hz)	Vmax (+)	Vmin (-)	Vrms
61.5	1.03	12.53	22.4	24.8	12.8
91.6	1.53	18.3	35.2	37.6	18.5
121.6	2.03	24.83	46	50	25.8
148.4	2.47	30.36	56	64	31.4
180.7	3.01	37.47	104	148	60.4

The voltage for Model 2A is graphed against the shaft speed as shown in Figure 32.

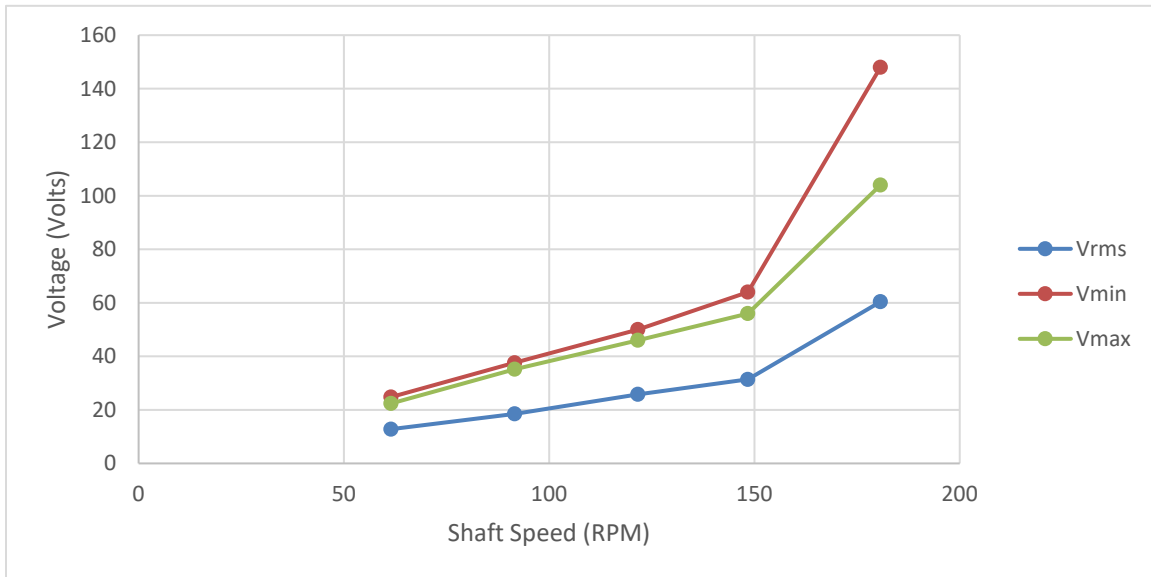


Figure 32. TENG Model 2A Voltage Data

The voltage data for Model 2B are tabulated in Table 7.

Table 7. Model 2B Voltage Data

RPM	Shaft Freq. (Hz)	Source Freq. (Hz)	Vmax (+)	Vmin (-)	Vrms
60.1	1.00	19.88	32	33.6	18.6
90.6	1.51	29.15	68.8	71.2	40.5
122	2.03	39.14	102	110	58.8
149.3	2.49	47.62	124	130	72.1
182	3.03	58.05	154	158	90.5

The voltage for Model 2B is graphed against the shaft speed as shown in Figure 33.

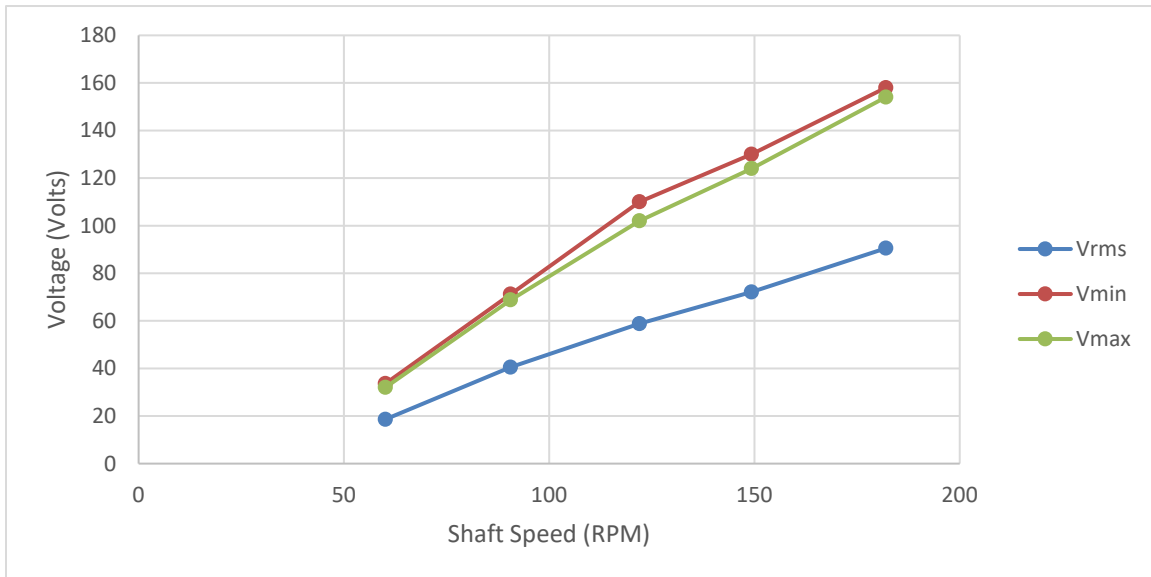


Figure 33. TENG Model 2B Voltage Data

2. Performance Comparison

The plotted graphs comparing Model 1A, 1B, 2A, and 2B are shown in Figure 34 and Figure 35.

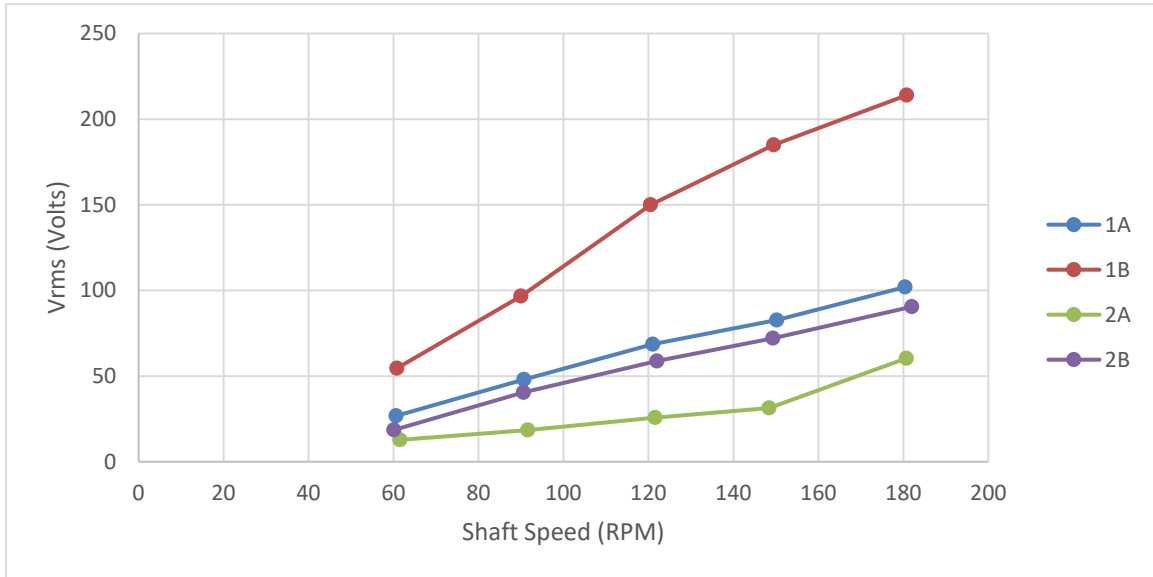


Figure 34. Effective Voltage (V_{rms}) Comparison between Models

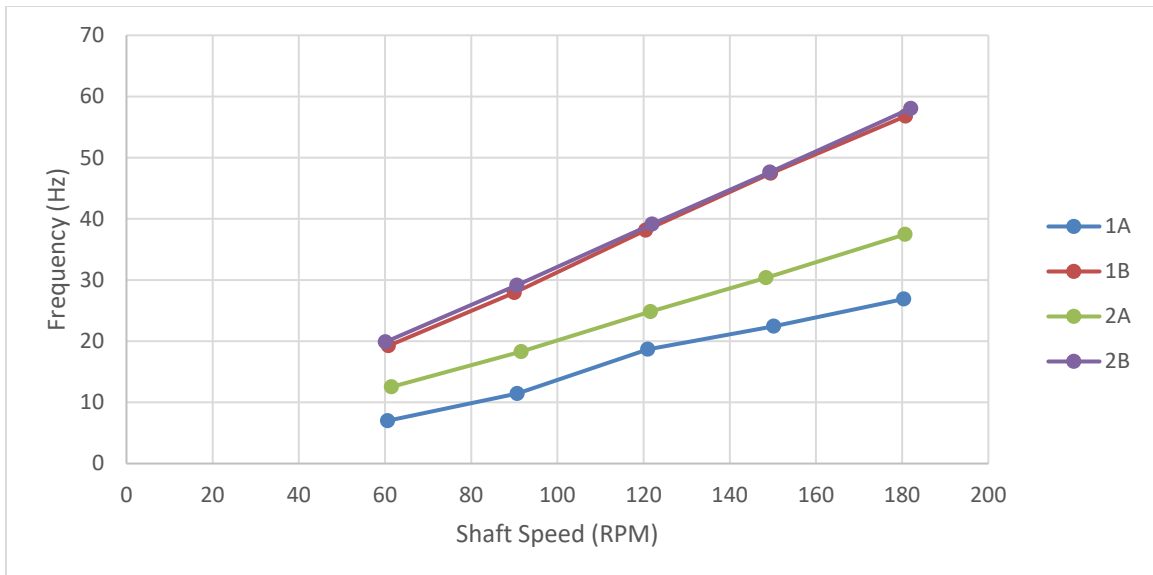


Figure 35. Frequency Comparison between Models

From comparing the performance of the four main models, Model 1B was chosen to be used for further analysis.

B. OPTIMUM PERFORMANCE ANALYSIS

When looking only at the frequency of each model, Models 1B and 2B were almost identical and both were higher than the frequencies for Models 1A and 2A. This was expected since the spacing between tapings for Models 1B and 2B were smaller than the spacing for Models 1A and 2A. However, in terms of voltage, Model 1B was significantly higher than Model 2B. In addition, Ohm's Law states that the current is directly proportional to the voltage and inversely proportional to resistance [9].

Therefore, based on the models that were tested, Model 1B outperformed all other models in terms of voltage. And since the induced resistance within the testing environment was a constant $10\text{ M}\Omega$ for all models, we can assume that the current flow for Model 1B also outperformed all the other models in accordance with Ohm's Law. The resistance rating for the oscilloscope cable that was used is shown in Figure 36.



Figure 36. Oscilloscope Resistance = $10\text{ M}\Omega$

To validate that the resistance provided by the oscilloscope cable was constant, the Keithley ammeter was used to measure the resistance with results as shown in Figure 37.



Figure 37. Validation of Cable Resistance

The results presented in the following section will depict the time it takes for Model 1B to store energy using a capacitor and how can that energy be displayed directly from the source using LEDs.

1. Performance with Capacitor

Using Model 1B, a $10\mu\text{F}$ capacitor was used to measure the amount of energy that could be stored depending on the speed of the shaft and how long it will take to reach that maximum. The general setup of this experiment is shown in Figure 38.

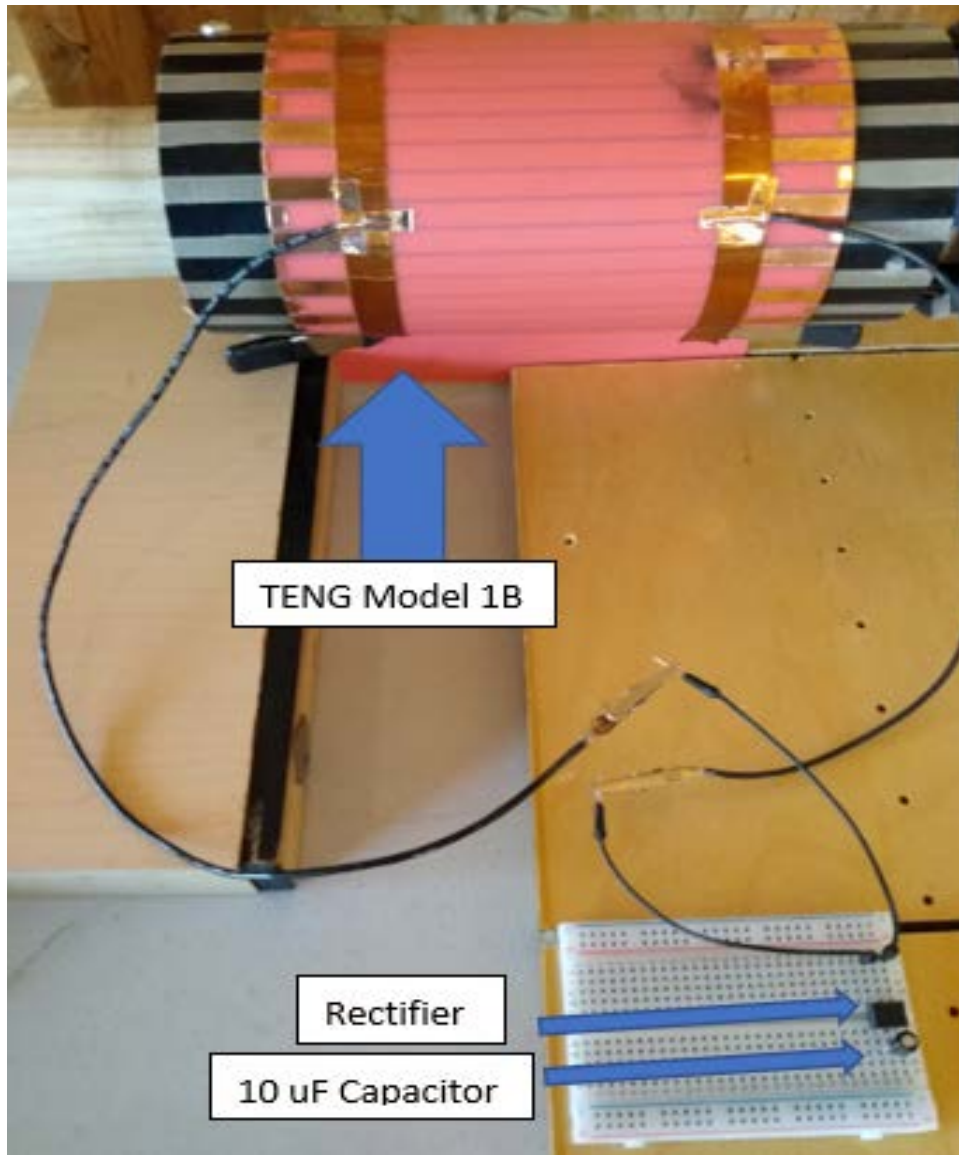


Figure 38. Configuration with Capacitor for electricity storage

The results from 10 μ F capacitor storage are tabulated in Table 8 and graphed as shown in Figure 39.

Table 8. Complete Charging of 10 μ F Capacitor

Shaft Speed (RPM)	Time (s)	Voltage (V)
50	413	40
75	357	54.00
100	227	66
125	171	68.00

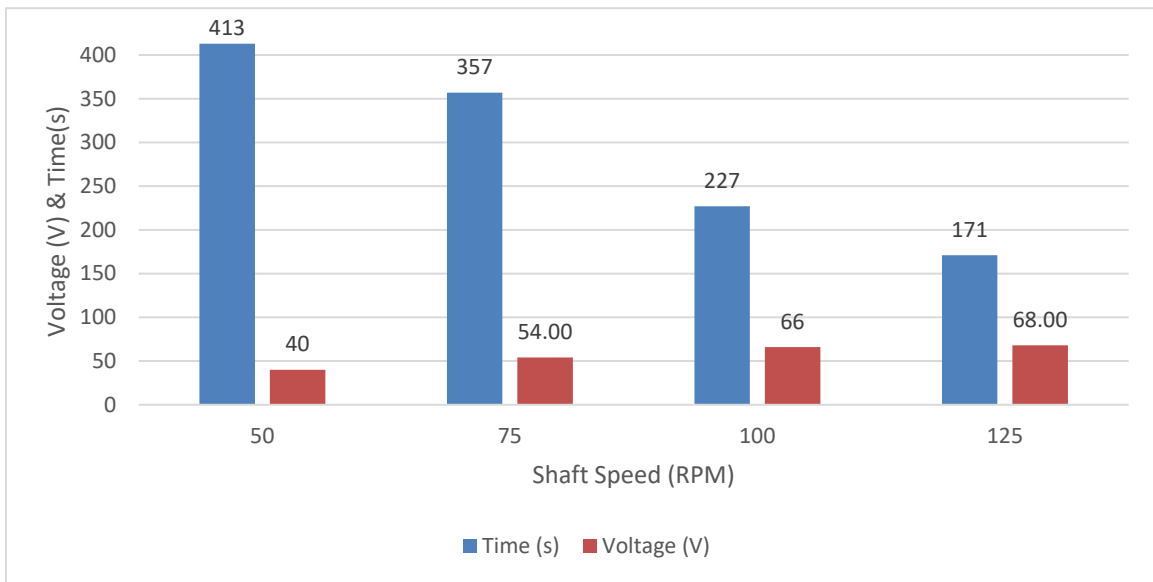


Figure 39. Voltage and Time to charge a 10 μ F Capacitor using TENG Model 1B

2. Performance with LEDs

Because LEDs have a small minimum voltage requirement to illuminate, a number of LEDs will be used to validate that there is electricity being generated by the TENG. And because Model 1B data resulted in very high voltage even at a very low shaft speed, the shaft speed was lowered even further to see how slow the TENG has to rotate to keep generating electricity.

The lowest RPM that could be achieved with the DC motor while maintaining stability was 30 RPM. And at that rate, the Model 1B TENG was generating a maximum voltage of roughly 24 volts. Therefore, the first set of LEDs tested were a combination of three red, three white, and three blue LEDs. This was because the minimum required voltage of those LEDs and the total voltage required for their combination are as shown in Table 9.

Table 9. LEDs Used in 1st Display Test

	Quantity	Vmin	Voltage Required
Red	3	2	6
White	3	3	9
Blue	3	3	9
		TOTAL (V)	24

Connecting the circuit to the TENG displayed the LEDs as shown in Figure 40.



Figure 40. Nine LEDs at 24 Volts from TENG

If the DC motor was set to 60 RPM to produce the initial results in Table 5, the maximum voltage from that test was 90 volts. Therefore, using 30 LEDs rated at 3 volts each, the TENG Model 1B can light all LEDs as shown in Figure 41.

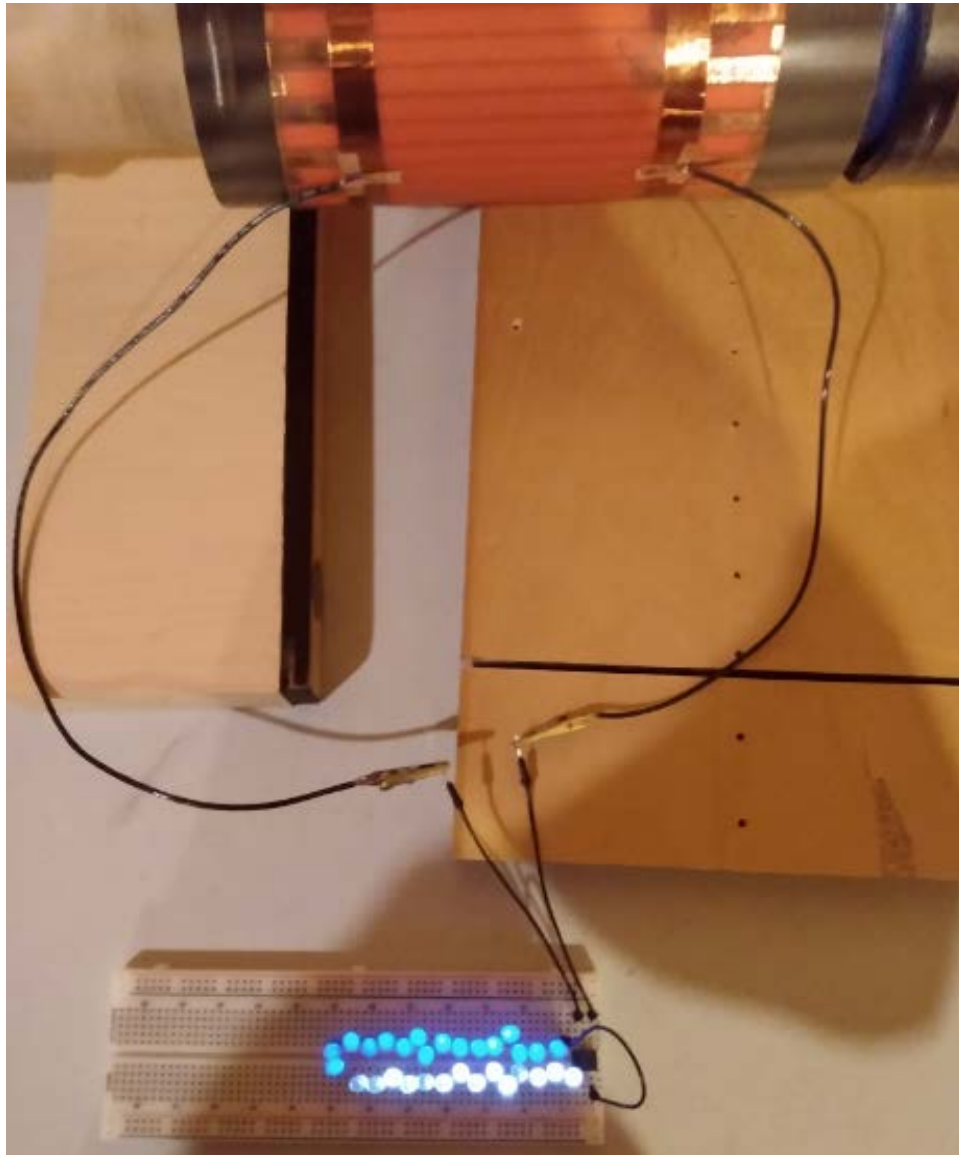


Figure 41. 30 LEDs at 90 Volts from TENG

And since the circuit board being used is limited on the number of slots available. The TENG Model 1B was finally used to see if it were capable of lighting the maximum number of LEDs in series that could fill the circuit board. In this case, 120 LEDs were connected in series as shown in Figure 42.



Figure 42. 120 LEDs

The lighting of the LEDs above was visible when the shaft was rotating at roughly 90 RPMs. And as the RPM increased, the frequency increased therefore allowing the LEDs to illuminate with almost unrecognizable dimming as the voltage alternates.

C. SERIES/PARALLEL TESTING RESULTS

The first test set was conducted for Model 3. And the similar procedures were repeated for Models 1A and 1B in series and parallel.

1. Experimental Results for Model 3

The voltage data for Model 3 with two identical TENG designs are tabulated in Table 10.

Table 10. Model 3 Voltage Data

	RPM	Shaft Freq. (Hz)	Source Freq. (Hz)	Vmax	Vmin	Vrms
RIGHT	90	1.50	28.02	5.00	5.00	4.29
LEFT	90	1.50	28.02	5.00	5.00	5.29
SERIES	90	1.50	28.02	9.00	10.00	9.97
PARALLEL	90	1.50	28.02	6.00	6.00	6.20

Model 3 showed lower voltages compared to previous models at the same speed. This may be due to discrepancies in the spacing of the copper and Teflon taping. The effective voltages for Model 3 are as shown in Figure 43.

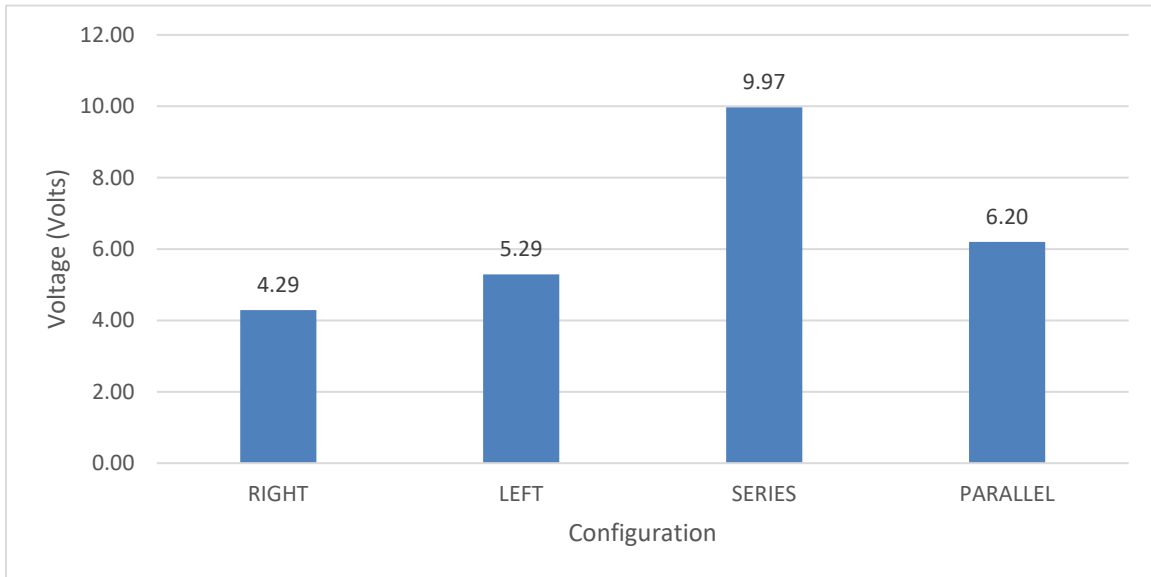


Figure 43. TENG Model 3 Voltage Data

From Figure 43, TENG models in series was more effective compared to models in parallel as expected for ideal combination of voltage sources.

2. Experimental Results for Model 1A and 1B in Parallel/Series

The voltage data for Model 1A and 1B are tabulated in Table 11.

Table 11. Series/Parallel Test (Model 1A and 1B)

	RPM	Shaft Freq. (Hz)	Source Freq. (Hz)	Vmax	Vmin	Vrms
Model 1A	92	1.53	13.77	126.00	140.00	56.80
Model 1B	88	1.47	28.09	106.00	96.00	60.60
SERIES	90	1.50	21.9	118.00	148.00	59.00
PARALLEL	90	1.50	24.126	152.00	228.00	94.60

The effective voltages and source frequencies for the series/parallel test for Models 1A and 1B are as shown in Figure 44.

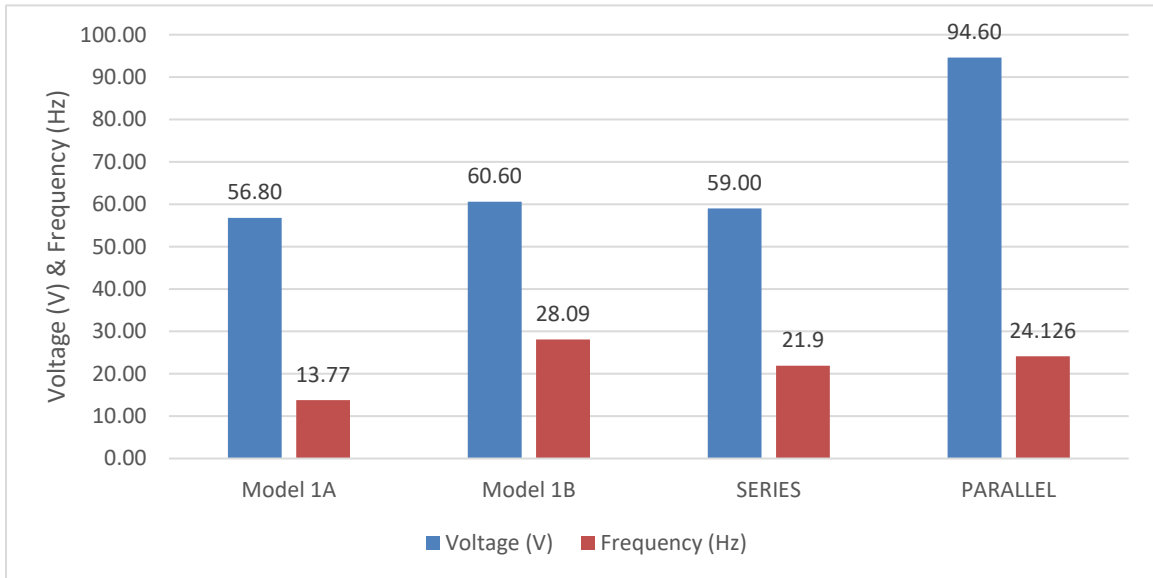


Figure 44. Series/Parallel Test (Model 1A and 1B)

From Figure 44, TENG models in parallel was more effective compared to models in series. Although surprising, this was expected since the previous NPS Rotational TENG models concluded with the same results [6]. Possible cause to this inconsistency may be due to “out-of-phase” combination of voltage sources.

In addition, parallel TENG models resulted in higher current due to proportionality with voltage. However, if more current is needed, transformers can be used. As a supporting example, Model 1B was set to generate 200 VAC and the Keithley Ammeter was used to measure the current being produced from the source and current being produced from using a 115-to-14 VAC transformer. The resulting currents are as shown in Figure 45.



Figure 45. Current without Transformer (left); Current with Transformer (right)

The results showed a significant increase in current from $36.88\mu\text{A}$ (without transformer) to 1.28mA (with transformer). Therefore, although different size models showed greater voltage in parallel, you are not taking advantage of having two voltage sources. The current may be higher for parallel voltage sources; however, that may be irrelevant since that is the primary purpose of introducing transformers into the circuit.

D. SUMMARY OF ANALYSIS RESULTS

Model 1B produced the most optimal results from testing the individual TENGs. And although Model 1B and 2B had relatively the same frequency, Model 2B did not produce as much electricity as Model 1B (or even Model 1A). Overall, Model 1B was the best performer and Model 2A was the poorest performer. A visual comparison of the first set of data at 60 RPM shaft speed is shown in Figure 46 and Figure 47.

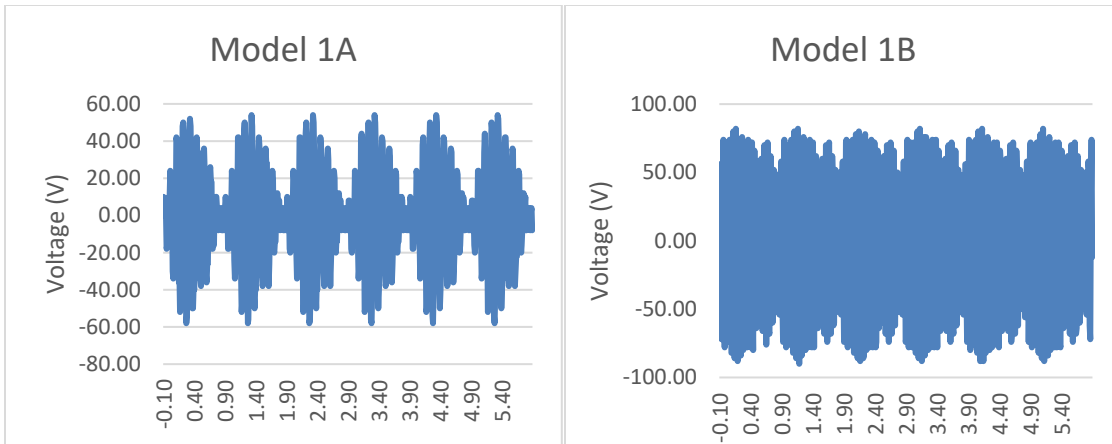


Figure 46. Model 1A and 1B at 60 RPM Shaft Speed

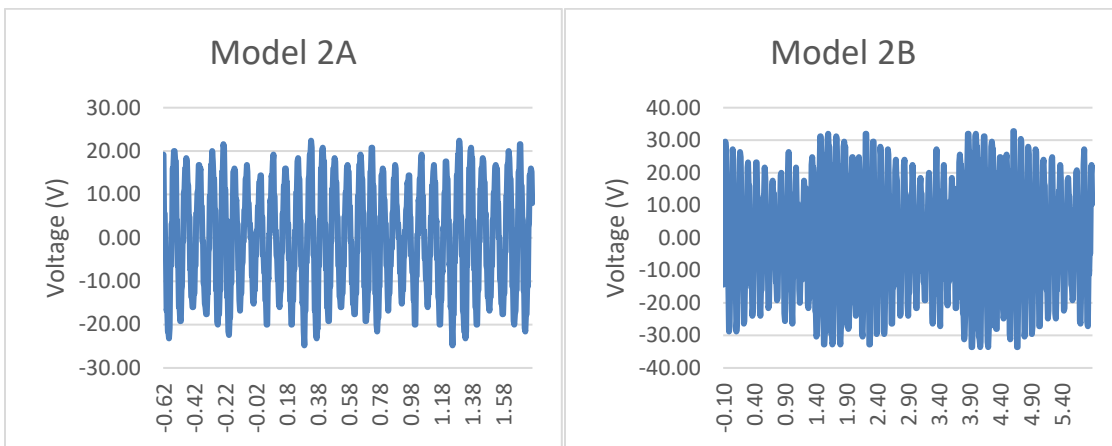


Figure 47. Model 2A and 2B at 60 RPM Shaft Speed

The voltage data above confirms that Model 1B has the highest voltage and frequency out of all the models. Although Model 2A had a much finer frequency compared to Model 1A, Model 2A still generated less electricity compared to Model 1A - that is why it was considered the poorest performer. The figures above also showed inconsistencies in the voltage values. This may be due to imperfections in the spacing of the copper and Teflon.

When using Model 1B to store energy with a $10\mu\text{F}$ a capacitor, a visual comparison of the capacitor charging at 50 RPM and 100 RPM is shown in Figure 48 and Figure 49.

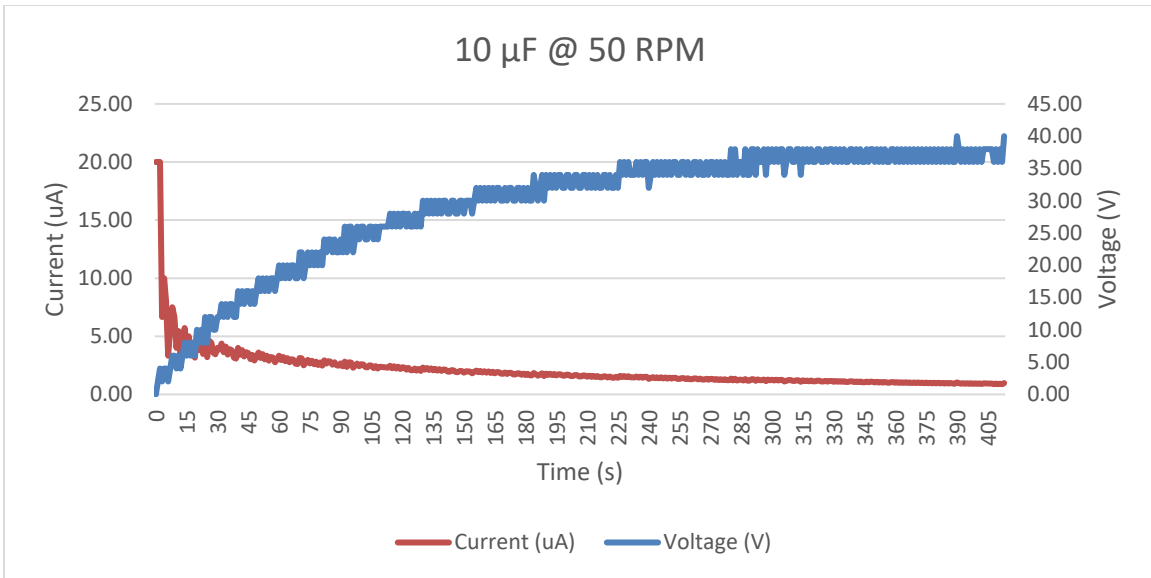


Figure 48. Voltage and Current for Model 1B at 50 RPM

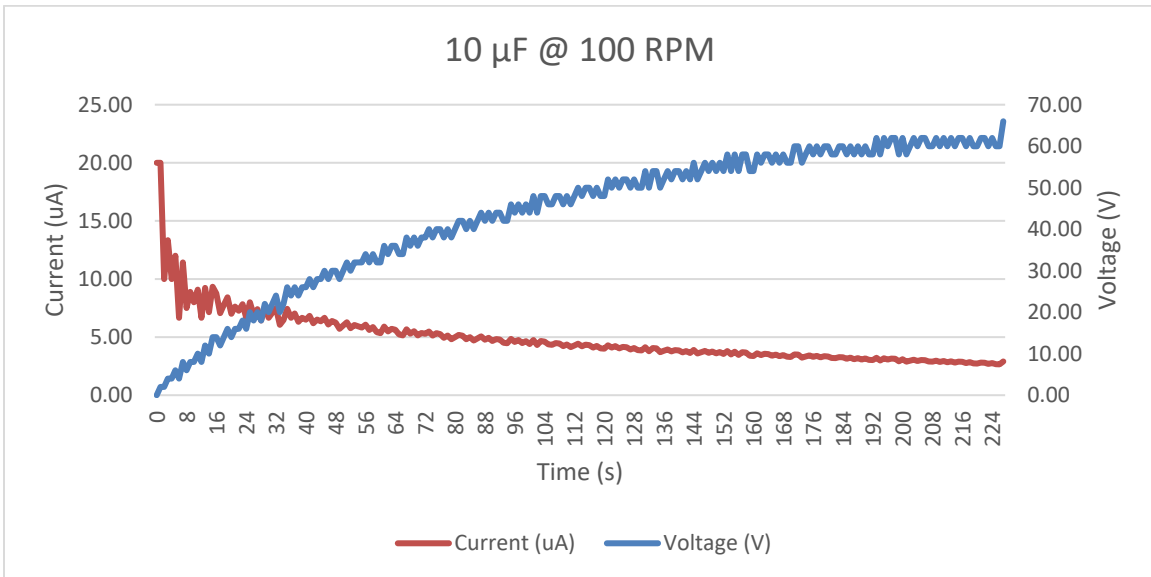


Figure 49. Voltage and Current for Model 1B at 100 RPM

The results validate that the TENG models can store energy within a capacitor. Figure 48 and Figure 49 also showed that at twice the speed, the 10 μF capacitor was able to reach a maximum charge in almost half the time at a higher charged voltage. Another noticeable result is that the depleting current during the charge were almost identical for both the 50 RPM and 100 RPM testing cycles. This can only mean that the current is

always the same no matter how fast the TENG is rotating. Therefore, in the case where a large load may be receiving electricity from the capacitor being charged, an increase in current may be necessary -if needed- with the help of transformers to supplement the charging of the capacitor. In addition, if a larger capacitor was being charged, it would still charge but it would take a longer time compared to the 10 μ F capacitor.

In terms of using LEDs to display electricity generation, Model 1B was used primarily because of its high frequency. All the other models were capable of lighting LEDs too; however, the low frequency models showed noticeable gaps in the lighting and dimming of the LEDs when the TENG models were tested. Either way, the LED testing showed potential for applications that require low frequency blinking lights (Ex: buoys) and/or high frequency steady lights (Ex: reading lamp).

For the series/parallel test, Model 3 showed that voltage sources in series produced the greater voltage. A visual comparison of the series and parallel data is as shown in Figure 50.

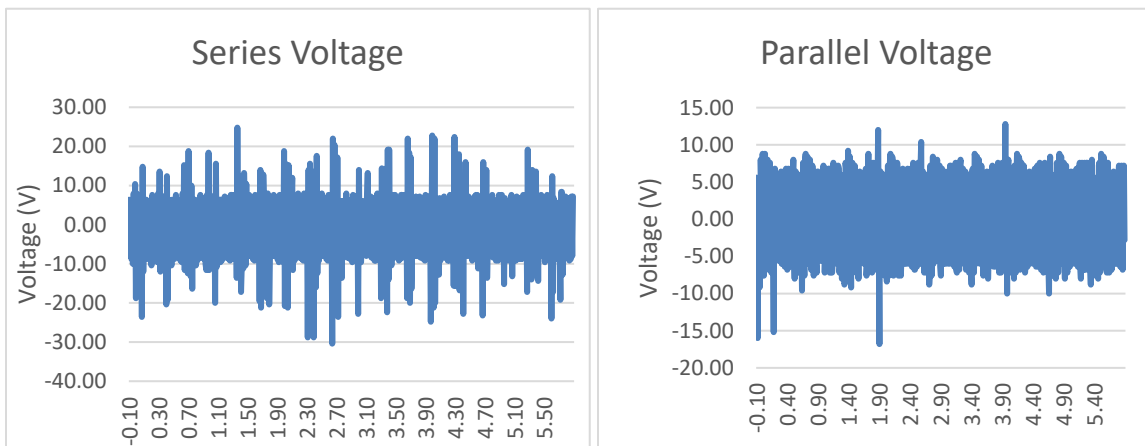


Figure 50. Series/Parallel Data for Model 3

The results above were expected since Model 3 had two “smaller” models on the same PVC pipe which should be alternating voltages at the same rate. However, there were irregularities shown in the figures above which may have been due to improper spacings in one of the two “smaller” models within Model 3.

However, when testing two separate models (Model 1A and 1B), the voltage sources in parallel produced the greater voltage. A visual comparison of the series and parallel data is as shown in Figure 51.

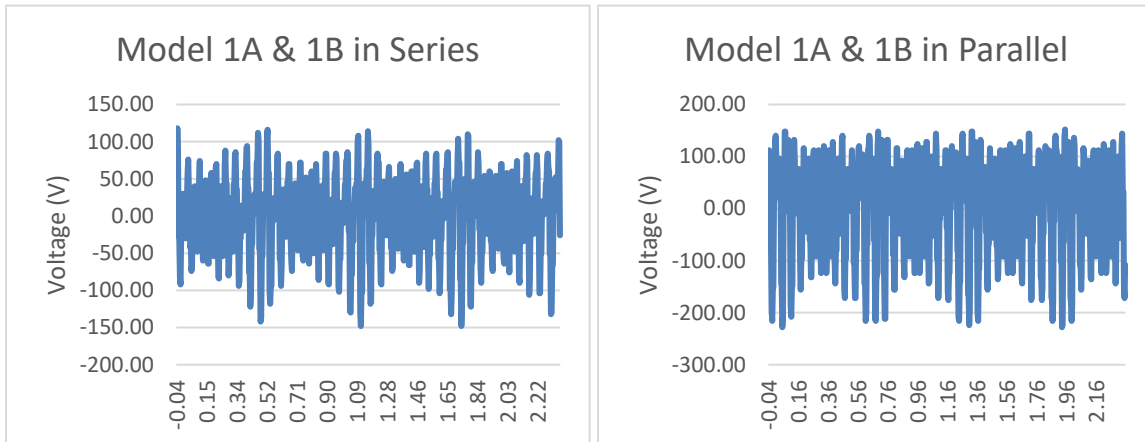


Figure 51. Series/Parallel Data for Model 1A and 1B

The contradicting results in comparison to Model 3 may have been due to the fact that Models 1A and 1B were operating at different sizes, different phases, or a combination of both. Either way, further research is needed to validate these assumptions.

E. DISCUSSION

At first glance, the longer models (2A and 2B) were expected to generate more electricity since they were larger than Models 1A and 1B. However, this experiment showed that the longer the models generated less electricity compared to its shorter counterparts. One possible reason may be due to the loss of precision due to accumulated human errors during the construction of the models. Because all models were built by hand, the longer models had more surface area that required taping. And the more surface area that required taping, the greater the chances of uneven laying of tape. Therefore, introducing small errors in lining up and causing accumulated deficiencies in the spacing and proper overlap of the copper and Teflon. Another reason why Models 2A and 2B generated less electricity may be due to the electronegativity properties of the materials

used. There might be a limit on the sizing and proportionality of the combination of copper and Teflon that was not covered in this research. A more detailed material analysis in terms of the electronegativity of the material used is required to validate this assumption.

In comparing the performance of the TENGs with respect to the width of the models, the thinner models (Models 1B and 2B) generated greater electricity compared to their wider counterparts (Models 1A and 2A). Possible reason may be due to the arc length contact of the copper and Teflon as shown in Figure 52.

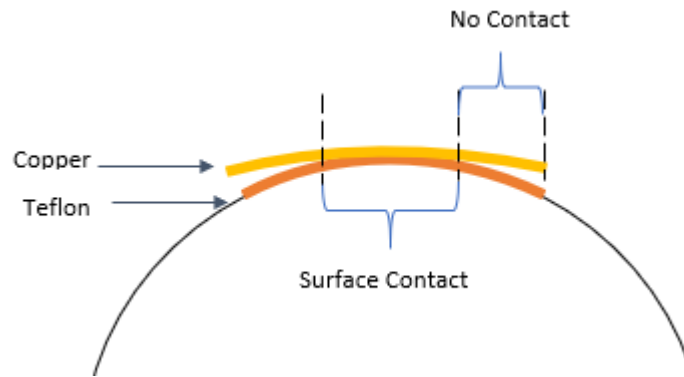


Figure 52. Gap in Surface Contact

Since the flexible plastic holding the copper taping can only flex so much to achieve full overlap and complete contact, the fabrication of the flexible plastic being used may need modifications to improve surface contact. In addition, this partial overlap may have also contributed to why the longer models generated less electricity.

Overall, Model 1B was ultimately chosen as most effective and was used for further testing primarily since the cable used for the oscilloscope was rated at $10\text{M}\Omega$ and the change in current would be directly proportional to the change in voltage [9].

When testing to store energy, the $10\mu\text{F}$ capacitor showed potential that a TENG is capable of storing electricity within a certain time depending on how fast the TENG is rotating. The increase in shaft speed increases the voltage and frequency generated by the TENG; therefore, allowing the capacitor to store energy at a higher voltage in addition to

decreasing the time it takes to charge. Overall, the TENG would require operating at higher speeds and/or with a transformer in order to attain a feasible capability of charging larger capacitors within a reasonable amount of time depending on the load it is required to provide electricity for. And since greater length in the TENG showed no improvement in voltage data, it would be unrealistic to assume that a larger model would have the capability to store a greater charge. However, separate systems in series or parallel may solve the problem; therefore, instead of having larger models, a combination of smaller models may have the potential to generate electricity for macro-scale applications.

In terms of the series/parallel test, Model 3 was constructed to emulate two separate models lined up with each other. Their frequencies were the same validating that the separate models were in phase with each other. Also, Model 3 showed that TENG models with the same phase will generate a greater voltage when connected in series vice parallel.

However, when testing the concept with Model 1A and 1B, the parallel connection yielded a greater voltage compared to the series connection. And although it is not ideal to connect voltage sources in parallel especially if they are not identical, further investigation is required to determine if this result is an advantage or disadvantage to the TENG system [9], [10]. The first factor is that Models 1A and 1B did not have the same effective voltage values. And secondly, both models were not in phase with each other. That is why the frequency of each model was included in the data collection process. And since the two Models were not in phase with each other and had different voltage values, the results can be unpredictable. For instance, when Model 1A peaks positive and Model 1B peaks negative at a certain instance in time, the total output voltage in series would be the sum of the two voltage values (which could be zero assuming both models peaked the same value at opposing current direction). On the other hand, the total output voltage in parallel would more than likely be influence by the greater voltage value between the two. During this experiment, this was the case and the parallel connection of two different size models showed a higher value in comparison to the series connection. However, further research is required to validate that parallel voltage source connections are more ideal in comparison to series connections before

incorporating such concepts into modern applications since the accepted practice is to always connect voltage sources in series rather than in parallel.

On the brighter side, despite all the minor problems with instability and precision, the results from all the TENG models were exceptional. Even the most outpaced model (Model 2A) was capable of generating an average of 126 VAC and 37 Hz at 180 RPM shaft speed. And considering the rating of wall outlets in the United States is roughly 120 VAC and 60 Hz [11], all the designed models may require improvements to perfect their performance. But overall, all the models showed potential that TENGs are capable of generating electricity for use on everyday applications.

The adaptability of the TENG models makes this technology highly marketable for consumers that may require wind, waves, and/or self-generation as sources for electricity generation. For example, in terms of self-generated electricity, TENG has great potential in becoming a reliable source of energy in the future for household applications. The models below were adapted unto a stationary bicycle using a set of gears and a chain (see Figure 53 and Figure 54).



Figure 53. Stationary Bike with Mounted Gears and Chain

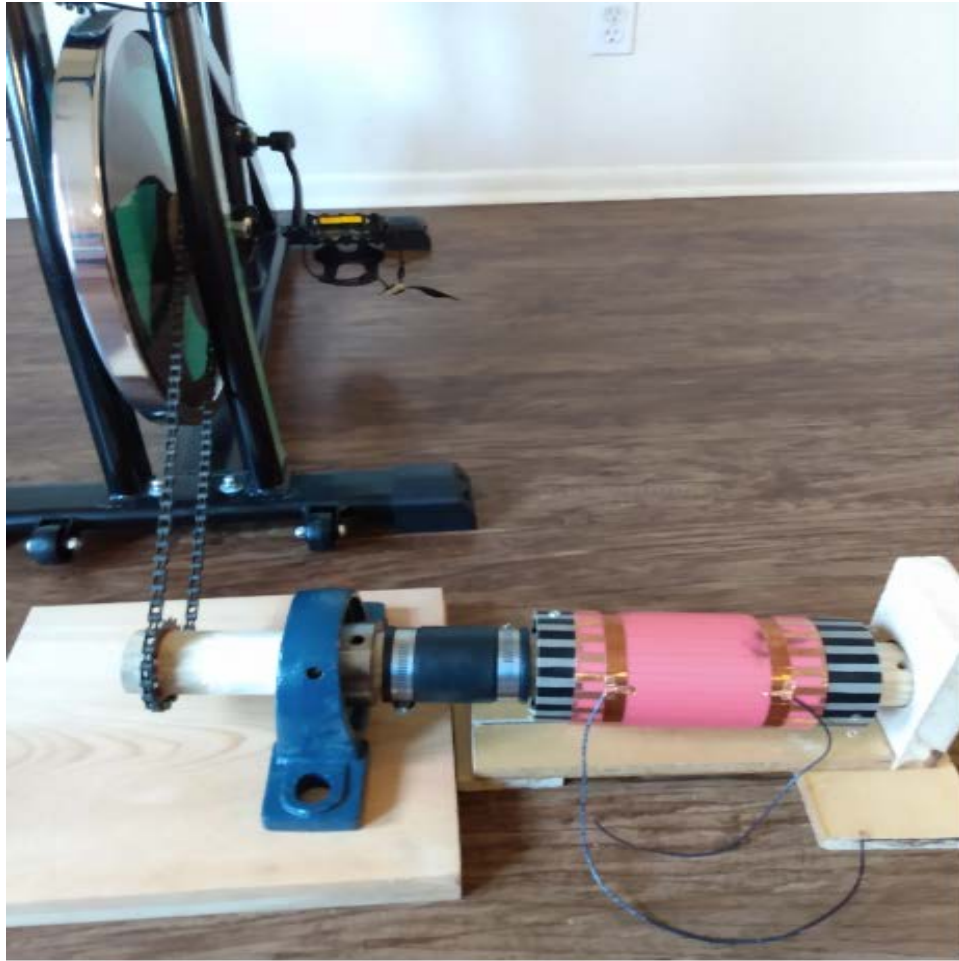


Figure 54. Stationary Bike with TENG

Therefore, without the need for wind or waves, the setup was capable of generating electricity as long as someone was peddling the stationary bike. For instance, when the stationary bike is generating an average rotational speed of 20 RPM, the TENG can generate an average of 100 VAC as shown in Figure 55.

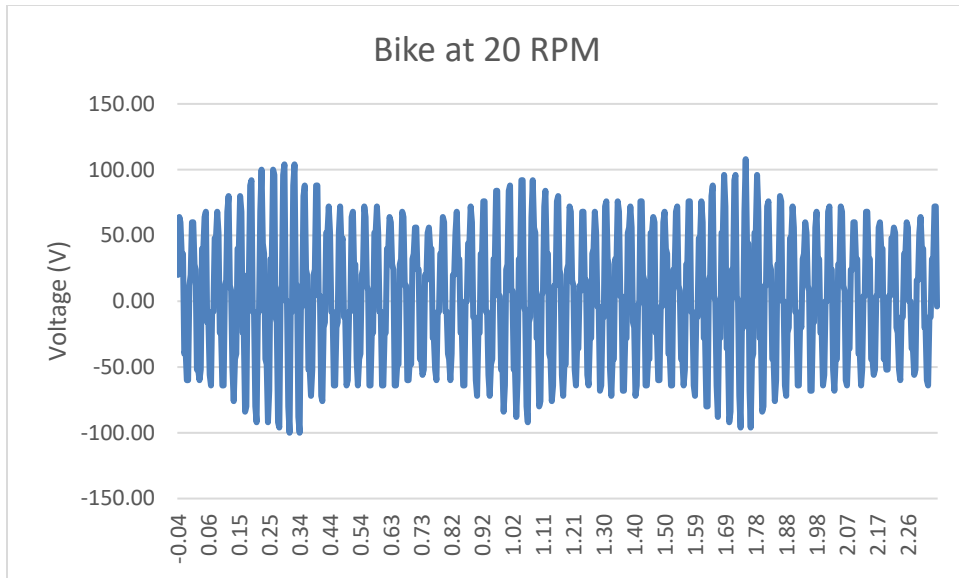


Figure 55. TENG Voltage Data at 20 RPM (Bike Speed)

In addition, the maximum number of LEDs used for this research were also tested with the stationary bike and the results are as shown in Figure 56 and Figure 57.



Figure 56. 120 LEDs connected to TENG with Stationary Bike

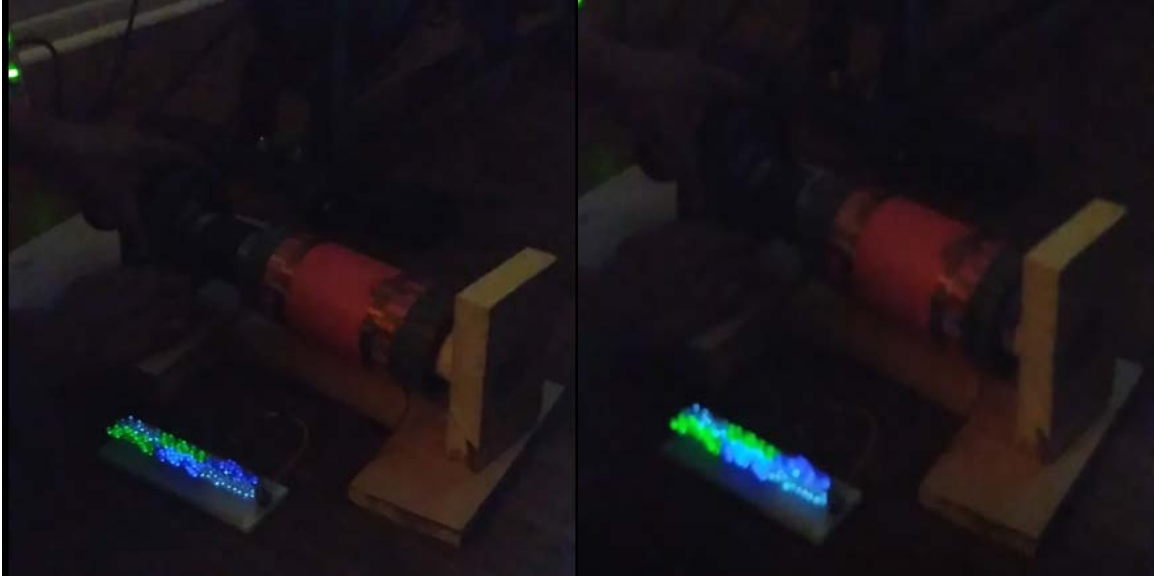


Figure 57. 120 LEDs when Stationary Bike is operating at 20 RPM (left) or greater (right)

The adaptation to the stationary bike shows great promise in the fact that it proves that TENG can be used alongside a self-generating source without the need for wind or waves to generate electricity.

THIS PAGE INTENTIONALLY LEFT BLANK

V. CONCLUSIONS AND FUTURE WORK

A. CONCLUSIONS

The experiments conducted for this research were conceptual in nature with intentions to further analyze and improve previous NPS TENG designs. The models constructed emulate the previous NPS Rotational TENG design in the fact that they utilize friction between copper and Teflon to generate electricity due to rotational motion. Major differences in designs include the construction materials and the size of the models. For this experiment, no materials were 3D printed. A cylindrical hardwood was used as the shaft to provide the rotational motion. A PVC pipe was mounted on the hardwood for placement of the Teflon taping. And the copper taping was laid on a polyethylene plastic that was then wrapped around the PVC pipe using clamps. The hardwood was then connected to a DC motor using a flexible coupling to generate rotational motion for data collection.

The main objective for the experiment was to validate the TENG's potential to generate electricity and to document its performance capabilities based on the size and speed of the model that was tested. The results from this experiment were significantly superior compared to all previous NPS TENG designs. All previous NPS designs resulted in maximum voltages less than 10 Volts and maximum current within the nanoamp range, while the models for this experiment resulted in current within the microamp range and voltages greater than 400 Volts. The only reason why maximum voltage could not be determined was because the oscilloscope could only read voltages less than 400 Volts. The most optimum model (Model 1B) achieved 399 Volts at 398 RPM in comparison to the previous NPS Rotational design which achieved less than 4 Volts at 360 RPM. Overall, this experiment achieved results almost 100 times greater in terms of voltage and 1000 times greater in terms of current compared to all previous NPS designs.

One main reason why the TENG models from this experiment outperformed all previous NPS models was probably due to the size of the models. Even though this experiment showed that larger models are not more efficient compared to smaller models,

there might be a limited range of size where rotational TENGs are most effective and the chosen sizes for this experiment were probably within or close to that range. Another reason may have been the simplicity of spacing for the copper and Teflon taping in this experiment. Since all taping were done by hand, 1.27cm and 0.635cm tapes were used since they can be purchased at the proper sizes with no need for cutting. A disadvantage previous NPS models had was the spacing between the copper was so small that a precision die-cutter had to be used. Although precise, small unnecessary overlaps between the copper and Teflon can through off the potential drop across the wire leads since the models were so small. And finally, future research should analyze the electronegativity of PLA. Although PLA is highly popular for 3D printing, its effect on the TENG has not been clearly studied in previous NPS designs. The use of PVC and polyethylene plastic as mediums for this experiment was solely to reduce electronegativity effects on the Teflon so that the copper would be the primary electronegative material against the Teflon with minimal effects from surrounding materials.

Nonetheless, there is still room for improvement. The experiment proved highly feasible for high voltage applications and showed its capabilities to adapt to different sources. However, the longer models proved to be inefficient compared to the shorter models. And the series and parallel test showed that a TENG is more effective in series if they are in phase with each other and effective in parallel if they are different sizes and not in phase with each other. Overall, more test on different size models are needed to determine the optimal size for a TENG in terms of width, length, and spacing. In addition, it is more efficient to ensure multiple TENGs are generating alternating current in phase with each other so to connect them in series to provide more voltage.

In terms of energy storage, it took roughly 413 seconds to charge a 10 μ F capacitor to 40 VDC at 50 RPM shaft speed and 171 seconds to charge to 68 VDC at 125 RPM shaft speed. Although the results may be impressive for small applications, further research needs to be conducted to improve the models. For instance, 10 μ F capacitors are usually used as filters for rectified voltages on circuit boards for larger applications (computers, TVs, refrigerators, etc.). If TENG is to be competitive in the Blue Energy

storage business, models have to be improved to store energy at a faster rate in larger capacitors.

The main idea behind this research was to use readily available material. A caveat to that was that it proved to be a great challenge to modify the materials used to form fit. Multiple hardware was needed to secure all the parts together; but the increase in number of hardware used only increased the instability of the system as a whole. Therefore, 3D printing of some parts might have been necessary to alleviate the need of certain hardware (screws, tape, nuts, bolts, etc.); but at the same time, it increases the need to replace a larger piece compared to hardware and smaller pieces. If this technology is to be globally distributed, design techniques have to improve at least to the point where maintenance, repairs, and/or replacements do not become a significant problem.

And finally, the greatest challenge for this experiment was the laying of the copper and Teflon taping by hand. Although time consuming, laying out the copper and Teflon taping correctly was probably the most important part of the assembly; otherwise, the TENG models would have been ineffective and/or possibly inoperable. Therefore, patience and dedication in the craft became the key in the execution of this research and experiment.

B. RECOMMENDATIONS

While the results showed great potential in rotational TENG technology, many modifications are needed to optimize the performance. First, a more precise technique has to be implemented in laying the copper and Teflon tape to achieve the correct spacing. Laying the tape by hand was a good start to prove the concept; but to pursue efficiency in the system, precision tools and equipment may be needed to supplement configuration of the taping.

The stability of the shaft and the polyethylene plastic could also use a little improvement. Since friction between the copper and Teflon is part of this design, there is tendency for the polyethylene plastic to slide off the model if the clamps came loose. No problem with the stability was encountered when tests were conducted at lower shaft speeds. However, as the speed increases (especially greater than 200 RPM), the

vibrations encountered by the model are capable of shaking the clamps loose if they are not secured properly. A recommendation would be to 3D print the shaft with modifications to readily install the PVC piping unto the shaft. This would minimize the need for multiple drilled holes and the use of nuts, bolts, and screws to secure the model. In return, the stability of the model during rotation should increase which would also decrease the chances of the polyethylene plastic flying off during high rotational speed testing.

C. FUTURE RESEARCH

The results from this research showed that a rotational TENG design is capable of generating significantly high output voltage at very low current. Future research should consider testing the behavior of this TENG model against a variety of transformers to determine the most effective means to increase the current while decreasing the voltage without generating too much heat loss.

Another interesting consideration is to combine TENG with other Blue/Green Energy source technologies to increase their power output. A good start would be to combine TENG with an electromagnetic generator (EMG) to analyze their energy generation capabilities. TENG generally is a high voltage and low current source while EMG is a low voltage and high current source. The polarity in the way these two technologies generate electricity have proven to complement each other very well. Research Scientist at NASA Ames proved this concept when testing a floating oscillator-embedded triboelectric-electromagnetic (FO-TEEM) generator which was proposed as a hybrid energy harvester platform that simultaneously utilizes both the mechanisms of a TENG and an EMG [12].

APPENDIX

The following graphs represent raw data from the oscilloscope for each TENG model. For Models 1A, 1B, 2A, and 2B each graph displays their alternating voltages at various shaft speeds. For Model 3 and Models 1A & 1B in series/parallel testing, each graph displays alternating voltage data at a set shaft speed for comparison. The capacitor storage data displays Model 1B charging time vs voltage and current for a $10\mu\text{F}$ capacitor.

A. MODEL 1A DATA

The figures below show voltage data for Model 1A at various shaft speeds.

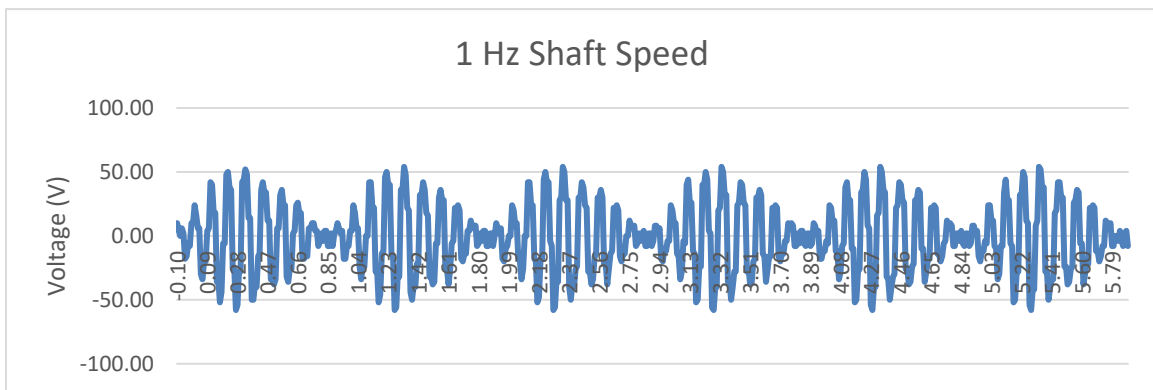


Figure 58. Model 1A Shaft Speed at 60 RPM

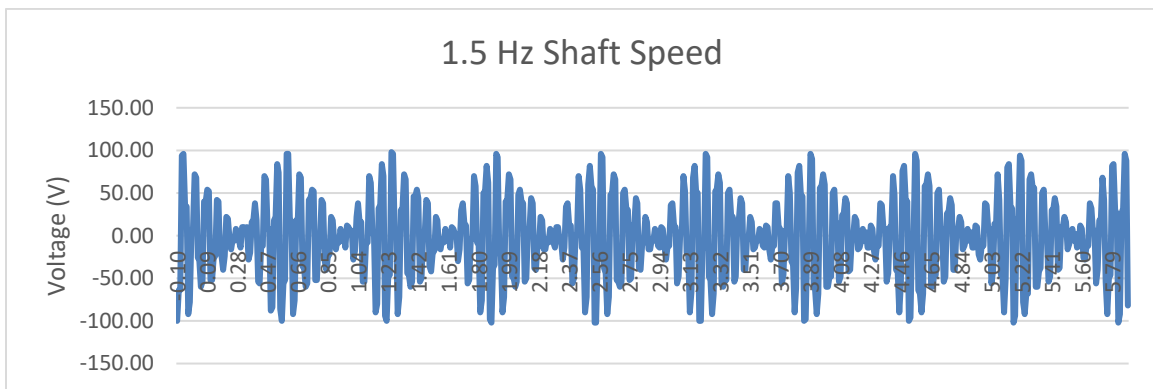


Figure 59. Model 1A Shaft Speed at 90 RPM

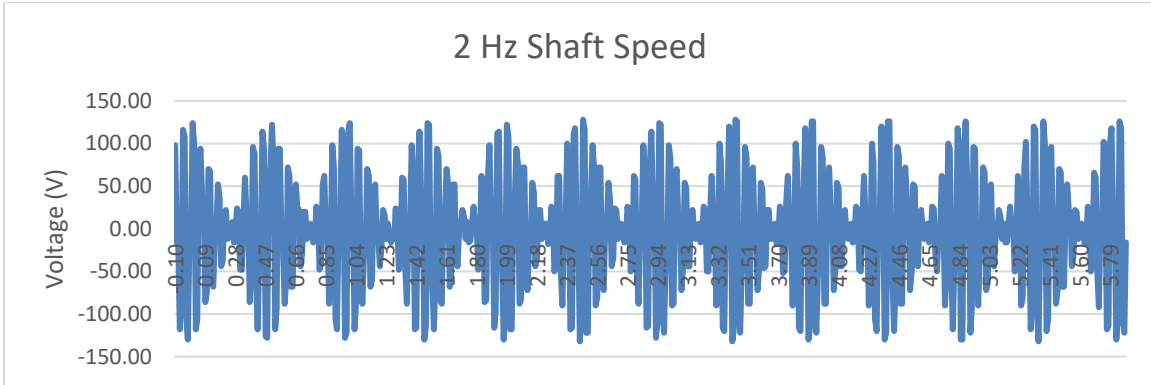


Figure 60. Model 1A Shaft Speed at 120 RPM

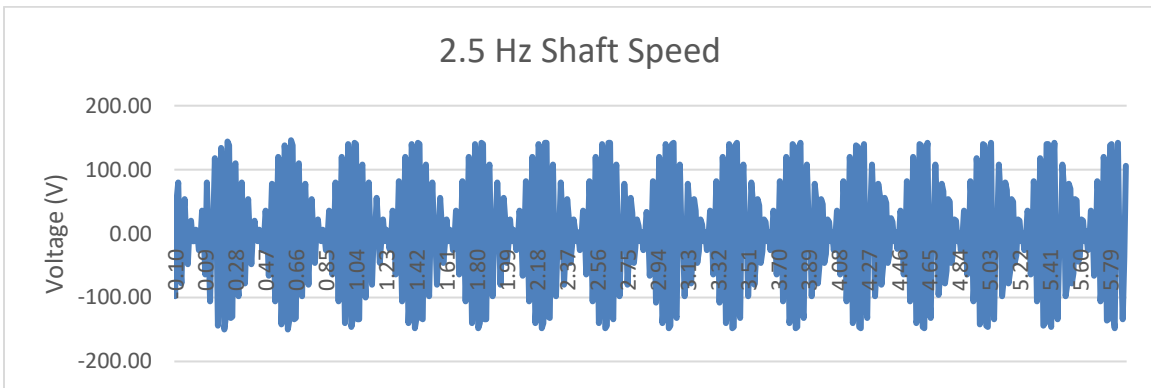


Figure 61. Model 1A Shaft Speed at 150 RPM

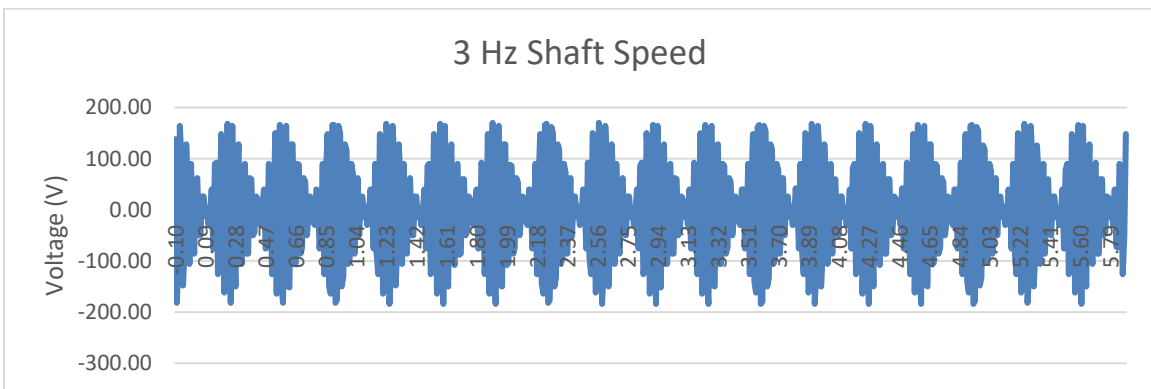


Figure 62. Model 1A Shaft Speed at 180 RPM

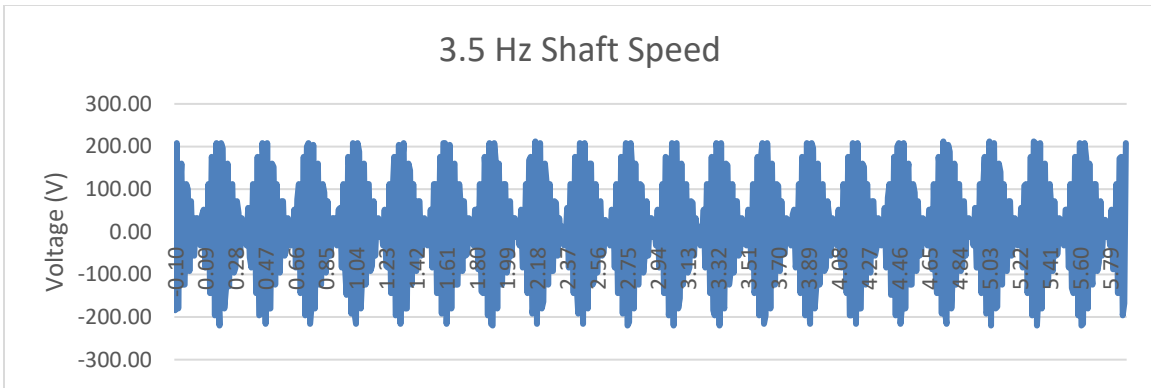


Figure 63. Model 1A Shaft Speed at 210 RPM

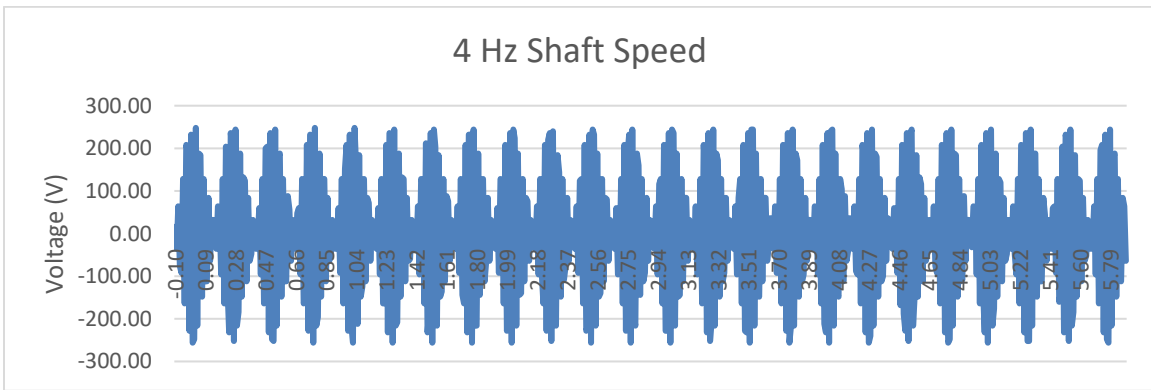


Figure 64. Model 1A Shaft Speed at 240 RPM

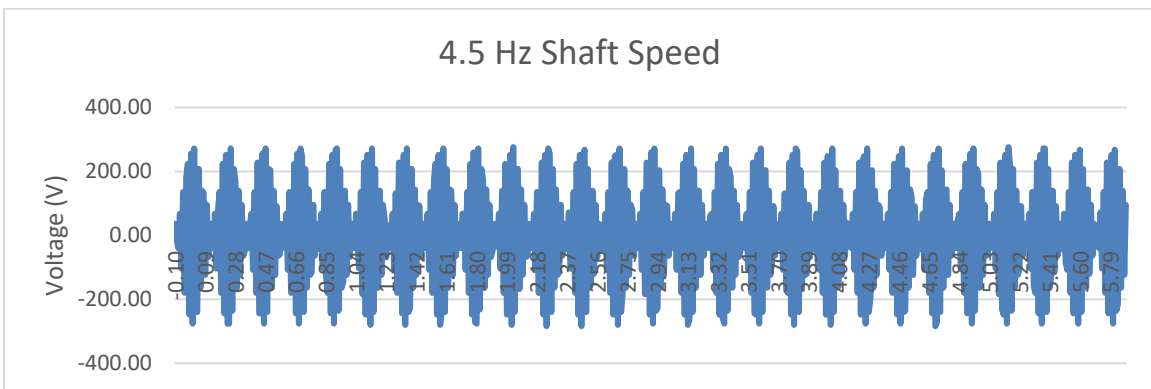


Figure 65. Model 1A Shaft Speed at 270 RPM

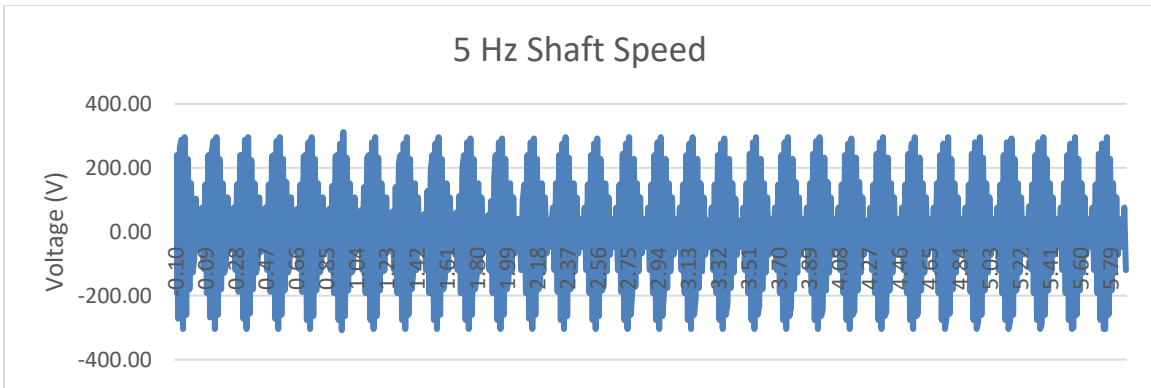


Figure 66. Model 1A Shaft Speed at 300 RPM

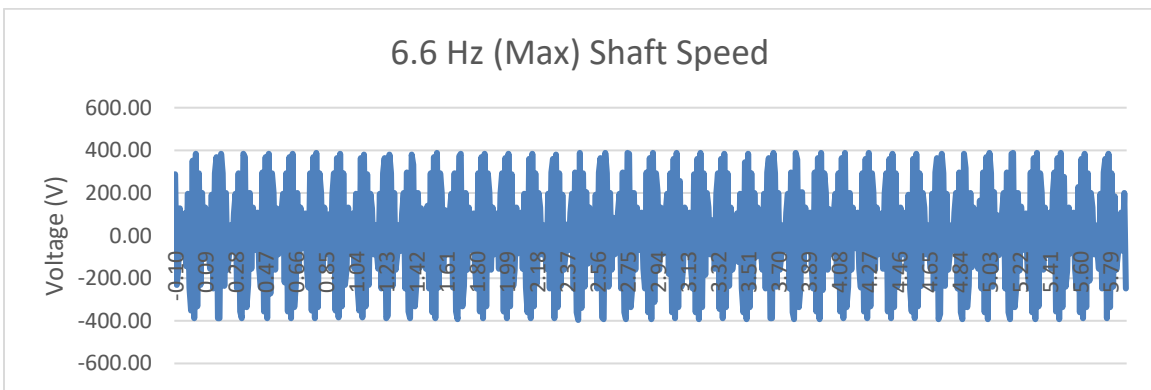


Figure 67. Model 1A Shaft Speed at 397 RPM

B. MODEL 1B DATA

The figures below show voltage data for Model 1B at various shaft speeds.

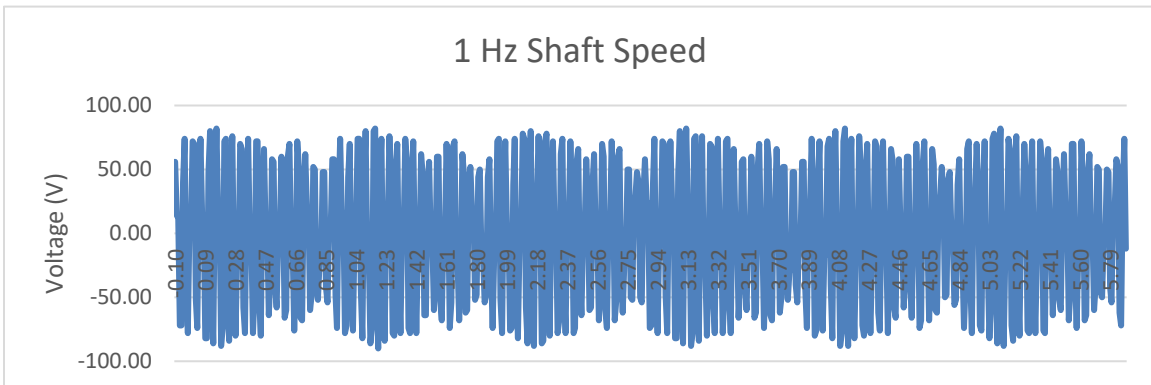


Figure 68. Model 1B Shaft Speed at 60 RPM

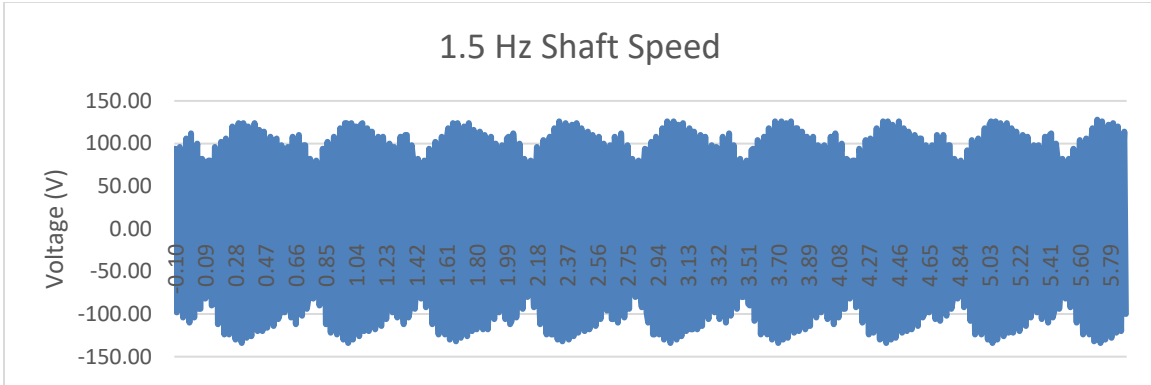


Figure 69. Model 1B Shaft Speed at 90 RPM

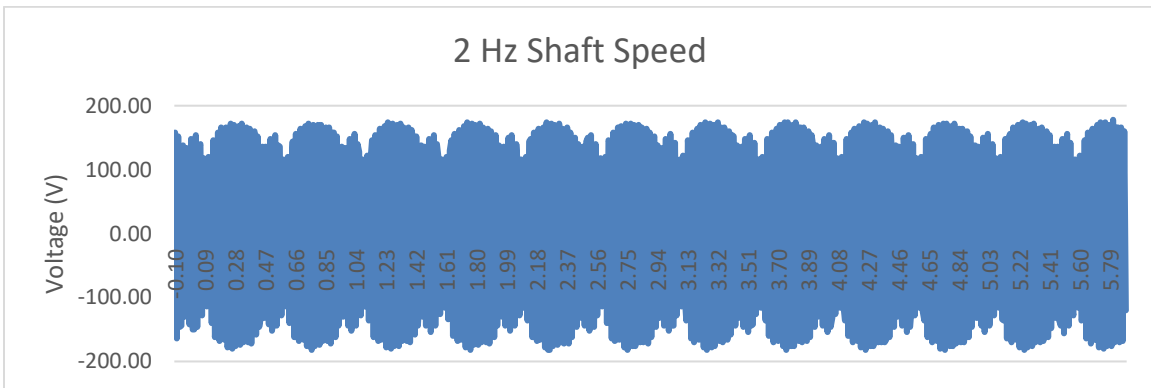


Figure 70. Model 1B Shaft Speed at 120 RPM

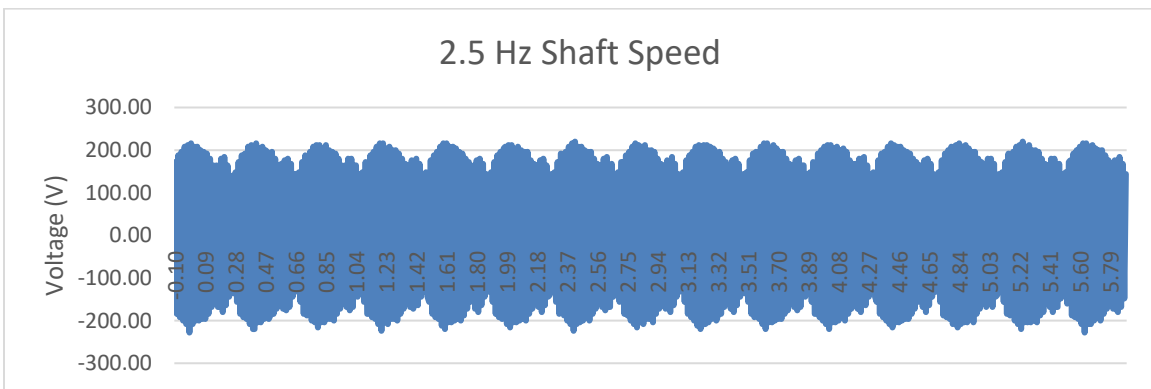


Figure 71. Model 1B Shaft Speed at 150 RPM

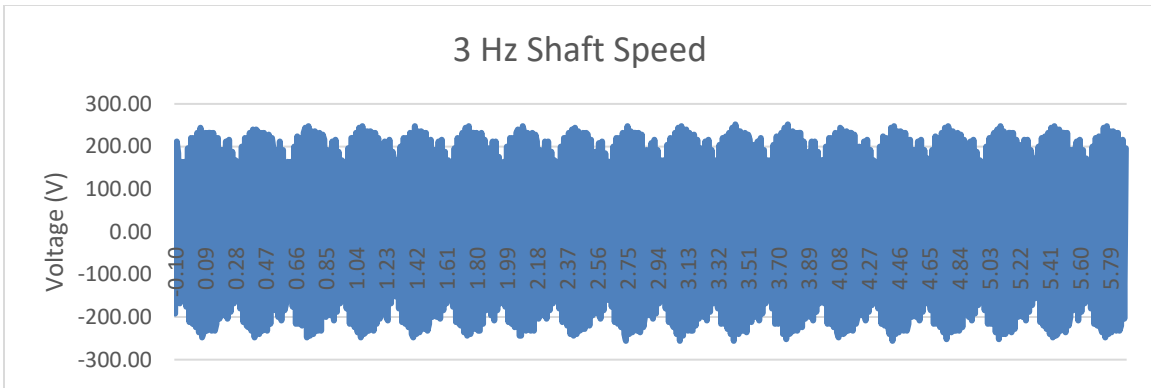


Figure 72. Model 1B Shaft Speed at 180 RPM

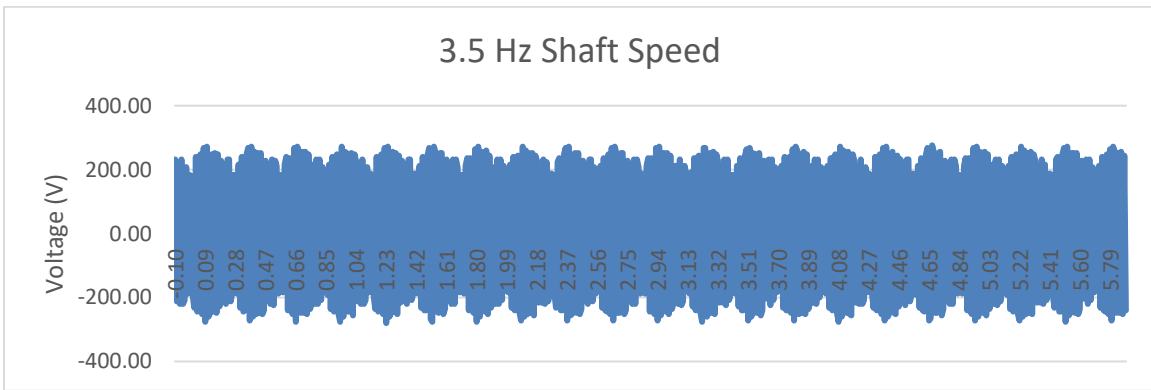


Figure 73. Model 1B Shaft Speed at 210 RPM

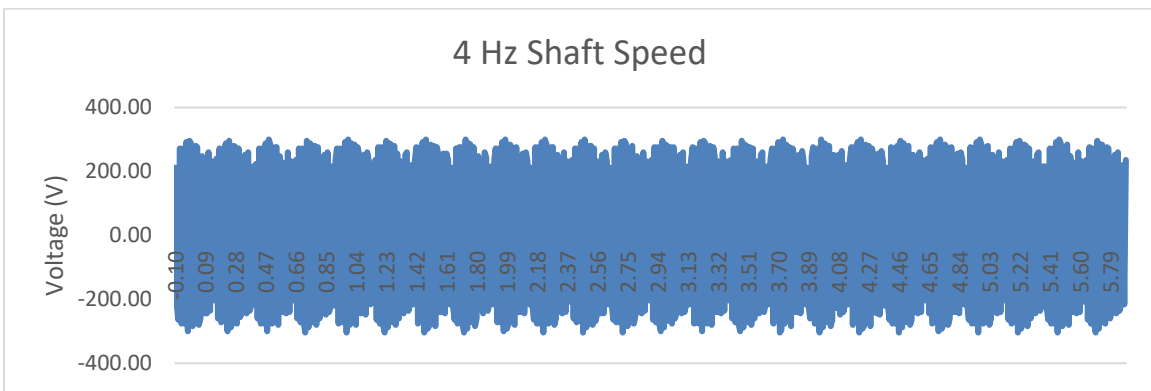


Figure 74. Model 1B Shaft Speed at 240 RPM

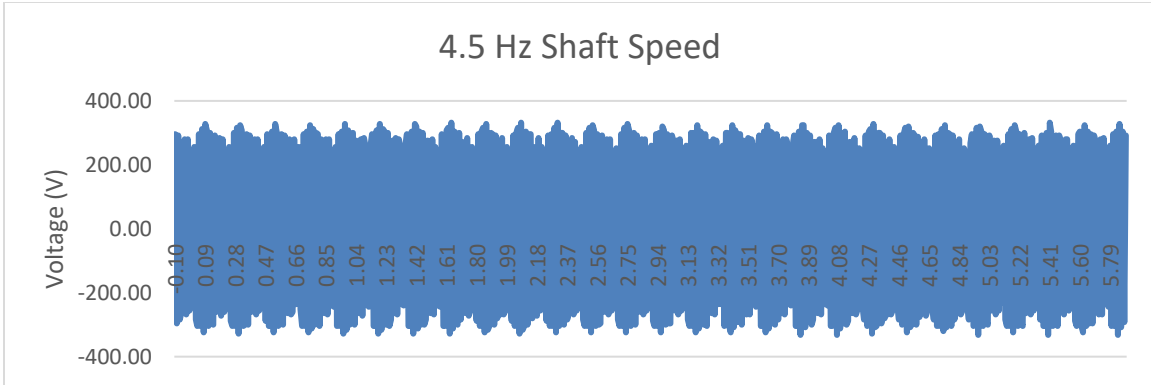


Figure 75. Model 1B Shaft Speed at 270 RPM

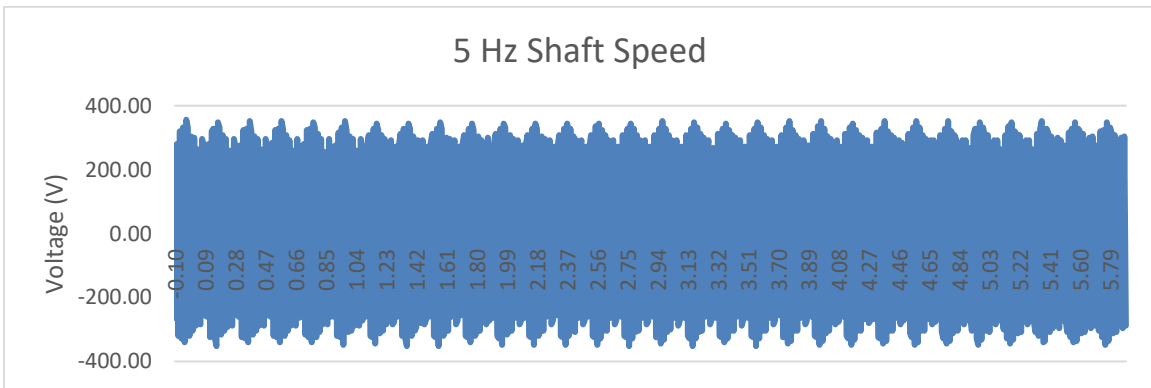


Figure 76. Model 1B Shaft Speed at 300 RPM

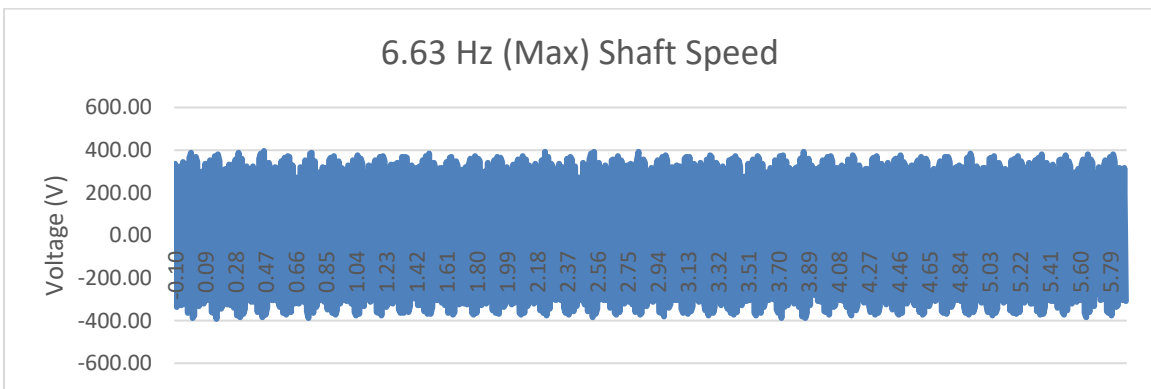


Figure 77. Model 1B Shaft Speed at 398 RPM

C. MODEL 2A DATA

The figures below show voltage data for Model 2A at various shaft speeds.

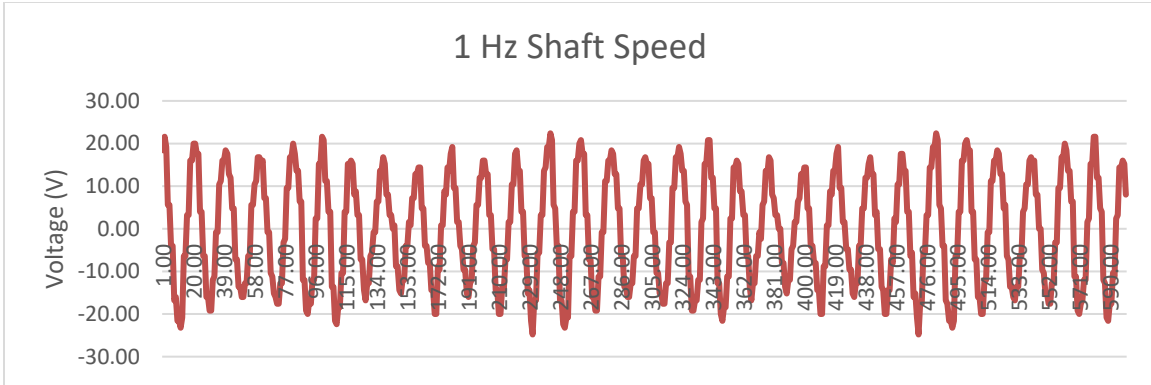


Figure 78. Model 2A Shaft Speed at 60 RPM

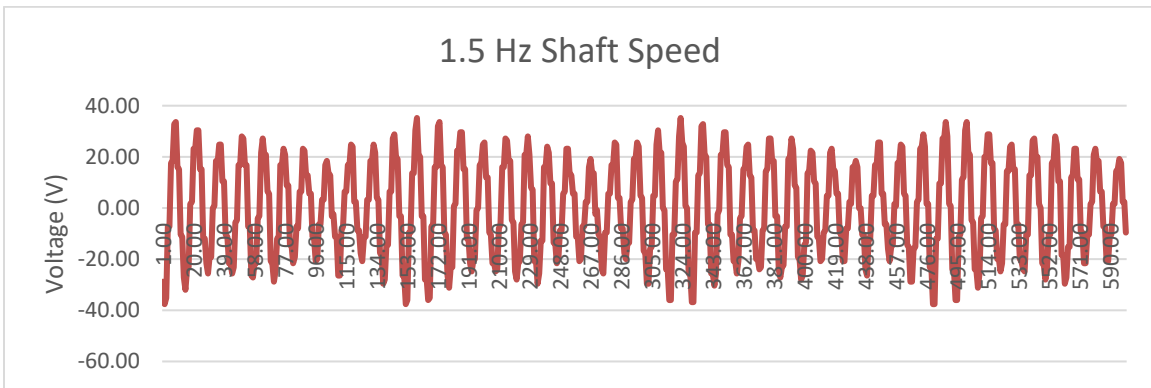


Figure 79. Model 2A Shaft Speed at 90 RPM

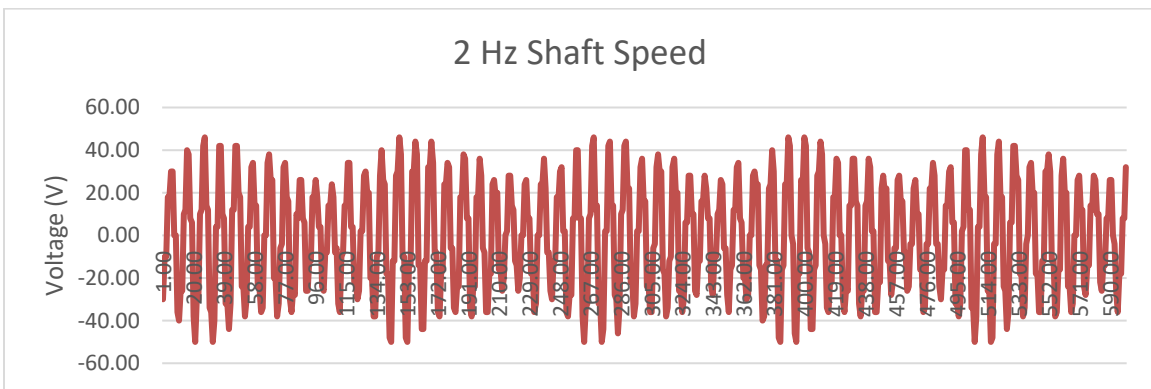


Figure 80. Model 2A Shaft Speed at 120 RPM

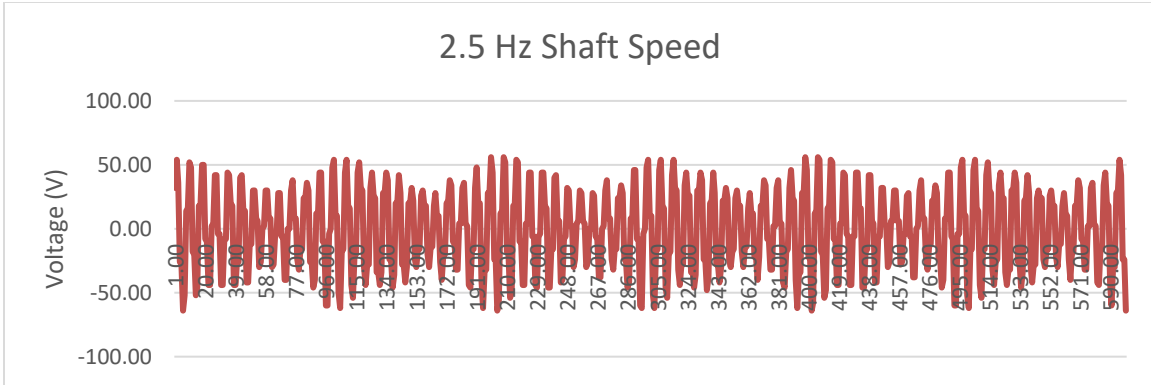


Figure 81. Model 2A Shaft Speed at 150 RPM

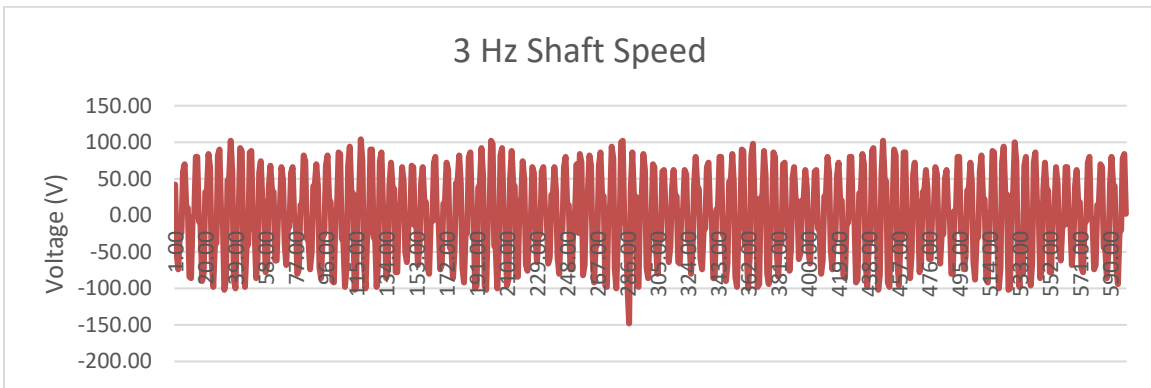


Figure 82. Model 2A Shaft Speed at 180 RPM

D. MODEL 2B DATA

The figures below show voltage data for Model 2B at various shaft speeds.

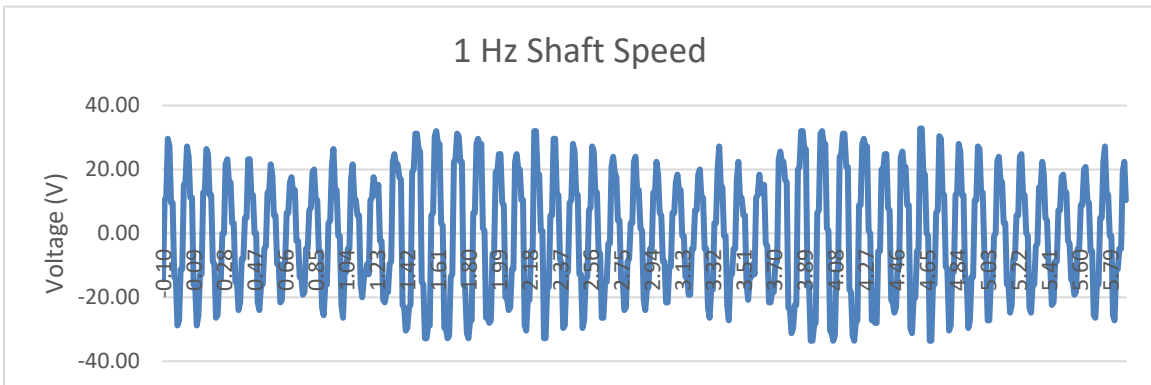


Figure 83. Model 2B Shaft Speed at 60 RPM

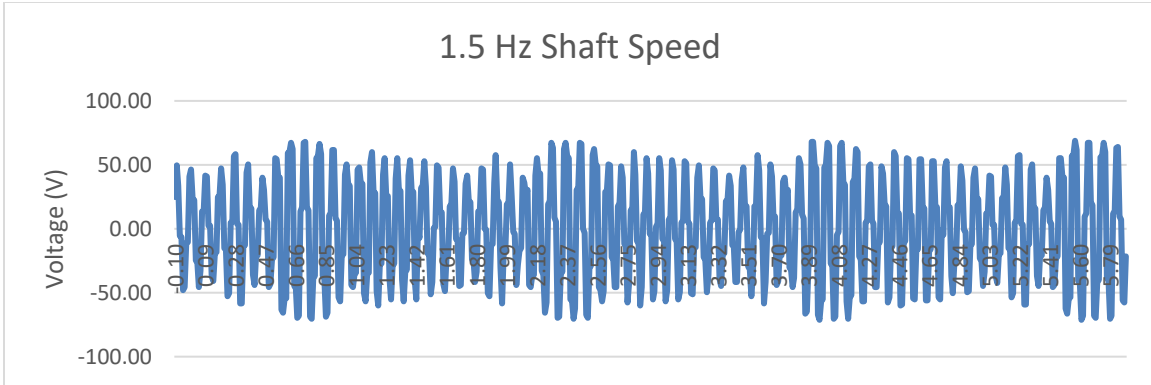


Figure 84. Model 2B Shaft Speed at 90 RPM

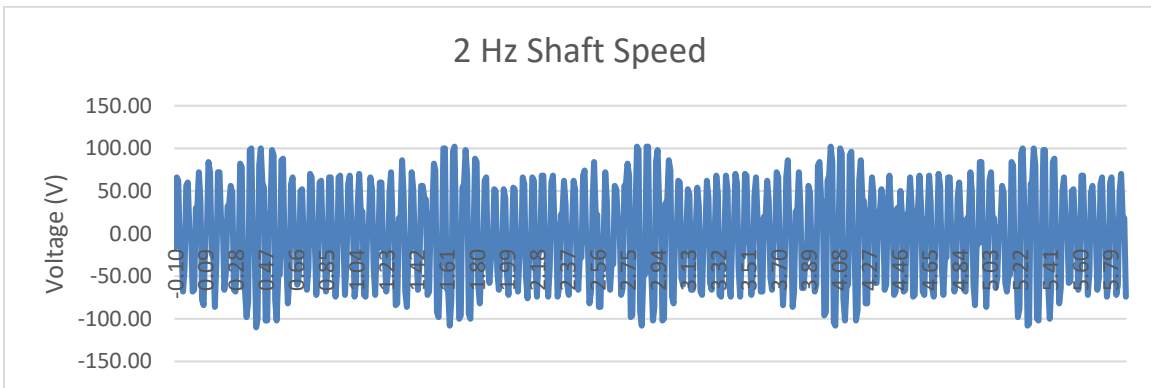


Figure 85. Model 2B Shaft Speed at 120 RPM

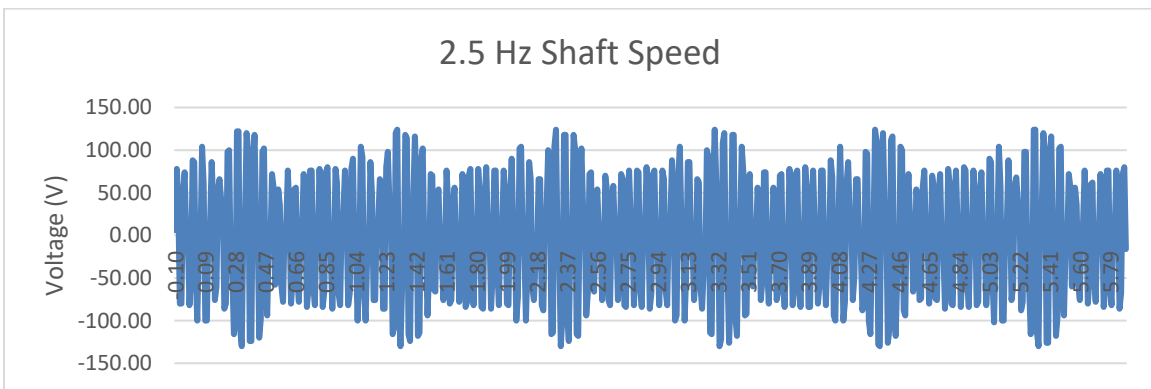


Figure 86. Model 2B Shaft Speed at 150 RPM

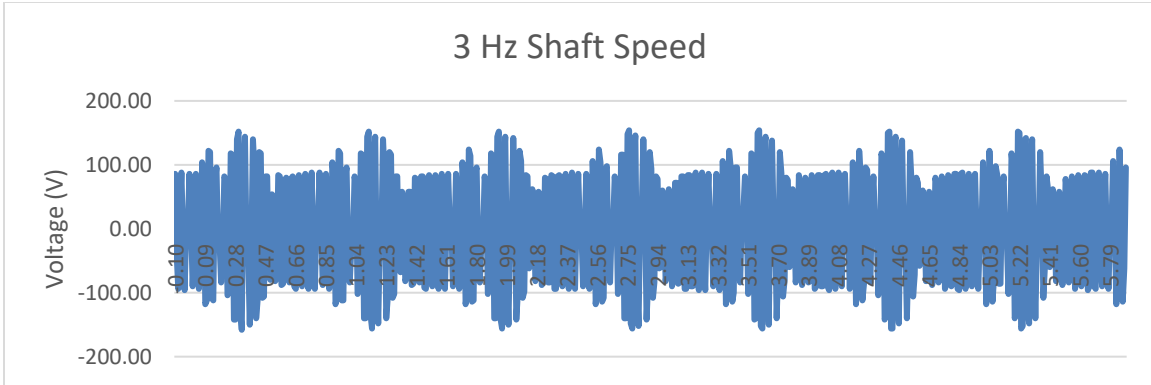


Figure 87. Model 2B Shaft Speed at 180 RPM

E. MODEL 3 DATA

The figures below show voltage data for Model 3 at 90 RPM shaft speeds.

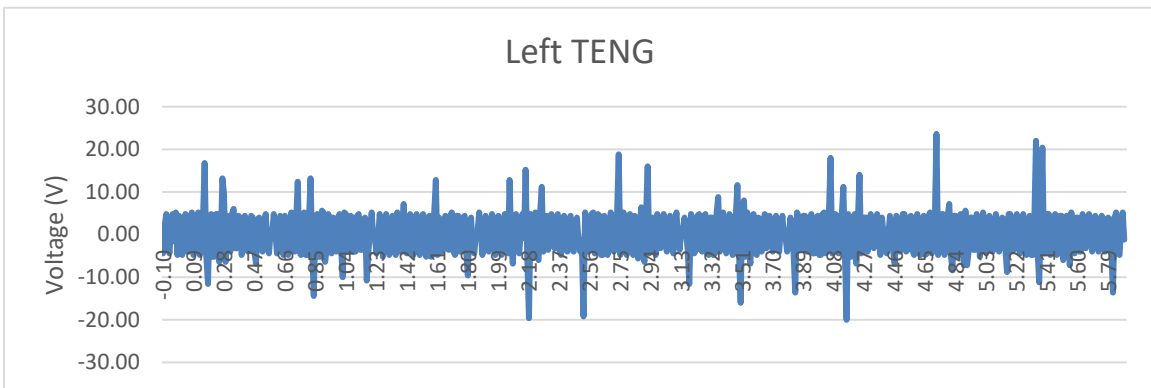


Figure 88. Left Side of Model 3 at 90 RPM

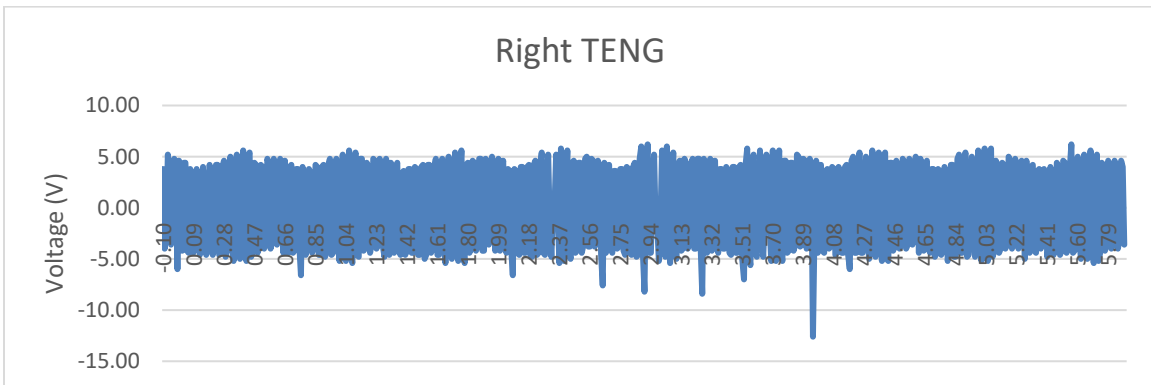


Figure 89. Right Side of Model 3 at 90 RPM

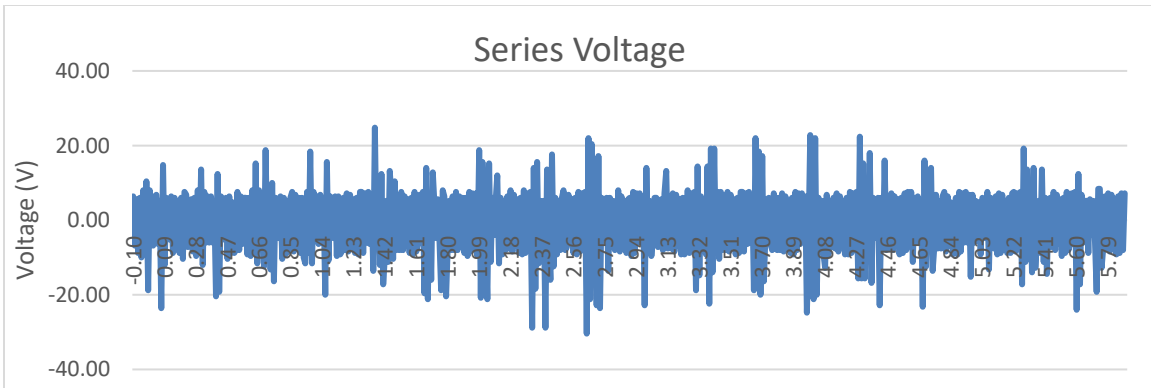


Figure 90. Model 3 Right and Left sides in Series at 90 RPM

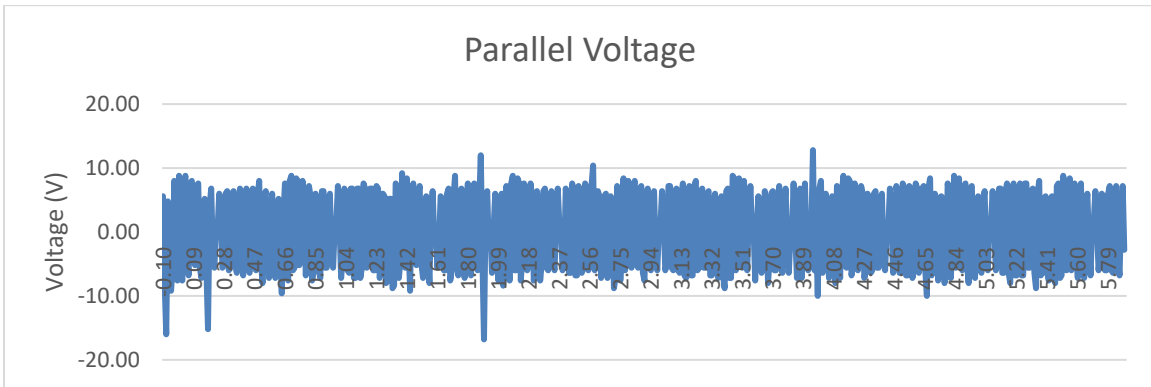


Figure 91. Model 3 Right and Left sides in Parallel at 90 RPM

F. MODEL 1A AND 1B SERIES/PARALLEL TEST DATA

The figures below show voltage data for Model 1A and Model 1B during Series/Parallel test between the two different models.

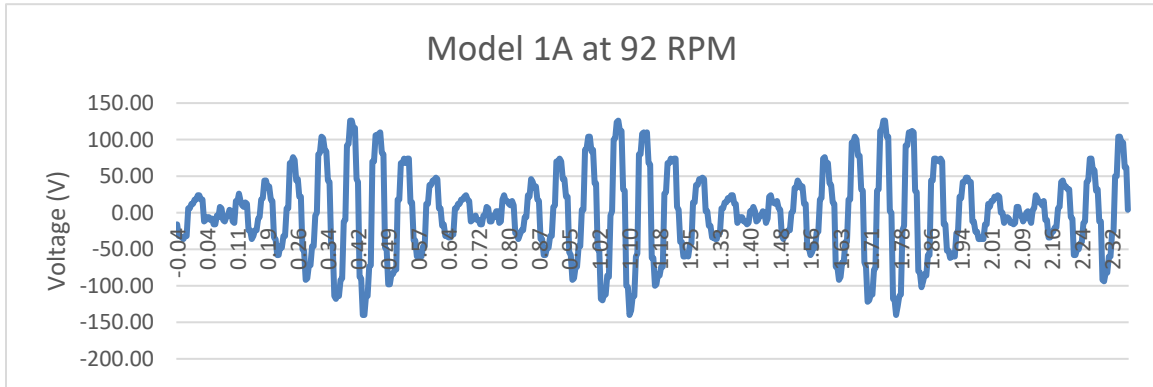


Figure 92. Model 1A prep for Series/Parallel Test

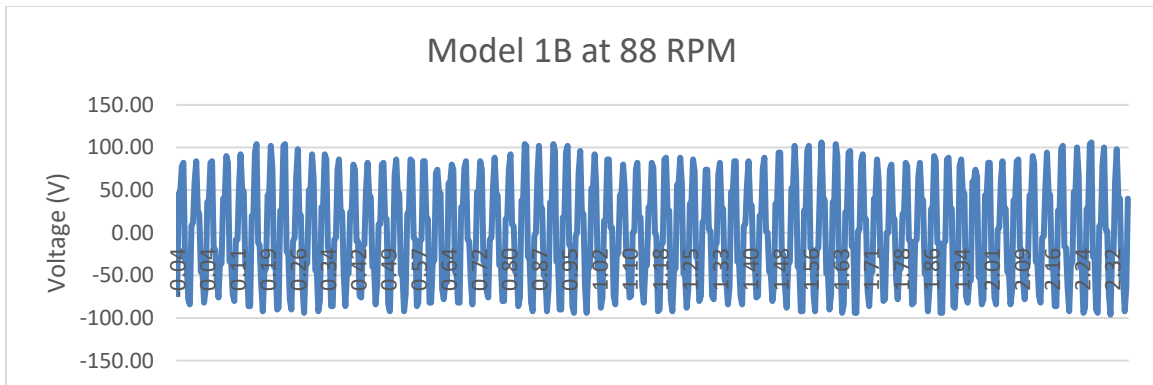


Figure 93. Model 1B prep for Series/Parallel Test

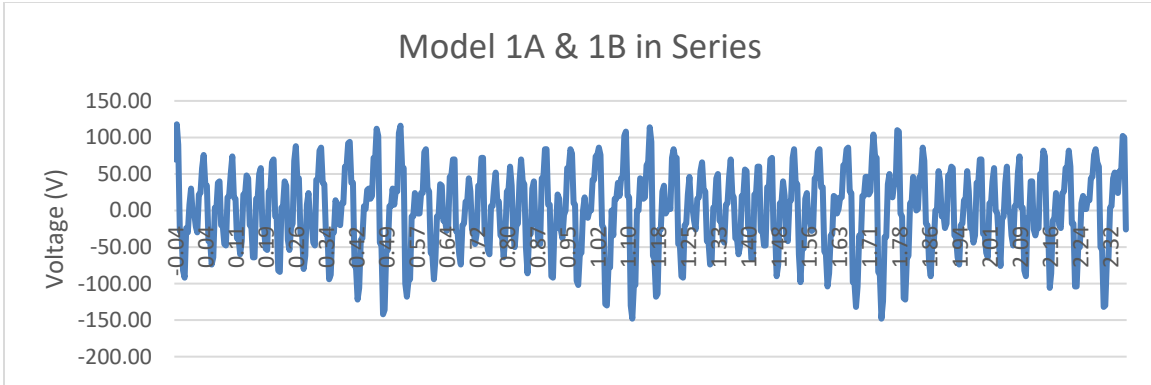


Figure 94. Model 1A and 1B in Series at 90 RPM

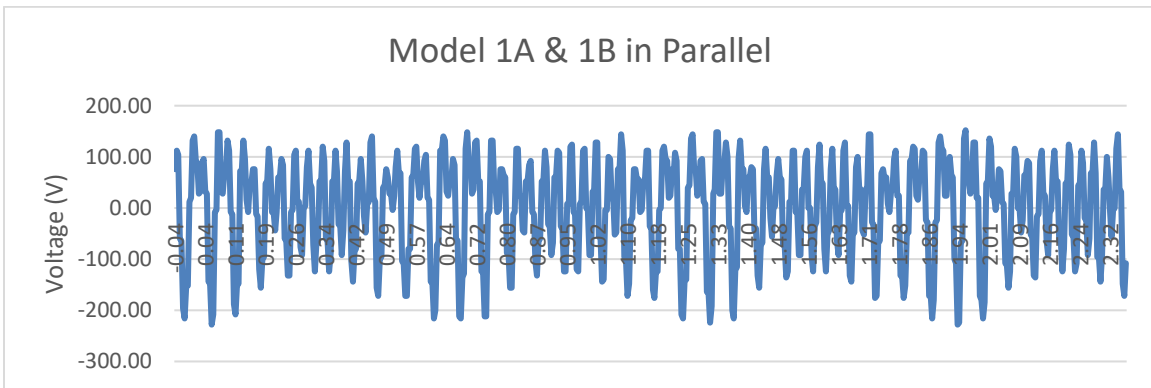


Figure 95. Model 1A and 1B in Parallel at 90 RPM

G. CAPACITOR STORAGE DATA

The figures below show voltage and current data for Model 1B during charging at different shaft speeds.

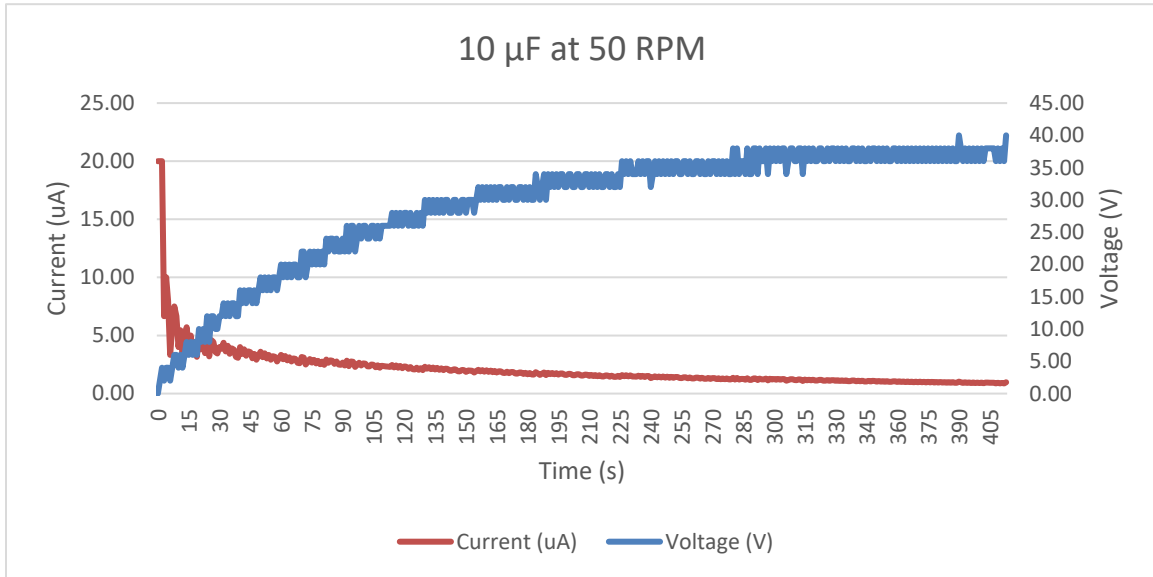


Figure 96. Model 1B Charging 10μF Capacitor at 50 RPM

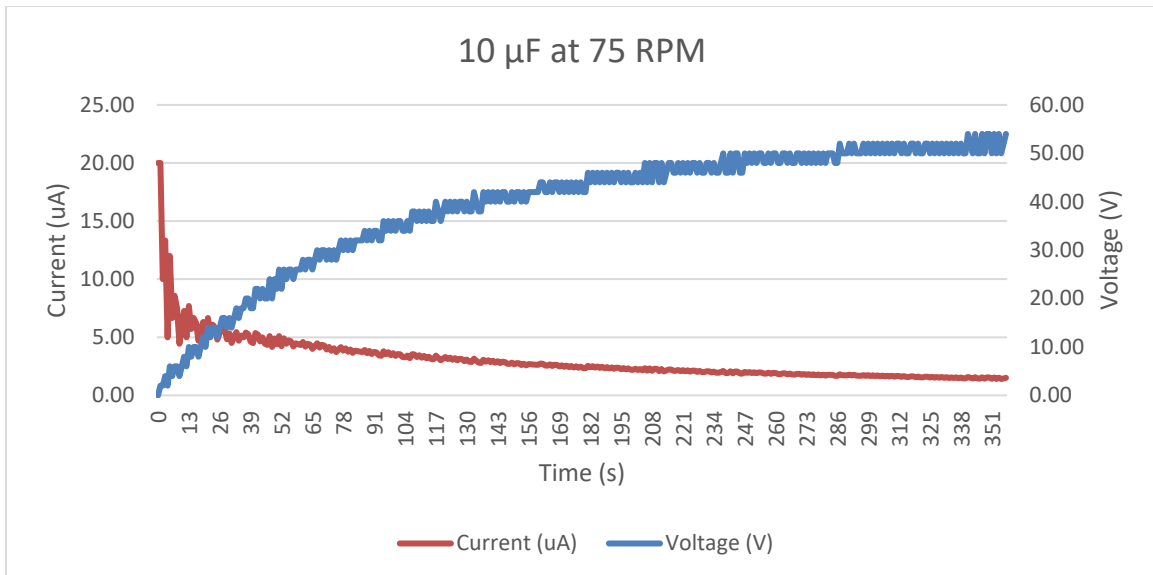


Figure 97. Model 1B Charging 10μF Capacitor at 75 RPM

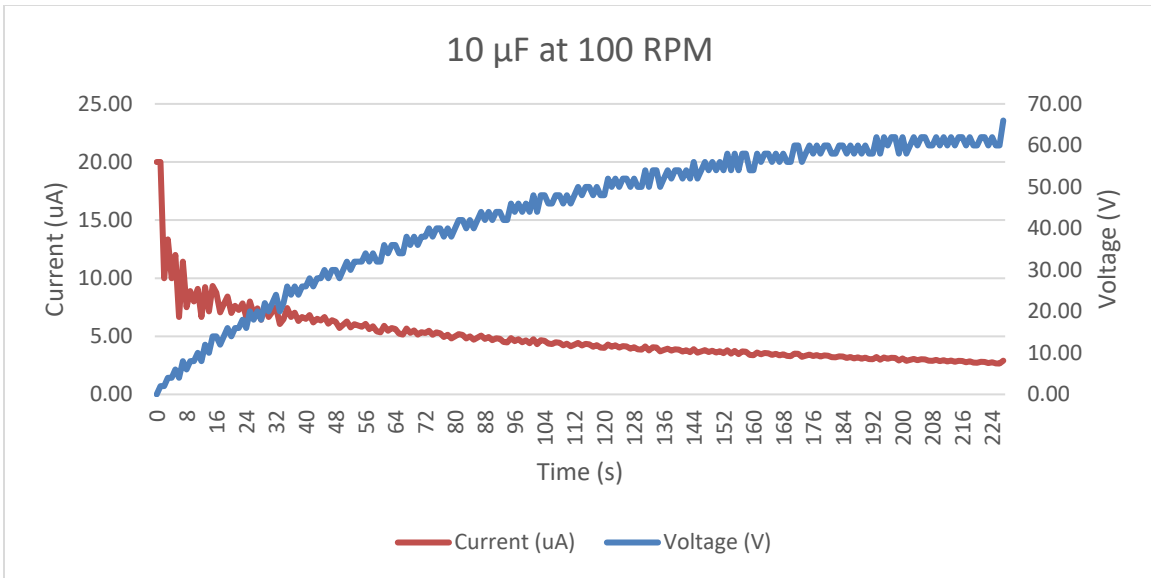


Figure 98. Model 1B Charging 10μF Capacitor at 100 RPM

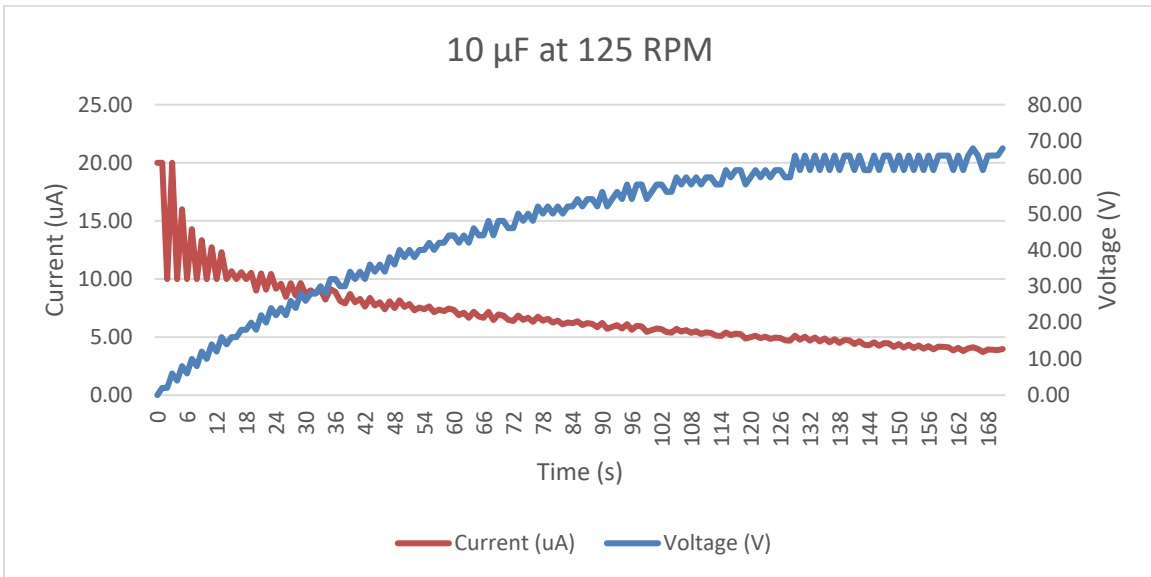


Figure 99. Model 1B Charging 10μF Capacitor at 125 RPM

LIST OF REFERENCES

- [1] BP, “Primary energy.” Accessed Sept. 12, 2020. [Online]. Available: <https://www.bp.com/en/global/corporate/energy-economics/statistical-review-of-world-energy/primary-energy.html>.
- [2] U. Khan and S.-W. Kim, “Triboelectric nanogenerators for blue nergy Harvesting,” *ACS NANO*, vol. 10, pp. 6429–6432, 2016.
- [3] Z. L. Wang, “Triboelectric nanogenerators as new energy technology and self-powered sensors – Principles, problems and perspectives,” *Faraday Discussions*, vol. 176, pp. 447–458, 2014.
- [4] K. Bayindir, “Motion and sound activated, 3D printed, chalcogenide based triboelectric,” *Advanced Materials*, vol. 27, pp. 2367–2376, 2015.
- [5] Z. L. Wang, “On Maxwells displacement current for energy and sensors: the origin of nanogenerators,” *Materials Today*, vol. 20, no. 2, pp. 74–82, 2017.
- [6] J. Kessopha, “Triboelectric nanogenerators (TENG) with rotational motion,” M.S. thesis, Dept. of Mech. Eng., NPS, Monterey, CA, 2020. [Online]. Available: <https://calhoun.nps.edu/handle/10945/64912>
- [7] S. Riley, “Triboelectric Nanogenerator with Ocean Wave Energy,” M.S. these, Dept. of Mech. Eng., NPS, Monterey, CA, 2019 [Online]. Available: <https://apps.dtic.mil/dtic/tr/fulltext/u2/1080384.pdf>
- [8] K. Mann, “Triboelectric Nanogenerator for Energy Harvesting,” M.S. these, Dept. of Mech. Eng., NPS, Monterey, CA, 2019 [Online]. Available: https://calhoun.nps.edu/bitstream/handle/10945/64018/19Dec_Mann_Katherine.pdf?sequence=1&isAllowed=y
- [9] T. L. Floyd and R. Donovan, *Electric Circuits*, vol. 2. Boston, MA, USA: Pearson Custom Publishing, 2007.
- [10] T. L. Floyd, *Principles of Electric Circuits: Conventional Current Version*, 8th ed. Upper Saddle River, NJ, USA: Prentice Hall, 2007.
- [11] WorldStandards, “Country-by-country list of plugs, sockets and voltages.” Accessed August 23, 2020. [Online]. Available: <https://www.worldstandards.eu/electricity/plug-voltage-by-country/>.

- [12] M.-L. Seol, J.-W. Han, S.-J. Park, S.-B. Jeon and Y.-K. Choi, “Hybrid energy harvester with simultaneous triboelectric,” *Nano Energy*, vol. 23, pp. 50–59, 2016.

INITIAL DISTRIBUTION LIST

1. Defense Technical Information Center
Ft. Belvoir, Virginia
2. Dudley Knox Library
Naval Postgraduate School
Monterey, California